



***Study on the key factors allowing the PEM fuel cell systems large commercialization: fuel cell degradation and components integration***

Denis Bona

I.D. number 178646

Supervisor: Prof.ssa Elena Maria Tresso

Applied Science and Technology Department, Politecnico di Torino

Electro Power Systems SpA

PhD in Electronic Devices (XXVI cycle)

Academic years 2011 – 2013



# Contents

|  |          |
|--|----------|
| <b>Acknowledgments</b>   | <b>1</b> |
| <b>Introduction</b>  | <b>3</b> |
| <b>1. The PEM fuel cells system</b>                                      | <b>9</b> |
| 1.1. PEM fuel cells .....  | 9        |
| 1.2. Power system features .....   | 11       |
| 1.2.1. Fuel cell stack.....  | 13       |
| 1.2.2. Fuel/oxidant conditioning and delivery .....                      | 14       |
| 1.2.3. Cooling system.....   | 15       |
| 1.2.4. Electrical power conversion.....                                  | 16       |
| 1.2.5. Control electronics .....   | 18       |
| 1.3. Market applications, status and forecast for near-term period ..... | 20       |
| 1.3.1. Automotive.....   | 22       |
| 1.3.2. Stationary .....  | 23       |

|  |           |
|--|-----------|
| 1.3.3. Back-up Power .....   | 24        |
| <b>2. State of the art on the PEM fuel cells degradation issues</b>                            | <b>26</b> |
| 2.1. PEM fuel cells system durability evaluation .....   | 27        |
| 2.2. PEM fuel cells degradation mechanisms and solutions.....                                  | 30        |
| 2.2.1. Membrane .....  | 31        |
| 2.2.2. Catalyst layer.....   | 32        |
| 2.2.3. GDL.....  | 35        |
| 2.2.4. Bipolar plate .....   | 36        |
| <b>3. Mitigation strategies for commercial PEM fuel cells stacks</b>                           | <b>38</b> |
| 3.1. Mitigation strategies against the membrane degradation .....                              | 39        |
| 3.2. Mitigation strategies against the Pt dissolution .....                                    | 41        |
| 3.3. Catalyst carbon support corrosion .....   | 45        |
| 3.3.1. Carbon corrosion during startups and shutdowns .....                                    | 47        |
| 3.3.2. Carbon corrosion during fuel starvation .....   | 49        |
| 3.3.3. Carbon corrosion detection methods.....   | 51        |
| 3.3.4. Material-based carbon corrosion mitigation strategies .....                             | 58        |
| 3.3.5. System-based carbon corrosion mitigation strategies .....                               | 64        |
| 3.4. Mitigation strategies testing and validation.....   | 69        |
| <b>4. Performance, compactness and cost improvement of the fuel cells system</b>               | <b>81</b> |
| 4.1. DC-DC converter integration with a fuel cells stack.....                                  | 82        |
| 4.2. Functionalized stack head with integrated heat exchanger for reactant gases processing    | 87        |
| 4.3. Sensors integration for the process parameters measurement directly inside the stack .... | 90        |

|   |            |
|---|------------|
| 4.4. Global advantages obtained and future developments ..... | 98         |
| <b>Conclusion</b>   | <b>101</b> |
| <b>References</b>   | <b>102</b> |



# Acknowledgments

I wish to thank all the persons who have supported me during the three years of PhD. It was not easy to both work in a company and carry on my PhD research but, finally, I succeed.

So, first of all I would like to thank my family and, above all, my wife Sabrina: without her support it would have been much harder to undertake all tasks always at the best.

Then, I would like to gratefully acknowledge all my colleagues in EPS and my PhD tutor Elena Tresso. They all helped and guided me in any situation, especially when the deadlines were close or when the tasks were particularly hard.

A special thanks to my friend Dennis Curtin: without his help and contribution it would have been almost impossible to succeed in publishing our article and other two works respectively at an international journal and at two international conferences.

Finally thank you very much also to all the people not mentioned here but who contributed, even in minor part, to my PhD work development.



# Introduction

The world energy demand is continuously growing due to the world population increasing and the developing countries rising. The U.S. Energy Information Administration (EIA) in the International Energy Outlook 2013 has estimated a 56% increase of the world energy demand by 2040 passing from 524 quadrillion British thermal units (Btu<sup>1</sup>) in 2010 to 630 quadrillion Btu in 2020 and to 820 quadrillion Btu in 2040 [1] (see figure 1). Much of the growth in energy consumption occurs in countries outside the Organization for Economic Cooperation and Development (OECD<sup>2</sup>), known as non-OECD, where demand is driven by strong, long-term economic growth. While North America, Europe, Japan and Oceania will show a modest energy demand growth (17%), the energy use in China, India and other developing countries in Asia, Africa and South America will increase by 90 percent. The EIA estimated that China and India will account for half of global energy growth through 2035 [2].

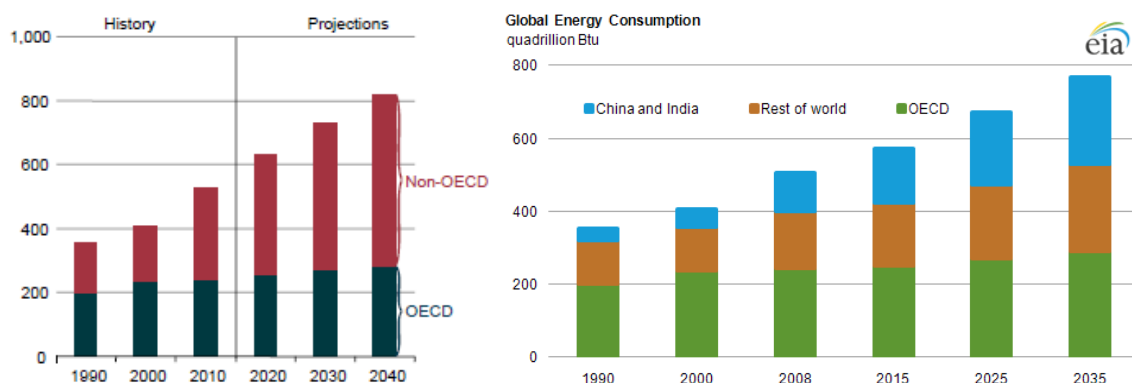


**Figure 1.** On the left: IEO2013 projections [1]; on the right: energy world demand trend by areas [2].

<sup>1</sup> Unit of energy equal to about 1055 joules; it is the amount of energy needed to cool or heat one pound of water by one degree Fahrenheit.

<sup>2</sup> OECD member countries: USA, Canada, Mexico, Austria, Belgium, Chile, Czech Republic, Denmark, Estonia, Finland, France, Germany, Greece, Hungary, Iceland, Ireland, Israel, Italy, Luxembourg, Netherlands, Norway, Poland, Portugal, Slovakia, Slovenia, Spain, Sweden, Switzerland, Turkey, United Kingdom, Japan, South Korea, Australia, and New Zealand.

## Introduction

The world is still recovering from the effects of the 2008-2009 global recession. In 2009, the world energy consumption decreased for the first time in 30 years by  $-1.1\%$  as a result of the financial and economic crisis, which reduced world GDP by  $0.6\%$ . As these effects continue to be felt, many unresolved economic issues add to the uncertainty associated with this year long-term assessment of world energy markets. Currently, there is wide variation in the economic performance of different countries and regions around the world. In particular, two contrasting trends can be observed: energy consumption growth remained vigorous in several developing countries, specifically in Asia. Conversely, in OECD, consumption was severely cut and was thus almost down to its 2000 levels. In North America, Europe and the CIS (Commonwealth of Independent States), consumptions shrank by  $4.5\%$ ,  $5\%$  and  $8.5\%$  respectively due to the slowdown in economic activity. China became the world's largest energy consumer ( $18\%$  of the total) since its consumption surged by  $8\%$  during 2009 (up from  $4\%$  in 2008).

According to the forecast of global oil production presented by the World Energy Outlook (WEO) [3], [4], the crude oil production from currently producing fields have already reached the peak in 2008 and is now depleting. So, right now, the efforts are concentrated in finding and developing new fields on one hand or producing non-conventional oil on the other in order to satisfy the continuously increasing world oil demand (see figure 2).

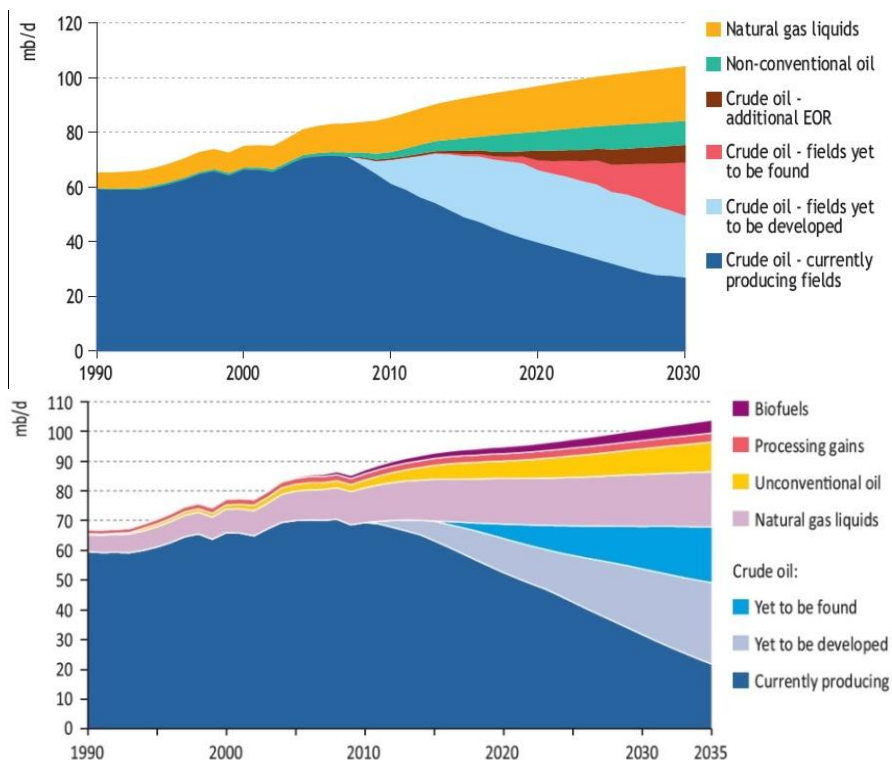


**Figure 2.** On the top: oil production forecast according to WEO2008 [3]; on the bottom: oil production forecast according to WEO2011 [4].

The issue is that typically new fields are in areas more difficult to reach and the non-conventional oil is more expensive to extract or obtain. So, as a result, considering the growing world oil demand, in the future

## Introduction

---

the oil price is expected to increase reaching 106 \$/barrel in 2020 and 163\$/barrel in 2040 [1] and the coal consumption will rise especially in the developing countries enhancing the CO<sub>2</sub> global production.

World energy-related carbon dioxide emissions will rise from 31.2 billion metric tons in 2010 to 36.4 billion metric tons in 2020 and 45.5 billion metric tons in 2040 in the *IEO2013* Reference case, so an increase of 46 percent over the projection period. Coal continues to account for the largest share of carbon dioxide emissions throughout the projection (see Figure 3).

According to IEA (2012), the climate goal of limiting warming to 2 °C is becoming more difficult and costly with each year that passes. If action is not taken before 2017, all allowable CO<sub>2</sub> emission would be locked-in by energy infrastructure existing in 2017. To limit global temperature to a hypothetical 2 °C rise would demand a 75% decline in carbon emissions in industrial countries by 2050 [5].

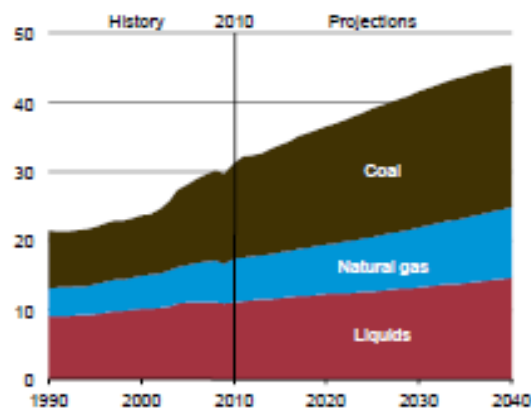


**Figure 3.** World energy-related carbon dioxide emissions by fuel type, 1990-2040 (billion metric tons) [1].

An important role is starting to be played by the renewable sources of energy (sun, wind, hydroelectric, geothermal). In 1990, renewable resources supplied about 14% of the world energy demand, 16% nowadays and are going to be one quarter by 2035, leading to an important reduction of ambient pollution.

The main drawback of this kind of resources is that their availability is non-constant on a fixed period of time, and cannot be linked with the power demand, since we are not able to control the power source itself. On the other hand, these resources are inexpensive and have a small environmental impact, compared to the pollution rate generated by fossil fuel or nuclear. Moreover, renewable resources can be effectively exploited in small-scale plants, introducing the concept of the so-called smart grid economy. In a smart grid scenario the energy production is distributed geographically in a large number of low power production sites, each of them connected to the grid in order to share peaks of production and demand over time. This solution features big advantages in terms of stability and availability and the reduction of energy losses due to energy transport, since most of the energy is consumed next to the production site.

In order to effectively use renewable resources, high-efficiency energy accumulator systems must be included as nodes to the smart grid. This kind of systems must be able to store the energy during the peak of

## Introduction

---

production or when the load adsorbs less power than the one that is produced by the renewable source, and to release the energy when the renewable resources perform at a lower production than the load demand.

As coal fueled the industrial revolution in the 18<sup>th</sup> and 19<sup>th</sup> century, the use of oil in the 20<sup>th</sup> century had been indispensable for the great technology development that was featured by the advent of the automobile, airplanes and the spreading use of electricity. The oil derivatives (gasoline, diesel, kerosene, etc.) are characterized by high heating density values; and the use of liquid fuels allows high versatility in many applications and facilitates the fuel transportation.

Once extracted, the oil can be considered as an energetic vector able to be used to feed a vehicle or to be transformed into electricity or heat in stationary applications. The oil usage would be useless without the presence of a huge infrastructure that is able to:

- 1) extract the crude oil
- 2) transport the crude oil from the well to the refinery
- 3) refine the crude oil in order to obtain suitable derivatives
- 4) transport the oil derivate to the end use

Every step requires high investment cost. Without considering the cost related to the research of new oil fields, drilling and building new wells in some areas or offshore can cost more than 2 billion \$ [6], an oil sea-tanker can reach 120 million \$ [7], an oil pipeline can cost up to 1.5 billion \$ for each 1000 km [8], [9] and a refinery plant can overcome 150 million \$ [10]. This huge investment can be sustained only by a few big companies in the world.

Also, hydrogen is an energy vector, but its availability is not correlated to a deposit from which to extract the fuel, and must be obtained by transforming other sources (principally fossil fuels or water). Considering a long-term vision, obtaining the hydrogen from fossil fuels is not convenient since the transformation of an energetic vector into another one involves energy losses and cost, so it is preferable to use the primary energetic vector (fossil fuel) instead of transforming it into hydrogen for the end use.

The alternative is to store the excessive renewable energy by transforming on-site the water into hydrogen and oxygen trough the electrolysis process. The **green hydrogen** obtained can be used: a) in nearby small and medium co-generation power plants or power systems able to feed nearby industries or houses, and b) in nearby hydrogen re-filling stations able to re-fuel a fuel cell electric car in 4-5 minutes [11]. Alternatively, a hydrogen pipeline similar to the existing natural gas pipelines can be built in order to feed distant co-generation plants, systems or re-filling stations.

To take an example, a 1.5 MW wind turbine coupled with an electrolysis plant of 1.5 MW and a gas compressed storage system at 250 bar could cost less than 2,000,000 € [12]. In a case study, Mura et al. estimated that the hydrogen production through electrolysis and a wind turbine placed in Sardinia (Italy) would produce every year 685,000 Nm<sup>3</sup> of hydrogen corresponding to 2,055,000 kWh of energy annually stored.

If a fuel cell power system or plant of 500 kW was coupled (cost 1,000,000 €), considering an efficiency of 50% (possible if the oxygen produced by the electrolyzer is exploited) then the electricity need of about

## Introduction

340 families could be satisfied at least for 16 years and the cost for every family would be 8800 €. Alternatively, the same energy could satisfy at least 5-6 industrial facilities of medium size. A further cost saving would be the heat exploited from the plant in a co-generative way. Other possible uses of the hydrogen would be a re-filling station for city buses or taxi fleets that would be supplied with fuel for at least 16 years without any operation or services costs.

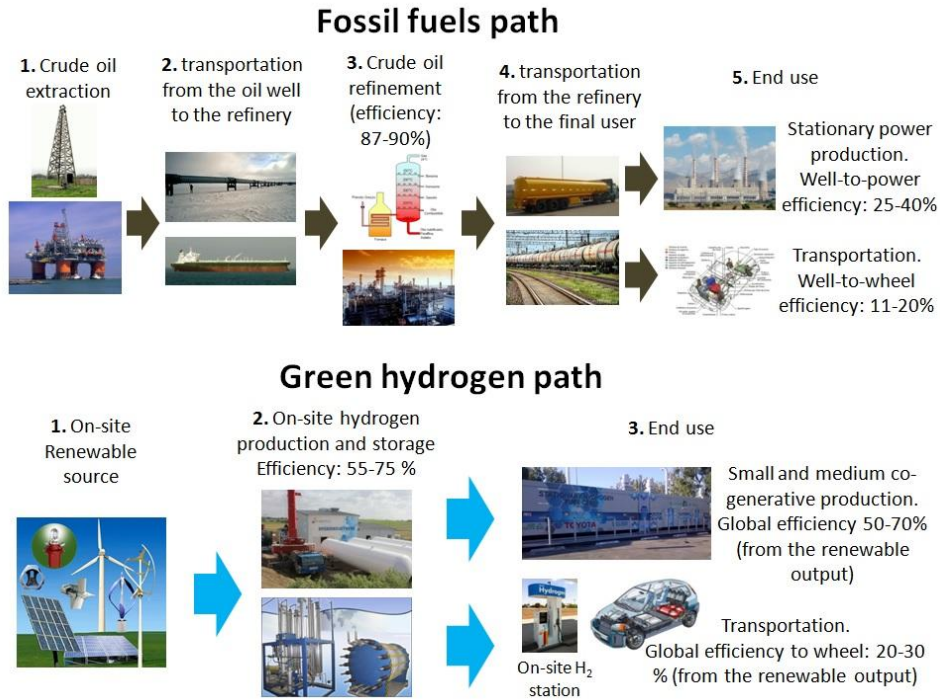


**Figure 4.** Comparison between fossil fuel and hydrogen as energy vector.

As the oil path between the production and the end use is featured by many steps, even the final stage, the energy production, is characterized by many intermediate steps that leads to a loss of performance (see Figure 5). Instead, the fuel cell plant can be considerably more competitive in terms of efficiency thanks to the single electrochemical stage that immediately provides the electrical output.

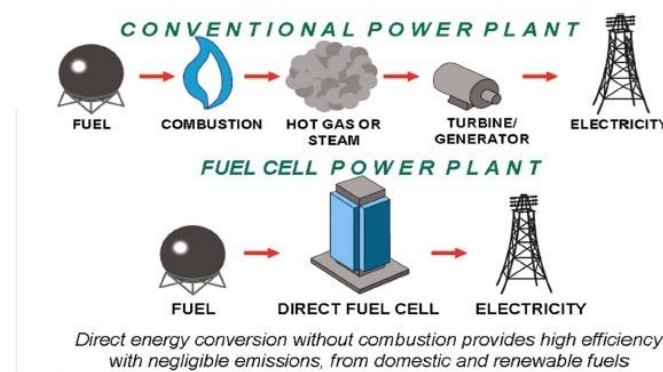


**Figure 5.** Comparison between the conventional power plants and the fuel cell plants for electrical energy production.

## Introduction

---

In some applications, a power cut due to a blackout or to a disturbance on the power line can be critical because of safety or economical fallouts; and a lot of different appliances that are classified under the name of UPS (Uninterruptible Power Sources) have been introduced to guarantee power continuity.

Since from its birth in 2005, Electro Power Systems SpA (EPS) has installed worldwide more than 500 telecom UPSs based on PEM fuel cell technology. In 2010, they developed and introduced into the market the first PEM fuel cell based power system for back-up purposes using oxygen as oxidant. This choice allows higher efficiency and a doubling of power density volume, compared with traditional power systems that use air as oxidant. During 2011, EPS integrated the power system with an alkaline electrolyzer, bundled in the same structure, to solve the problem of the logistic of the reactant gases. This solution can be used in grid-connected sites, but paves the way for a completely new niche of off-grid, isolated sites. In the same year EPS started the first experimentation of ElectroSelf™ integrated with renewables at Cellarengo (Italy).

Now, using the experience collected on field at Cellarengo, EPS is exploring the possibility to use ElectroSelf™ together with renewable sources for the energy storage market in a smart grid context or in isolated off-grid sites. Two parallel projects, Alcotra and HySolWind, were started in 2012, and have the goal to test the ElectroSelf™ coupled with renewable sources (mainly photovoltaic modules and small wind turbines) for stationary applications.

In the back-up market for developed countries (Europe, America, Japan), some factors as cost and durability are less important with respect to others such as the reliability. The customer here is more interested in having a system able to start in any kind of condition (in some cases also extreme cold or hot ambient temperature) and even after a consistent time of non-operation (1-2 years). A failure to start during a blackout can have serious consequences: in a hospital, surgical operations cannot be performed and medical devices cannot work; in a supermarket, large amounts of frozen food risk spoilage; and in the telecom applications the operator cannot supply the phone and internet services. In these countries, however, the blackouts have low frequency and the average hours of operation is in the order of 5-10 h/year. So, in this context, the reliability is fundamental but the number of operation hours is so low that even a lifetime of 500-1000 h can be enough.

Instead, in the energy storage market and in the back-up market for developing countries (where the numbers and hours of blackout are considerably higher), the durability and cost are important factors that can become determinant for the success of the fuel cells introduction and spreading. For this reason, during the last three years EPS has deeply investigated the PEM fuel cells degradation mechanisms in order to find proper and effective mitigation solutions able to improve the fuel cells lifetime. In the same time, EPS has also explored new technologic solutions able to effectively reduce the system cost.

The study of PEM fuel cells degradation and the investigation of new technology solutions for system cost reduction had been the aim of this thesis work. The efforts have been focused on one side in finding new mitigation strategies able to improve the PEM fuel cell stack lifetime and, on the other, in saving materials or optimizing the system components so that the same power output is obtained at a lower cost and improved compactness.

# Chapter 1

## The PEM fuel cells system

### *1.1. PEM fuel cells*

Fuel cells are devices able to convert the chemical energy contained in hydrogen or hydrocarbon molecules into electrical and thermal energy. The exothermal reactions taking place in any fuel cell generate water as byproduct and, if the fuel used is a hydrocarbon, carbon oxides.

The first commercial application of fuel cell appeared in the 1960s with the NASA Gemini program. It had a solid electrolyte made of a thin layer of polymer, so a PEM (Polymer Electrolyte Membrane) fuel cell. Many different solutions have been proposed since then: the main difference between the classes of fuel cell is the electrolyte that limits the working temperature range of the devices.

Devices operating at higher temperature can use hydrocarbons (e.g. methane) or methanol as fuel since they can perform an implicit steam reforming next to the reaction sites.

**Polymer Electrolyte Membrane (PEM) Fuel Cells** feature a perfluorosulfonic acid membrane synthesized as thin film between two reaction sites, anode and cathode. The membrane is a polymer, containing sulphonated groups capable to carry protons if properly hydrated by the water produced at cathode by the reaction itself. In order to maintain the membrane well hydrated, the operating temperature at low reactant pressure (300-400 mbarg) must not overcome 70-75 °C. Since the low operating temperature

does not allow the on-site hydrocarbon molecules division, the PEM fuel cells are able to process only pure hydrogen.

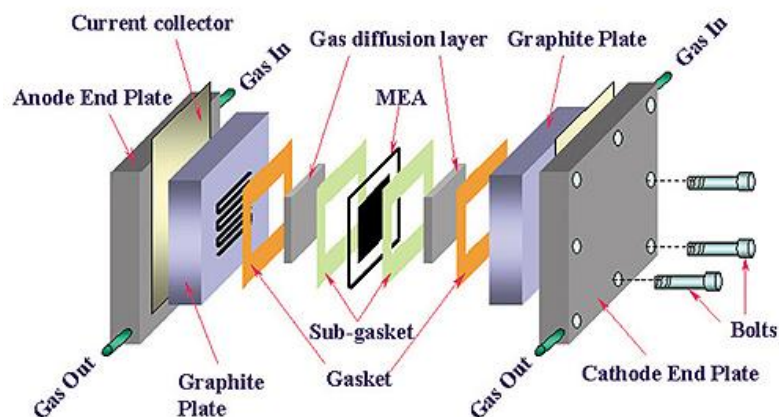


**Figure 1.1.** PEM fuel cell scheme [13].

Catalyst layers are applied to both sides of the membrane and can be constituted by pure platinum metal (Platinum Black) or a mix of carbon supported platinum catalyst (Carbon Black) and an ionomer phase (material similar to the membrane). With the Carbon Black solution, the support modifies the morphology of the catalyst surface, basically increasing the area using tridimensional structures. In this way the catalyst activity can be high enough even with a low Pt content. The disadvantage instead is the oxidation tendency of the carbon support leading to the catalyst detachment and dissolution into the ionomer phase.

Contacting the catalyst layers, the membrane has two porous backing electrodes. The electrodes must have good electrical characteristic (low electrical resistance), they must be able to transport the gas to the reaction sites and to drain the water out. This portion is named Gas Diffusion Layer (GDL). Optimal performances have been reached with carbon-based cloth, non-woven pressed carbon fibers or felt-like materials applied directly to the catalyst coated membrane in order to have an intimate electrical contact.

The membrane together with the catalyst layer and the gas diffusion layer form the Membrane Electrode Assembly (MEA), commercially available.

The anode and the cathode compartments are made from special plates with some narrow channels designed to transport homogeneously the gas reactants to the active area. The plates can be made of graphite (usually mixed with a polymer in order to have better mechanical properties) or metal with a surface treatment to reduce oxidation. The shape and the number of channels are computed in order to obtain uniformity in the gas distribution and to optimize the water management of the cell according to the nominal thermodynamic conditions. The surface of the plates in contact with the reactants is covered with a hydrophobic layer in order to ease the water drag by the gas flow and facilitate the elimination of liquid water that is produced by the reaction.

The closing pressure of the two bipolar plates (anode and cathode) is an important design parameter of the cell: it influences the contact resistance between the plates and the gas diffusion layer, the depth of the

porous electrodes and the gas channels, the gas seals and the mechanical durability of the plates, especially if they are made of fragile materials as graphite. The optimal closing pressure can be obtained using springs that can keep the pressure constant even when the pressurized gases are applied to the cell or during temperature gradients due to startup or shutdown of the device.

A single fuel cell can typically produce a few hundred watts, depending on the electro catalyst active area exposed. So in order to reach higher power output, usually more fuel cells are assembled in series to form a fuel cell stack. Typical back-up power stack can have 50-100 cells, while for automotive stacks the number of cells can reach up to 300-400.



**Figure 1.2.** 56-cell PEM fuel cell stack assembled by Electro Power Systems.

### *1.2. Power system features*

A power system is a device containing many functional blocks integrated into a single box. The main functional blocks are:

- Electrochemical conversion (fuel cell stack)
- Fuel and oxidant conditioning and delivery circuits
- Cooling system
- Electrical power conversion
- Control electronics

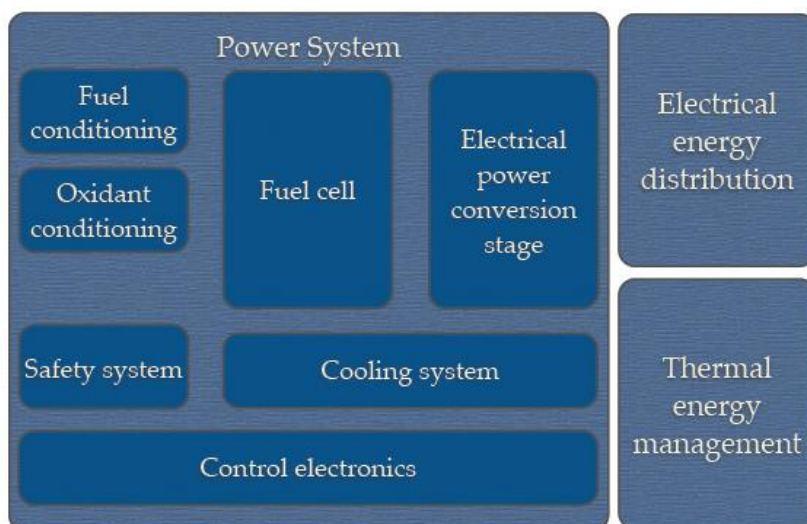


**Figure 1.3.** Functional blocks scheme of the PEM fuel cells power system.

Fuel cell stack, fuel conditioning circuits and cooling circuits form the so-called Balance of Plant (BOP). In following, two examples of power system scheme are reported, respectively using air and oxygen as oxidant.

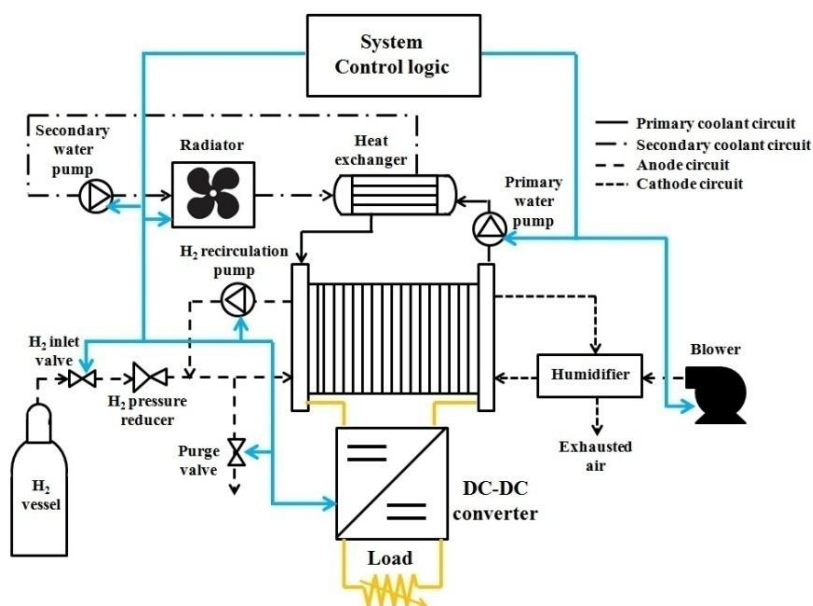


**Figure 1.4.** Scheme of a fuel cell power system using air as oxidant.

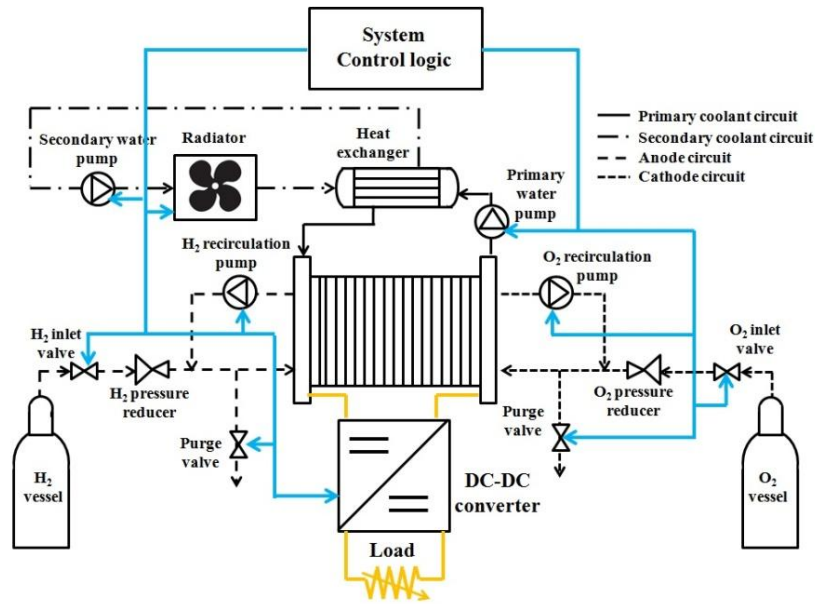


Figure 1.5. Scheme of a fuel cell power system using oxygen as oxidant.

### 1.2.1. Fuel cell stack

The fuel cell stack converts the chemical energy of the fuel into electrical energy providing a decreasing DC voltage for increasing current values. According to the fuel and oxidant flow rates and pressures, the operation temperature and the water content inside the polymer electrolyte membranes, the fuel cell stack will provide different performances. For example, using pure oxygen instead of air, the increased partial pressure reduces the losses due to the reaction activation, resulting in an increase (actually doubling) of the power density of the stack.

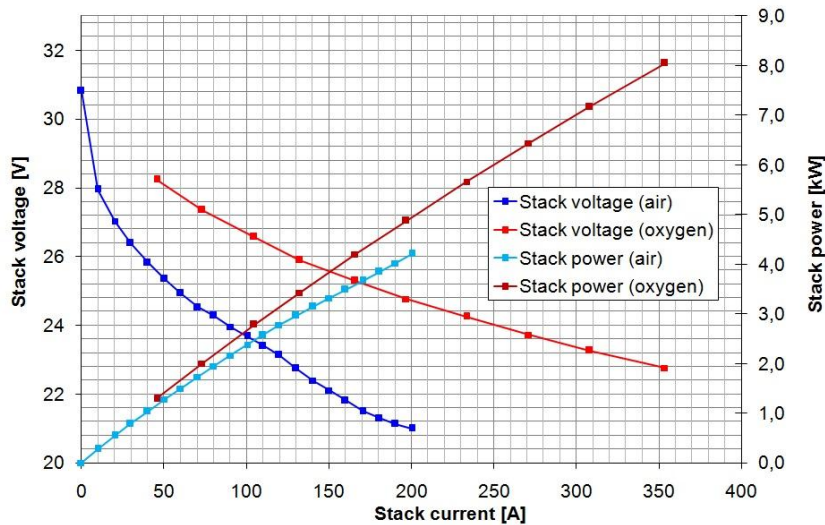


Figure 1.6. Reference curves relative to a 32 cell stack for air applications and a 32 cell stack for oxygen application.

### ***1.2.2. Fuel/oxidant conditioning and delivery***

Fuel and oxidant must be conditioned before reacting in the fuel cell. Pressure must be regulated as well as temperature, in order to control the dynamic humidification of the polymer electrolyte membranes.

Each fluid adduction system must include a mechanical pressure reducer, having one or more reduction stages, and a couple of valves connected in series to guarantee the shut-off of the gas in case of one of the two is leaking.

The simplest circuit is called open-ended. In this case, the outlet of the reactant manifolds are open at ambient pressure, so that the gas amount that is not taking part to the reaction is released into the ambient and wasted. This solution features a very poor efficiency since the system typically does not include a precise Mass Flow Controller (MFC), but just a pressure regulator so the amount of gas must be more than stoichiometric ratio in order to guarantee the minimum flow in any condition. Usually, the open-ended circuit is used for the air circuit, including a blower or a compressor that supplies the ambient air and generates the needed gas pressure at the stack inlet.

Another option is the so-called dead-end operation: in this configuration the outlet is closed and the efficiency is optimized since the entire supply of gas can react. The problem rises in long-term operation, since the gas always contains a small fraction of inert or other chemical species; this quantity can influence the partial pressure, especially if the reactants are not gas intended for industrial application. This small fraction cannot take part in the reaction, but tends to accumulate in the cells channels and manifolds, leading to a reduction of the partial pressure of reactants and lowering the performance of the stack. A good solution is to create a purge made of a valve with controlled duty cycle to release a small fraction of reactants together with the inert parts into ambient. The same result can be obtained using calibrated converging-diverging nozzle that chokes the maximum flow rate that is dispersed toward the ambient air.

The last possible configuration is recirculation: reactants not taking part into the reaction are pumped back using a vacuum pump toward the stack inlet and mixed together with fresh reactants. The vacuum pump is usually a volumetric pump that is able to recover the pressure drop caused by bipolar plate channels and to force the fluid into a defined direction in the stack. This method offers an indirect control of the inlet gas humidity content: the electrochemical process creates water vapor as byproduct that mixes with the non-reacting fraction of gas output. Being the process at an average temperature of 80 °C and the gas coming from the cylinders at ambient temperature, the mixture of the fluids causes liquid water condensation that must be removed using water drainers. To remove the inert part of the gases a calibrated nozzle is used as if the configuration is a dead-end one.

The nozzle can be bypassed by an electro-actuated valve. A Programmable Logic Controller (PLC) can manage to bypass the nozzle increasing the amount of gas wasted in particular stack conditions. The increased purge is used during the startup of the fuel cells in order to eliminate most of the inert gases,

mainly nitrogen, that remain in the stack when it is not working. The bypass valve can be used to increase the flow (operating in pulsed width modulation mode) when the performances of the stack are poor due to local accumulation of liquid water. This feature improves the water management of the fuel cells.

Particular attention must be paid in the choice of the recirculation pump. Optimal efficiency can be reached for low pressure drop (10-100 mbar) and flux around 0.5 Nl/s by using an oscillating membrane pump with an actuated DC brushless motor. The material of the membrane must fulfill the compatibility requirement to be used in hydrogen atmosphere and oxygen atmosphere, and it must be able to withstand contact with pure water. The best choice is to have a double membrane pump to prevent leakage.

Both circuits and components need to be chosen according to the application. Although the overall circuit is fueled with gas at relative pressure of 300 mbar and the physical volume of the gases is just few liters, the materials of pipes, joints and fitting must be carefully chosen. Low carbon stainless steel (AISI316) for fittings and Rilsan® polyamides for pipes are all compatible with hydrogen as well as oxygen.

Special precautions must be taken during the manufacturing process of the oxygen circuit. Oil or traces of other organic material can locally increase the friction of the oxygen in the pipes. If the heat generated by friction is enough, the organic material can burn in presence of oxygen and raise the gas pressure leading to explosions and severe consequences.

The pressure reducer and the pipes must be dimensioned to guarantee the flux consumed by the stack.

### ***1.2.3. Cooling system***

The hydrogen oxidation and the oxygen reduction taking place at the electrodes are not 100% efficient. This means that the chemical energy is not totally converted to electrical energy but a certain part is dissipated into heat. Furthermore, the electron and ion fluxes produce ohmic losses generating heat. So all this heat needs to be dissipated by a dedicated liquid cooling circuit in order not to damage the MEA components (principally the membrane and the ionomer phase present into the catalyst layer). The water cooling circuit is usually connected to an external heat exchanger in order to dissipate the thermal energy into the environment or use it for co-generating purposes.

Usually more than half of the power contained in the fuel is lost due to heat generation. One option could be to use this thermal energy to do combined heat and power generation, but in case of back-up power the thermal source is not continuous and it is difficult to forecast the blackout occurrence.

The liquid that cools the fuel cells is in contact with all bipolar plates: the conductivity of the liquid must be low; otherwise, an ionic current can flow into the cooling liquid when the stack is operating, causing losses. In order to keep the conductivity of the circuit low usually demineralized water is used with a proper ionic exchange resin filter inserted into the circuit. This filter can have cationic and anionic resins mixed together to form little spheres. When the water passes through those spheres, the ionic part is attracted by the filter resins and remains inside the filter. The resin amount needs to be evaluated in order to be enough to

control the normal ionic release for at least 2 years of continuous operation. After that time, the filter must be replaced, and the used resins can be regenerated to their original ion exchange capacity. A resistive heater can be used when the temperature falls near 0 °C to prevent freezing of the cooling water and of the water content inside the polymer electrolyte membranes. The heater is not required when the fuel cells are operating since the electrochemical conversion process produces heat.

The membranes humidification is a property that has a strong relation with the temperature. In nominal operations the BOP should be able to limit the thermal excursion between the inlet and the outlet of the stack to 5°C, otherwise the water content of the portion of membranes next to the inlet manifold of the coolant can be higher or the warmer part can be dryer than the other membranes.

The coolant enters the stack and removes some of the generated heat, which is transferred to the heat exchanger that dissipates the heat to the ambient. Usually the heat exchanger needs to dissipate the thermal energy with a minimum temperature gradient of 15 °C, which is the difference between the working temperature of the stack and the maximum allowed ambient temperature (typically 45 °C).

The airflow can be generated using variable speed fans, in order to better modulate the heat transfer from water to air and the consequent inlet temperature of the fuel cells. An optimal stability of the stack temperature can be achieved using a PID (Proportional Integrative Derivative) controller. This controller samples the error quantity as the difference between the measured value and the expected one, in this case the stack temperature. The error is used to compute the derivative and the time integral of the error itself and the linear combination of these three elements (with different weights) is used to compensate a setpoint of an actuator.

### ***1.2.4. Electrical power conversion***

During normal operation of a fuel cell or of a stack, the current changes according to the load requirements and it is difficult to determine a single working point of the stack precisely in order to dimension the active surface area and the number of the cells of the stack.

As the current density changes, the stack voltage changes consequently and the output impedance of the source changes according to the derivative of the characteristic curve.

Conventional loads for telecom back-up applications require a constant DC voltage at input terminals, so the use of a static DC-DC converter is mandatory.

A DC-DC converter or adapter is a device capable to convert electrical power between two different voltage levels. The total power is conserved, neglecting the losses due to electronics, so the output current of the device is a linear function of the input current multiplied by the ratio between input and output voltages.

Including the overall efficiency of the converter (usually dependent from the working point), we can write the following equation:

$$i_{out} = \eta_{DC-DC} \frac{V_{in}}{V_{out}} i_{in} , \quad (1.1)$$

where  $i_{in}$  and  $i_{out}$  are respectively the input current and the output current,  $V_{in}$  and  $V_{out}$  are the input voltage and the output voltage and  $\eta_{DC-DC}$  is the efficiency of the conversion.

The conversion is static, meaning that it involves electronic and electromagnetic components only and it is not done through any mechanical or thermodynamic cycle.

The fundamental principle of a DC-DC is the dynamic behavior of current in a complex impedance circuit, obtained using electronic switching devices, such as MOS transistors.

Other fundamental devices for a DC-DC converter are capacitors and inductors able to store electrical energy. In particular, they can eliminate the non-zero frequency components produced by the commutation process operated by the MOS transistors.

Three types of DC-DC converters can be distinguished: buck, boost and buck-boost. The first two respectively convert into a lower voltage and into a higher voltage, while the buck-boost is more flexible configuration and is able to provide a certain output voltage whenever the input is lower or higher.

Typical application usually features multiple symmetrical converters of the same topology, each one of them called a leg. Each leg MOSFET device is driven with a phase lag with respect of the others, in order to reduce the output ripple. Using this technique it is also possible to reduce the current switched into each leg.

The switching frequency is an important design parameter: higher frequency of the modulator allows a reduction of the size of the inductor, but the commutation losses are proportional to the switching frequency.

In order to control the switching frequency and duty cycle, a digital oscillator with programmable duty cycle is required. Typically, this function is done by a Digital Signal Processor (DSP) or by a dedicated CPU, which measures the output voltage and currents and modulates the  $V_{GS}$  (voltage applied between the Gate and the Source of the MOSFET) for each leg. The DCP features over-current and short circuit protections to prevent damages to the converter itself due to failures of the load or if the load has an impedance that is lower than the minimum value the DC-DC can drive.

The main losses in a DC-DC converter are due to residual magnetic field and hysteresis phenomena in the inductor cores during the switching cycles and to the commutation losses of the MOSFETs. MOSFET devices always have a characteristic parasitic ohmic resistance of the channel even if it is operating in saturation mode: this generates heat due to Joule effect mechanism. The parasitic capacitance due to the interface between the gate and the channel (the metal oxide layer) basically acts as an integrator filter that limit the maximum commutation speed, smoothing the gate voltage ideal square wave signal. This behavior limits the transition speed between cut-off and saturation of the channel leading to losses due to Joule effect. This kind of losses is proportional to the number of commutations per time unit, or to the fundamental frequency of the converter.

In order to reduce the losses related to the MOSFET, two approaches can be used: a) using devices with a low saturation resistance that is related to the physical size of the channel and to the material used for the bulk; or b) using devices with a low gate source parasitic capacitance that are more sensitive to the electrical noise or to electrostatic accumulation of charges in the gate region.

### ***1.2.5. Control electronics***

The system usually features control electronics made of different independent PLCs. All controllers share information and status data on a single serial bus. A possible configuration can be the following:

- I. Main controller
- II. Auxiliary board
- III. Cell voltage monitor

#### ***I. Main controller***

The main controller features the main finite state machine of the power system and gives the consent to open the main hydrogen valve if it is not detecting any fault conditions. The main state machine can have, for example, the following states:

0. Initialization: the software checks for different options installed and initializes all the CPUs, waiting for all the software to be ready at runtime.
1. Stand-by: the machine waits for a start signal or for a drop in the 48V bus, and monitor the possible events of failure.
3. Start: the fuel cells channels are fed with the reactants and the voltages are monitored to be in the appropriate range, without actually starting the commutations of the DC-DC. In this status, the fuel cell is not providing current.
4. Production: the fuel cells produce electrical power that is consumed by the load. The DC-DC regulates the output voltage of the system. The information about cell voltages is used to limit the maximum current according to the working conditions of the different cells.
5. Stop: the reactant adductions are closed, and the remaining gas amounts are removed by controlling the current transferred by the DC-DC to the 48 V bus or using some resistors shunts.
6. Fault: in case of failure in any of the previous states, the machine stops its normal operation and remains in the fault status. This is the safety condition and the user must manually accept the errors in order to reset the state machine to the stand-by condition.

The main controller also interfaces the input and output devices with the final user, through an HMI (Human Machine Interface) and, possibly, an Ethernet port for remote connection and data sharing. The main application software that controls the balance of plant is located in controller memory.

### **II. Auxiliaries board**

The auxiliaries board is a simple channel expansion that contains the input and output channels to drive the valves, pumps and fans and to read pressure, conductivity and temperature sensors. It is programmed with a watchdog feature that forces the inlet valves to be in a closed status when the communication with the main controller is lost: in this condition all the outputs are switched to a default safe status.

### **III. Cell Voltage Monitor**

A CVM (Cell Voltage Monitor) is a device that continuously scan the different cells with a couple of synchronous multiplexers and measures the cell voltage. The single sample and hold ADC (Analog to Digital Converter) is capable to sample each cell in 80 ms time, so the voltage of any cell is measured with a frequency of 0.625 Hz. The electronics can be tailored to the application, since the device must guarantee an isolation of 24 V and must be able to measure for each cell a voltage below 1.2 V with an accuracy of 1 mV. In order to isolate the ADC from the stack voltage, the front-end electronics (multiplexers and high impedance operational amplifier) can be powered directly from the stack (first and last cells are used), while the CPU and the ADC are powered by a regulated 48 V bus through a dedicated switching power supply.

The challenge in developing such a meter is that precise accuracy (mV range) is required on a relatively high voltage range. A typical stack for back-up power application can have more than 60-80 cells that can generate a stack voltage of 60-80 V in Open Circuit Voltage (OCV) condition.

The topology chosen in the device used by Electro Power Systems is a modular one. The device is made of different blocks, each capable of continuously monitoring 16 cells. The first module features four AD converters and the CANopen interface. Each block has front-end electronics isolated from the rest of the device, and powered directly by the corresponding 16 cells array. This part consists of 16 resistors limiting the current flow from the stack to the measurement device in case of misbehavior, and four analog eight-channels MUXs. The MUXs are operated synchronously, switching their output to a differential rail-to-rail amplifier, again powered by the stack voltage that generates an insulated differential signal proportional to the cell voltage (the gain is set at 5 to generate a signal for a 0-5V AD converter). While switching the MUXs, the voltage applied to the differential inputs of the amplifier corresponds to the difference between two adjacent cells ( $V_n - V_{n-1}$ ). Each module has a reference to the previous one to measure the first cell voltage and provides the reference voltage to the next module.

Since the power is supplied from the voltage of the monitored cells group, the output differential allows the use of commonly available MUXs and operational amplifiers, while guaranteeing the required isolation for the analog to digital converter.

The backend part of the main block is powered by a regulated 5 V supply, isolated by a DC-DC converter from the stack voltage. This part is made of four AD converters (10 bit resolution over a range 0-5

V), and a logic capable to handle the commands to the MUXs and the communication with the external CANopen serial bus.

The modularity allows the device to be used in different stacks, having cell number multiples of 16. Also, a modified device with only two MUXs was designed to allow monitoring 8 cells for increased flexibility. The 16 cells front-end electronics requires at least 8 volts to operate consistently, which means that cell voltages cannot be measured if the average stack voltage is below 500 mV per cell; however, this condition is considered as abnormal.

The logic transmits to the CANopen interface the stack minimum and maximum cell voltages and corresponding cell number, average cell voltage and standard deviation of the cells.

The resolution is set by the AD quantization (10 bit): 1024 levels are measured over the range of 0-1 V, so the minimum appreciable difference is 0.98 mV.

The acquisition speed is sufficient to monitor the stack under test. The MUX has an average switching time of 20 ms, and the AD converter has a typical sample-and-hold time of 60 ms; so a single measurement can last up to 80 ms. A complete scan of each block requires 1.3 s, and the four different blocks can be scanned together. The current consumption of the device is less than 50 mA, so the current leak is negligible.

### ***1.3. Market applications, status and forecast for near-term period***

Fuel cells are becoming well established in a number of markets where they are now recognized as a better technology option than conventional internal combustion engine generators or batteries. Shipments of fuel cell systems in 2012 continued to grow, almost doubling versus the previous year to reach a total of 45,700 units. In 2013, the shipments should have approached 67,000 units, 46% more than the previous year [14].

Despite a shortfall in the portable sector, continued growth in unit shipments of fuel cells for transportation and a significant increase in unit shipments of stationary fuel cells led to an increase overall. The stationary sector is by far the standout performer for fuel cell technology, finding application across all scales: from small-scale grid-connected micro combined heat and power units for residential use, to off-grid backup power systems providing uninterruptible power supplies to critical infrastructure, to prime power for buildings and even to megawatt-scale installations designed as grid-connected power stations.

In terms of megawatts shipped, the stationary sector continued to lead the fuel cell industry in 2012 thanks to the large size of individual units. The total megawatts shipped through 2013 should have reached 215 MW (see Figure 1.7).

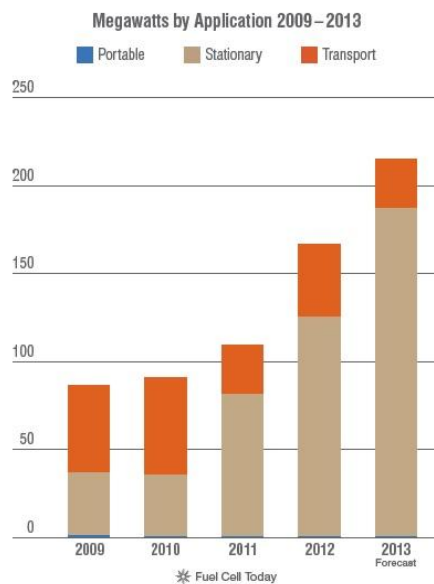


**Figure 1.7.** Cumulative fuel cell power installed up to 2013 [14].

Regionally, Asia has been the dominant adopter of fuel cell technology during the past six years, and this dominance has grown each year (61% of units shipped in 2012 went to the region). In terms of megawatts, the dominance is not so pronounced thanks to the sizeable market for large stationary fuel cells in North America. Nevertheless, Asia still accounted for 52% of megawatts shipped in 2012, and should have grown to 57% in 2013.

PEM fuel cell technology continues to prove the most popular type of fuel cell with regards to unit shipments. This can be attributed to its wide flexibility across all applications, unlike other fuel cell types, and its suitability for use at both small and large scales. In terms of megawatts, the picture is distributed more evenly between PEMFC, MCFC and SOFC. Interest in fuel cell technology has never been stronger: in the last year several high-level partnerships were forged, particularly in the automotive sector, and significant technology acquisitions took place.

The fuel cell industry continues to consolidate as it progresses from an investment-led technology industry to a market-led commercial industry. With an increasing number of truly global companies utilizing and investing in fuel cell technology and with the supply chain improvements and technology recognition that will come with the mass manufacture of passenger vehicles, the fuel cell industry is becoming increasingly well aligned for global success.

The PEM fuel cells show high efficiency, low operating temperature, fast startup time and favorable power-to-weight ratio and are able to satisfy a power output range in the order of 1 kW up to few MW. For the above mentioned features, the most suitable applications for PEM fuel cells are:

- Automotive
- Stationary co-generation
- Back-up

### ***1.3.1. Automotive***

In the last 10-15 years, almost all automotive companies have developed several fuel cells car prototypes. Recently the market is starting to move on pre-series. Hyundai, Toyota and Mercedes Benz have announced they will introduce production models between 2014 and 2015.

Toyota is confident that fuel cell vehicles will be price competitive against other zero-emission cars before 2030, and beyond 2020 fuel cell cars will be considered just one alternative of the eco cars. Toyota is hoping that dramatic reductions in the cost of fuel cells will help it sell between 5,000 and 10,000 units when the production version of its Fuel Cell Vehicle (FCV) Concept goes on sale in early 2015. When the company built demonstration vehicles in 2007, each fuel cell system cost nearly 750,000 euros. Now it expects the cost of the system will be less than 5 million yen (35,900 €) by 2015, or about half the car 72,000-euro price tag [15].

Hyundai has offered a first glimpse of its Intrado fuel cell concept vehicle, which will be unveiled at the Geneva auto show in March 2014, and says it will begin selling a hydrogen-powered Tucson compact SUV in 2014. Hyundai says this will be the first mass-market hydrogen vehicle available in the US [16].

On May 2013, the US Department of Energy confirmed the launch of H<sub>2</sub>USA, a Hydrogen Infrastructure Project [17]. Daimler is introducing a hydrogen filling station network to Germany. The so-called “H<sub>2</sub> Mobility” plan includes the realization of 100 hydrogen filling stations by 2017 and 400 by 2023 [18]. In Japan, to achieve the goal set by government to reduce 80% of CO<sub>2</sub> in the transportation sector by 2050, the scenario lays out a distribution of 2 million FCVs and construction of around 1,000 hydrogen stations in 2025, which then are needed to expand FCV/hydrogen stations driven by market forces [19].

In the transportation market, PEM fuel-cell-powered forklifts provide significant benefits over both petroleum and battery powered forklifts as they produce no local emissions, can work for a full 8-hour shift on a single tank of hydrogen, can be refueled in 3 minutes and have a lifetime of 8–10 years. Fuel-cell-powered forklifts are often used in refrigerated warehouses, as their performance is not degraded by lower temperatures. Many companies do not use petroleum powered forklifts, as these vehicles work indoors where emissions must be controlled, and instead are turning towards electric forklifts. According to Fuel Cells 2000, there were over 4,000 fuel cell forklifts in use in the U.S. in 2013 and the orders are growing exponentially for 2014. So the forklift market seems to be already started and the future developments are very promising [20].



**Figure 1.8.** Fuel cell powered forklift during the re-fuelling operation [14]. The average re-fuelling time is around 3 minutes against the 8-10 hours of re-charging time of a traditional battery powered forklift.

### ***1.3.2. Stationary***

Considering even all other fuel cell technologies (SOFCs and MCFCs included), unit shipments of stationary fuel cells showed a continued increase in 2012, with support from both large and small-scale applications, to finish the year 50% higher than in 2011 and 53% in terms of installed power capacity. The stationary sector is by far the biggest contributor to the annual megawatts shipped figure with 124.9 MW shipped in 2012, accounting for 75% of the total for that year. New regional markets are opening for residential micro-CHP, and support is continuing for installations of large megawatt-scale fuel cells. For example, in 2012 and 2013 a consistent growth in small stationary fuel cell systems occurred in Japan and is expected to further increase in 2014.

In 2012, Japan invested approximately \$240 million in fuel cell and hydrogen energy programs including \$112.77 million in subsidies for residential micro-CHP systems [21]. According to energy consultants Delta-ee, fuel cell micro-combined heat and power (micro-CHP) systems outsold conventional engine-based micro-CHP systems for the first time in 2012, accounting for 64% of global sales. This emergence as the dominant technology for micro-CHP is led entirely by uptake under the Japanese Ene-Farm scheme, which should have installed around 50,000 systems in 2013.

South Korea's national government offers 80% subsidies for micro-CHP fuel cell plants, plus up to an additional 10% subsidy from local governments [21].

The major markets for prime power application are the USA and Korea. Some pilot power plants using the by-product hydrogen generated in chlor alkali chemical plants are already working [22].

A 1.1-megawatt fuel cell system has been installed at Toyota Motor Sales U.S.A., California. The system enables Toyota to satisfy peak and mid-peak power needs using electricity either from the clean energy fuel cell system or from the power grid. Hydrogen fuel is delivered directly to the system by means of an existing pipeline, which also supplies a local fuel cell vehicle fueling station. Pipeline hydrogen used on the Toyota campus will be offset with the purchase of landfill generated renewable bio-gas [23].

In the future, other demonstrations of PEM fuel cell plants using the hydrogen produced by landfill or municipal waste will provide valuable electricity and heat, and utilize gas that is often otherwise flared.



**Figure 1.9.** 1.1 MW PEM fuel cells Ballard system installed at the Toyota Motor Sales in USA [23].

### ***1.3.3. Back-up Power***

Together with the forklift application, back-up power is the other existing market up in 2013. If the power system is combined with an electrolyzer, the advantages with respect to traditional technology (lead acid batteries and diesel gensets) are lower maintenance costs and no fuel logistics and transportation costs. In 2012, the U.S. companies added 31.7 MW of fuel cell power mostly in data center applications while the number of installed telecom back-up power systems exceeded 800 units [24]. Also, Italy started to invest in fuel cell back-up power with more than 300 back-up power units installed and a cumulative power capacity exceeding 1.8 MW. Hurricane Sandy passed over the East Coast of the USA in October 2012 with devastating effect, but during this time fuel cell powered cell phone towers remained in operation for extended periods for customers in New York, New Jersey and Connecticut. The 60 fuel cell systems installed in the disaster area functioned normally during and immediately after the storm [14]. The more frequently fuel cells are seen to provide reliable power during similar events, the more interest there will be from around the world in utilizing the technology.

Asia, and in particular China, represents a huge potential market for fuel cell technology as mobile phone adoption increases at an exponential rate. Here a number of companies are involved in trials with major telecommunications providers.

One of the aspects of fuel cell technology that appealed to telecoms customers was the replacement of widely used fuels such as diesel, which historically have been prone to theft. One telecom provider in the Philippines had installed methanol-fuelled systems, but was finding that, in some instances, even the

methanol was being stolen. In response, a few companies are providing a self-regenerating backup power system that incorporates a fuel cell and an electrolyzer, meaning the unit can operate in backup mode autonomously without the need for re-fuelling. During operation when grid power has failed the unit provides power using its on-board store of hydrogen. When grid power resumes, the unit replenishes its fuel supply using water electrolysis.

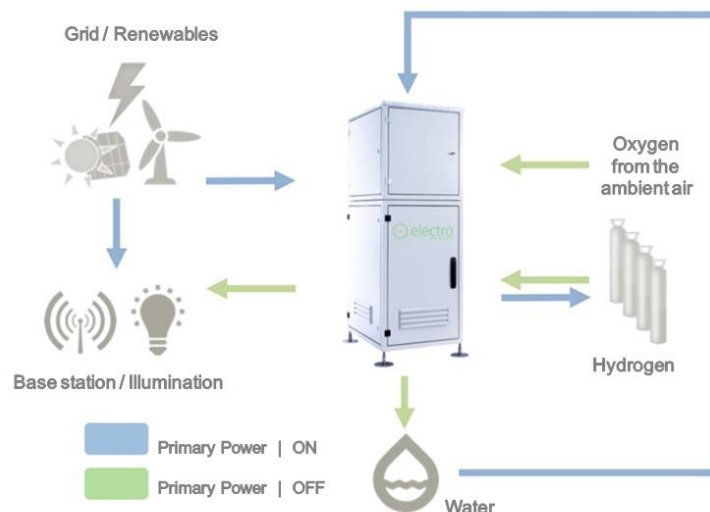


**Figure 1.10.** ElectroSelf™ provided by Electro Power Systems. It consists of a PEM fuel cell power system able to supply 1.5 – 10 kW and integrated with an alkaline electrolyzer for the hydrogen re-filling.

## Chapter 2

# State of the art on the PEM fuel cells degradation issues

During operation, a PEM fuel cells stack is subjected to many causes of mechanical and chemical degradation leading to a loss of performance.

A fuel cell's lifetime is deeply dependent upon the operating conditions. Since every application is characterized by different operating conditions, the same fuel cell can show a different lifetime for different applications.

In back-up applications, the fuel cell usually operates for short periods and is characterized by very long periods of inactivity. In this case, a long operating time is not required but a very short startup is necessary. So the fuel cells stack always works in non stable, non steady-state conditions and needs to startup quickly with dry electrolyte membrane. This is a stressing condition that leads to a high degradation rate for each startup/shutdown cycle.

The stationary application instead requires very long operating lifetime in order to make the system work for at least 15-20 years. In this case, the stack operating conditions are less stressing because the startups can occur more slowly, starting with already humidified electrolyte membrane. Then most all of the operational time is in steady-state conditions. However, the challenge is the very long lifetime requirement that implies a perfect system management control and resistant fuel cell materials in order to achieve a very low degradation rate.

Finally, the automotive application is the most stressing above all. As with back-up, the stack has to startup quickly, but a further issue in this case is the extremely variable load causing continuous voltage and current cycles. This condition damages considerably the fuel cell materials (the catalyst in particular) and gives very high degradation rates.

In the last decade the US Department of Energy (DoE), the European Hydrogen and Fuel Cell Technology Platform (HFP) and the Japanese New Energy and Industrial Technology (NEDO) have established severe durability targets that are required in order to satisfy the market needs for each PEM fuel cell application. Apart from some minimal differences, every institution agrees in the following durability requirements: 5,000 h for automotive, 10,000 h for back-up and 40,000 h for stationary [25].

However, it should be noted that every application could show different requirements depending on the country. For example, for back-up application, the 10,000 hours of operation are excessive in Europe, America, Australia and Japan where the number of blackout hours in a year are in the order of 10-50. While they are necessary in Asian and African countries where the blackout time can reach even 6-8 hours a day. Concerning the degradation rate, a value of 2–10  $\mu\text{Vh}^{-1}$  is commonly accepted for most applications [26], [27].

### ***2.1. PEM fuel cells system durability evaluation***

Normally, the fuel cell system manufacturers design their own systems with a certain power output margin in order to compensate for stack performance loss in time. The only way to have this margin is to over-size the stack, for example increasing the number of the cells. However, this is translating to an increase in the stack cost, so the power output over-sizing cannot exceed a certain percentage of the nominal power. The stack should be designed in order to be able to provide the required power for auxiliaries and load without consistently affecting the system cost, even when the Beginning of Life (BOL) performance is reduced up to 90%.

For a better understanding, a practical example of stack power sizing for a power system is explained. Taking into account a power system with an output nominal power of 3 kW and with a power consumption of 1 kW for auxiliaries, then the minimum stack power able to make the system supply the nominal output is 4 kW. This must be the power that the stack is able to supply immediately before the End of Life (EOL): if a further performance degradation occurs, the system will not be able to supply the nominal output of 3 kW.

So, if at the EOL the stack power output is 4 kW, at the Beginning of Life (BOL) the stack must supply 4.44 kW (EOL power / 0.9). In this way, even if the stack loses 10% of performance, the system will continue to supply the nominal power output.

In the above mentioned case, the power output margin is 0.44 kW, so the system at the Beginning of Life is able to supply 3.44 kW even if the required nominal output is 3 kW.

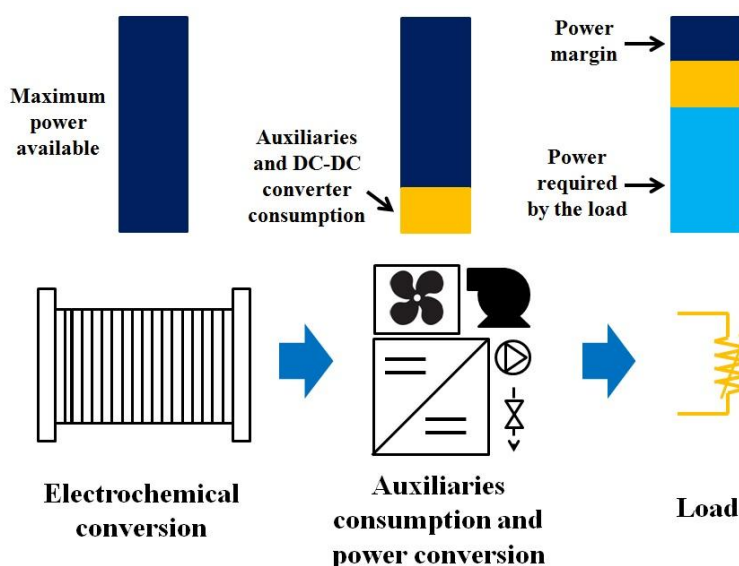


**Figure 2.1.** The maximum power that the stack can supply is not totally exploited: the power margin obtained subtracting the auxiliaries consumption is used to compensate the performance degradation in time.

Similar calculations can be done using the stack voltage instead of the power. In this case, another parameter must be introduced: the maximum stack current. This depends on two factors:

- a) **maximum tolerable input current for the DC/DC or DC/AC converter.** According to the required voltage and current output, the converter is able to transform a certain range of current and voltage values. For a certain active area, the current point where the stack shows the power peak depends on the fuel cell design and the operating conditions. However, once the operating conditions and the design are fixed, two cases can occur:
  - i. the maximum tolerable converter input current is higher than the current related to the power peak. In this case, the maximum power that the system can supply is limited by the stack.
  - ii. the maximum tolerable converter input current is lower than the current related to the power peak. In this case, the stack current cannot overcome the converter maximum tolerable input value, and the maximum power that the power system can supply is limited by the converter.
- b) **minimum tolerable cells voltage threshold.** The fuel cell voltage value decreases with the current rise due to some irreversibilities. At high current density, the mass transport losses are the prevalent type of irreversibility and the cell is at risk to suffer from fuel or oxidant starvation. A minimal fluctuation in the temperature or RH values can produce more water than the cell is able to expel. So, the bipolar plate channels or the GDL can remain blocked from the reactant feed and the fuel cell voltage can become negative. In order to avoid this situation it is preferable that the fuel cell

## Chapter 2 – State of the art on the PEM fuel cells degradation issues

works in a non mass-transport regime. According to the cell design or the operation conditions, the mass transport regime can start at different current and voltage values. Some companies decide to fix a cell voltage limit that ensures that above this limit the cell works in non mass-transport regime.

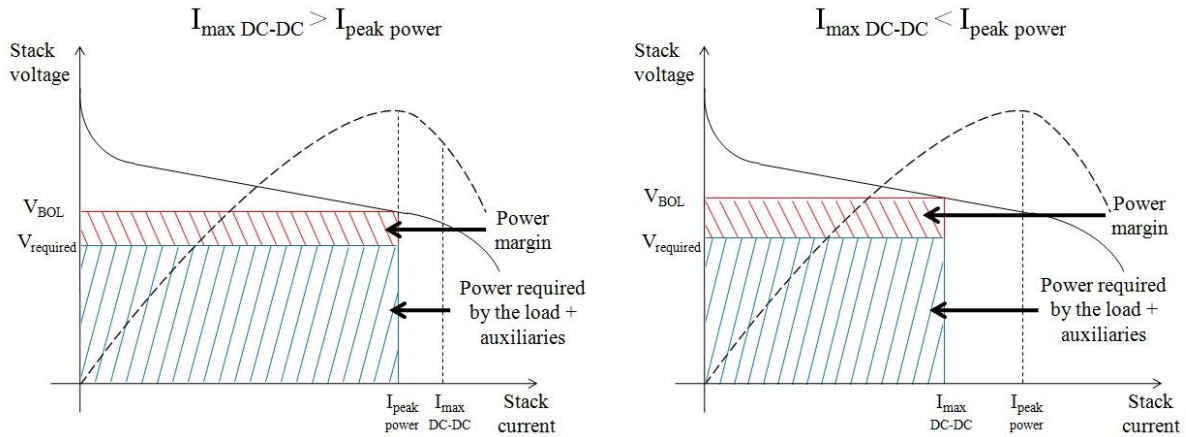


**Figure 2.2.** On the left: stack-limited maximum system power; on the right: converter-limited maximum system power.

Once the maximum stack current is fixed, the single cell voltage at this current, with certain operating conditions and for a particular stack, is practically fixed. In fact, it depends on the fuel cell design and the component materials; and under the same operating conditions, the cell voltage is approximately the same for the same design. So this can be considered as the BOL performance, while the EOL voltage is defined as 90% of the BOL value.

If for example the maximum stack current is 200 A and the single cell voltage at this current is 0.555 V, then the EOL voltage will be  $0.9 \cdot 0.555 \text{ V} \sim 0.5 \text{ V}$ . So the voltage margin for each cell is 0.055 V or 55 mV. Referring to the above mentioned case, the number of cell needed to reach 4 kW is:

$$\text{EOL stack power} / (\text{EOL cell voltage} \cdot \text{maximum stack current}) = 4000 \text{ W} / (0.5 \text{ V} \cdot 200 \text{ A}) = 40 \text{ cells}$$

At the BOL the same stack will supply  $0.555 \text{ V} \cdot 40 \text{ cells} \cdot 200 \text{ A} = 4440 \text{ W}$  (or 4.44 kW). The power margin of 0.44 kW at the BOL is approximately equivalent to the power supplied by 4 cells. So in this case an additional cost due to these 4 cells (10% of the total number) has to be considered. A further increase of the cells is possible but not advisable because the fuel cells are the most expensive components of the system and a 10% of performance margin is enough to guarantee the durability system requirements in most of the cases.

Apart from not predictable incidental failure events (such as a pressure reducer break leading to the membrane failure), the fuel cell lifetime can be defined as the operating time elapsing from the BOL performance and the EOL performance giving the minimum power able to supply the system nominal power output.

The degradation rate can be found by dividing the average cell voltage margin by the operation hours:  
number of operation hours = average cell voltage margin / degradation rate.

Taking into account the above shown case, where the single cell voltage margin was 55 mV, the degradation rate requirements for each application are:

- Automotive →  $55 \text{ mV} / 5,000 \text{ h} = 11 \text{ } \mu\text{Vh}^{-1}$
- Back-up →  $55 \text{ mV} / 10,000 \text{ h} = 5.5 \text{ } \mu\text{Vh}^{-1}$
- Stationary →  $55 \text{ mV} / 40,000 \text{ h} \sim 1.4 \text{ } \mu\text{Vh}^{-1}$

So, it is clear that the stationary application has the most challenging degradation rate requirements. In order to avoid an excessive fuel cells stack over-sizing, the R&D efforts must be focused on investigating the degradation mechanisms so that the information obtained could help improve the fuel cell stack and the system lifetime.

## ***2.2. PEM fuel cells degradation mechanisms and solutions***

In general, two different ways of durability improvements can be adopted: a) choose more resistant materials and b) use degradation mitigation system strategies.

In the first case, the proper material adoption for membrane, GDLs, catalyst layers and bipolar plates can enhance the chemical and mechanical degradation resistance of these components.

In the second case, instead, appropriate system design and control software are adopted with the precise aim of limiting the mechanical stress and chemical events.

In the following, a thorough investigation on the degradation mechanisms and on material and system strategies solutions is presented. Four sections are included, each one discussing one of the key fuel cell stack components (membrane, catalyst layers, GDL and bipolar plates) and describing the mechanisms and investigated solutions.

### ***2.2.1. Membrane***

The perfluorosulfonic acid (PFSA) membranes are currently the state of art for PEM fuel cells stacks. They are typically no more than 25-30  $\mu\text{m}$  thick and are characterized by relatively high proton conductivity at low temperature (usually in the order of 0.1 S/cm for well-hydrated membrane).

Two failure modes exist for the membrane:

- a) A pinhole develops and propagates within the polymer leading to reactant gas crossover. The fuel cell cannot operate even if a small amount of gas is able to permeate the membrane. The gas crossover is linked to a reduction of the Open Circuit Voltage (OCV) value, which means a decrease in fuel cell performance; furthermore, the crossover enhances the risk of direct combustion.
- b) The fuel cells can also fail if an electronic current passes through the membrane causing the system to short. If the short is “soft” and the current passing through the cell is relatively low, only a fuel cell performance reduction occurs. In this case, the cell voltage is reduced due to the higher current density provided by the cell and made by two contributions: the current required by the load and the parasitic current passing through the membrane. If the short is “hard”, usually the greater portion of the current passes through a very narrow area causing an overheating condition that will destroy the membrane. The membrane damage leads to gas crossover and the direct combustion will cause a definitive fuel cell failure.

Three primary root causes of membrane failure can be distinguished:

1. Chemical degradation: direct attack of the polymer membrane by radical species generated as by-products or side reactions of the fuel cell electro-chemical reactions causing polymer decomposition. In the end, the failure mode is pinhole formation. As previously described this leads to gas crossover and enhances the risk of direct combustion.
2. Mechanical degradation: membrane fracture caused by cyclic or fatigue stresses imposed on the membrane via humidity and thermal fluctuations in a constrained cell. Even in this case the membrane mechanical degradation leads to pinholes formation.
3. Shorting: electronic current passing through the membrane caused by cell over-compression and/or topographical irregularities of the neighboring components (electrodes, GDL) leading to local over-compression and creep.

In order to satisfy the challenging performance and cost requirements needed for a large scale commercialization, in the last decade researches have focused on developing membrane materials with reduced proton transport resistance in both wet and dry conditions. The proton transport resistance reduction is the only way to enhance the performance of the membrane. The two primary means to achieve it is to (a) increase the polymer proton conductivity and (b) reduce the membrane thickness.

However, there exists a great challenge to simultaneously address the performance and durability demands of PEM fuel cells systems. This is because many of the approaches to reduce membrane proton transport resistance tend to increase the risk of membrane failure. For example, membranes with lower Equivalent Weight (EW) or higher concentration of acid sites typically exhibit higher proton conductivity. However, lower EW membranes also exhibit greater swelling upon exposure to water. Higher swelling leads to greater stresses imposed on the membrane during the fuel cell operation and, consequently, reduces the membrane lifetime. Another way to reduce proton transport resistance is to use thinner membranes. In this

case, the negative effects are an increase of the gas crossover and a lower electron transport resistance. So, typically, thinner membrane are more susceptible to shorting and show enhanced voltage decay rates and earlier membrane failure.

Similarly, many of the approaches to improve the membrane durability can cause a decrease in performance.

One of the common approaches to improve the membrane mechanical durability is to incorporate a reinforcing or support layer into it, such as expanded polytetrafluoroethylene ePTFE. While the mechanical reinforced membrane have led to longer life in accelerated humidity cycling stress tests, the addition of a non-conductive support increases the proton transport resistance of the composite membranes. Similar concerns about performance loss exist for other approaches that use composite membranes to increase the mechanical stability.

The most effective approaches able to prevent chemical degradation of the polymer membrane from radical species utilize stabilization additives. These additives may be metal ions, such as  $Ce^{3+}$  or  $Mn^{2+}$ , and typically incorporated into the membrane as either salts or oxides. However, such ions can bind to the cation exchange sites in the membrane or the ionomer in the electrodes, thus lowering the proton conductivity of these respective layers.

Two relatively simple approaches can be applied to reduce the risk of membrane shorting caused by local over-compression. Fuel cell stacks are normally compressed at least to 1.5 MPa in order to minimize the electronic contact resistances in the cells, particularly between the bipolar plates and the GDL. While lower stack compression can significantly reduce the risk of shorting, the increased associated contact resistances lead to unacceptable performance losses. Another approach is to utilize a thick Micro-Porous Layer (MPL) between the GDL and the electrodes. This layer can cushion any topographical irregularities of the GDL that lead to local high compression. However, addition of a thick MPL adds to both the electronic and gas transport resistances in the cell, thus creating undesirable performance losses. Shorting can also be mitigated by careful fuel cell system control to prevent voltage spikes or cell reversal.

### **2.2.2. *Catalyst layer***

The conventional Catalyst Layer (CL) is typically composed of Pt nano-particles supported on a high surface area carbon black in close contact with a controlled amount of ionomer. The carbon black support allows the Pt nano-particles to have a high dispersion (2-3 nm) and provides a porous, electronically conductive structure. This structure plays a critical role in providing transport for reactants and electrons to the Pt nano-particles as well as removal of water and inert gas. The ionomer, which coats the entire support surface, maintains discrete hydrophobic and hydrophilic domains for reactant and protonic access to the Pt active sites.

## Chapter 2 – State of the art on the PEM fuel cells degradation issues

---

In addition to the Hydrogen Oxidation Reaction (HOR) and Oxygen Reduction Reaction (ORR), undesired parasitic and corroding electrochemical reactions also take place, degrade the MEA components and limit fuel cell lifetime. These parasitic reactions include:

- a) Pt dissolution, diffusion through the ionomer and consequent re-deposition on another Pt particle forming a large particle or diffusion into the membrane to form a band.
- b) Carbon support corrosion to carbon dioxide and resulting disintegration of the CL leading to Pt agglomeration. A secondary effect of the carbon corrosion is then the formation of OH groups leading to hydrophilic or wettable carbon surface that flood easily and impede the transport of oxygen to the Pt.
- c) Generation of reactive species such as hydrogen peroxide ( $H_2O_2$ ), hydroperoxyl radical ( $\bullet OOH$ ) and hydroxyl radical ( $\bullet OH$ ) that cause chemical degradation of the membrane/ionomer.
- d) Reversible and irreversible adsorption of contaminants from air, fuel, MEA and bipolar plate degradation products on Pt nano-particle sites.

Overall, these reactions result in a loss of electrochemically active catalyst sites that become manifest as a loss in mass activity of the catalyst, a rise in membrane/ionomer resistance and in mass-transport resistance in the catalyst layer, all of which result in fuel cell performance degradation over time.

Under normal operation, the PEM fuel cell stack experiences a variety of loads that may be constant or cyclic and fast transient response (a transient from 10% to 90% in few seconds is not uncommon). Then it is also subject to a range of ambient environmental conditions of pressure, temperature, humidity and air/fuel quality. The principal modes of operation of PEM fuel cells that cause electrode degradation are:

- a) OCV/idling/low load. This condition favor the formation of peroxides and radicals that attack the ionomer, lowering the proton transport.
- b) Load cycling. A load cycling is translated into a catalyst potential cycling, which is particularly dangerous for the platinum dissolution reactions. The Pt dissolves into the ionomer and re-deposit into another Pt nano-particles or into the inner part of the membrane.
- c) Startup/shutdown cycles. During the startup or the shutdown at the anode, a hydrogen-air boundary is formed dividing the cell in two different areas. In the hydrogen-rich zone, the usual operating reactions (HOR at the anode and ORR at the cathode) take place. Instead in the anode oxygen-rich zone, the ORR occurs at the anode while the Carbon Oxidation Reaction (COR) takes place at the cathode. So the catalyst support is damaged by the Carbon Corrosion Reaction (CCR), and the Pt can be agglomerated into large particles or dissolved into the membrane.
- d) Fuel starvation. In some particular circumstances, the fuel feed can be blocked due to ice formation, water flooding or excessive inert gas presence. When a cell of a stack is fuel starved the HOR is substituted by the Oxygen Evolution Reaction (OER) and the COR, and the cell voltage becomes negative. If the water content is sufficient, the OER is prevalent; while on the contrary, the COR becomes dominant at low water contents and the cell shows consistently negative potentials.

- e) Fuel/air contaminants. The high surface area carbon blacks and the PFSA ionomer can act as a filter and easily absorb impurities from the fuel and atmospheric air. Pt is susceptible to the absorption of various contaminants that may reversibly or irreversibly occupy the sites necessary for the ORR or the HOR. The reformat hydrogen typically contains small quantities of CO, NH<sub>3</sub> and H<sub>2</sub>S while pollutants such as SO<sub>2</sub>, NO<sub>2</sub> and NO are common in some city and industrial environments.

Advanced materials (possessing a higher activity and dissolution resistance) that are likely to be introduced in the near future include supported binary and ternary Pt alloy nano-particles, extended thin film electrocatalyst structures, supported ‘core-shell’ catalyst that employ monolayer Pt or Pt alloy shells over a base metal core. These materials should help decrease the dissolution rate of the Pt into the ionomer. However, some of the advanced materials that are employed in extremely thin catalyst layer show mass-transport issues. On the other hand, other system mitigation strategies can be employed, such as controlled smooth cell voltage profiles.

Meanwhile promising research concerning catalyst dispersed on highly corrosion-resistant conductive supports are under study. These new materials include graphitized carbon blacks, single walled and multi-walled carbon nanotubes and other non-carbon supports such as doped TiO<sub>2</sub>, TiC and TiN. The challenge here is in overcoming high preparation cost, as for graphitized carbon blacks and carbon nanotubes, or low electron conduction, as for TiO<sub>2</sub>, TiC and TiN.

Presently, the most effective methods able to mitigate the catalyst carbon support corrosion are again several system strategies able to prevent fuel gas blockage, high electrode potentials, and H<sub>2</sub>/air boundaries at the anode side during a startup or a shutdown.

Based on the literature [25], the loss in performance due to fuel and air contaminants is quite severe in case of sulfur compounds, less in the case of the nitrogen compounds. However some tests demonstrated that a potential hold of 0.9 V or higher can oxidize the Pt-S to sulfate, thus freeing up active sites of Pt for the ORR. Again, the loss in performance due to the anode Pt site contamination caused by CO can be completely recovered if the fuel cell runs for a certain period of time fed by ultra-pure hydrogen. Even the chloride ions coming from de-icers, sea mists, or certain catalyst preparation precursors lower the ORR activity but these can be flushed out by fuel cell operation at high current densities with the generation of water.

### 2.2.3. *GDL*

The Gas Diffusion Layer (GDL), also called Gas Diffusion Medium (GDM) plays an essential role allowing the reactants to diffuse uniformly on the active sites and electronically connecting the bipolar plates with the catalyst layer. The GDL also facilitates the by-product water removal and prevent water flooding, which would block electrocatalyst active sites.

There are two types of GDLs, namely: carbon papers and carbon cloth. The carbon papers are made by non-woven carbon fibers, and are usually cheaper and most commercially diffuse. The carbon cloth are made of woven carbon fibers and are characterized by higher water removal properties at high current density and high reactant RH values. In both cases, the carbon fibers are coated by a hydrophobic agent, normally PTFE, which gives to the GDL the water removal property.

Usually a Micro-Porous Layer (MPL) made of carbon and a hydrophobic agent is applied onto the GDL surface between the catalyst layer and the GDL to enhance water removal from the catalyst layer, minimizing the electrical contact resistance with adjacent catalyst layer, and preventing the catalyst ink from migrating into the GDL.

GDL degradation can be detected by changes in its characteristics and properties. Namely, two main changes can be observed:

- a) wetting behavior changes due to loss of the hydrophobic agent and carbon surface property changes
- b) changes in the structure of the GDL due to carbon corrosion and mechanical stresses

Very limited literature is available on GDL degradation, as the focus in PEM fuel cell studies has been concentrated mostly on catalyst and membrane development. Due to the difficulties in separating the GDL degradation from MEA sub-components in in-situ experiments, GDL degradation studies are often performed by ex-situ testing.

GDL degradation can be categorized into electrochemical, mechanical and thermal degradation.

The chemical degradation of GDL is due mostly by the carbon oxidation reaction, also known as carbon corrosion. The main effect of carbon oxidation is essentially an enhanced flooding tendency, but there are two factors intervening in two different phases that causes it.

At the beginning, the carbon oxidation changes the surface properties of the carbon fibers in the GDL or of the carbon blacks in the MPL. These surfaces starts to show hydrophilic hydroxyl and carboxyl groups that increase the wettability of the carbon fiber or the carbon blacks [28], [29], [30], [31].

Then when the carbon corrosion starts to damage the carbon fiber or the carbon black, the PTFE detachment further increases the wetting behavior leading to severe water flooding. So, the fuel cell shows high mass transport loss especially at high current density.

Normally the carbon fibers of the GDL and the carbon blacks of the MPL are graphitized. In fact, graphitized carbon has a higher oxidation resistance and can be used in PEM fuel cells to mitigate oxidation losses.

High relative humidity and high temperature generally enhance the carbon corrosion. However, the carbon oxidation reaction is negligible during normal fuel cell operation because of its low kinetics. The only two conditions generating the predominance of carbon corrosion are fuel starvation [32], [33] and fuel cell startup and shutdown [34], [35]. Several mitigation strategies have been proposed in order to mitigate carbon corrosion for the catalyst layer [28], [36-41] and, in principle, can be adopted to mitigate the carbon oxidation in the GDL and MPL.

GDL mechanical degradation occurs due to high clamping pressures applied during PEM fuel cell assembly, erosion by the reactant flows, and water freezing at low temperatures.

High compression results in GDL deformation and changes in thickness due to the breakage and displacement of the fibers under high pressures. The variations in GDL thickness are irreversible and result in a change in electrical and thermal resistance, together with a decrease in porosity. So, the fuel cell starts to show high ohmic loss and higher operation temperatures leading to the membrane drying. At the same time, the lower porosity enhances the mass transport loss, and the fuel cell performance at high current density decreases significantly.

The GDL mechanical degradation can occur due to uneven pressure applied by the bolts on the edge of the cell leading to local over-compression. Also, the temperature and RH cycling can lead to a periodic non-uniform distribution of stress across the MEA due to the membrane swelling.

It has been observed that the reactant flows may erode the GDL surface, resulting in a loss in GDL hydrophobicity due to the loss of the PTFE from both the fibers and the MPL. This mechanism is enhanced and accelerated at increased flow rates and temperatures.

A few studies have addressed the effect of freezing conditions on GDL performance, and the formation of ice between GDL/CL/membrane interfaces. Under freezing conditions, the most significant loss is the contact resistance due to the presence of trapped pools water leading to the gap formation between the GDL and the membrane. However the freezing effect can be easily avoided by either purging the PEM fuel cell (removing any accumulated water), or using low RHs before freezing conditions are experienced.

No significant studies have been reported in the literature that address the effect of temperature on GDLs. In any case, high temperature significantly affects the GDL's maximum strain, resulting from wakening PTFE within the GDL and enhancing carbon corrosion.

### **2.2.4. Bipolar plate**

PEM fuel cell commercialization and market penetration necessitate the mass production of bipolar plates. Therefore, they are required to be made of materials with excellent manufacturability and suitable for cost-effective, high volume, automated production systems.

Pure graphite has been considered as the PEM fuel cell industry reference standard for bipolar plates because of its excellent corrosion resistance and low Interfacial Contact Resistance (ICR). However, due to its brittleness and lack of mechanical strength, pure graphite is not suitable for automotive application. Then, in stationary and back-up applications, the issue is its relatively poor manufacturability and cost effectiveness for large production volume. For this reason, before a large commercialization can occur, finding another material with good mechanical properties and large-scale manufacturability at low cost is fundamental. The two candidate materials are the carbon-based composite and coated metal.

## Chapter 2 – State of the art on the PEM fuel cells degradation issues

---

The carbon-based composite plates enjoy good chemical stability and high corrosion resistance. They also have low contact resistance due to the absence of a passive surface film and can be molded with considerable advantage in terms of production rate and cost. Most of the composite materials are prepared using proprietary methods, so the exact material composition and production steps are not in the public domain. In any case it is possible to state that the typical composite molded plate is manufactured starting from a carbon (or graphite) powders mixed with some polymer precursors that polymerize inside the mold at high compression pressure and temperature of 200 °C or higher. The result is a material composed of conductive carbon (or graphite) powders held together by the polymer resin that provides the mechanical resistance.

Metal is the material favored in the automobile industry because it provides higher mechanical strength, better durability to shocks and vibration, no permeability to H<sub>2</sub> gas and more flexibility in fabrication. The main challenge of a metallic bipolar plate, however, is that corrosion-resistant metal, such as stainless steel, develop a passive oxide layer on the surface. Although this passive layer protects the bulk metal from the progression of corrosion, it also causes an undesirable effect of high interfacial contact resistance. This causes the dissipation of a considerable amount of electric energy into heat and a reduction in the overall efficiency of a fuel cell stack. So, metallic bipolar plates should be coated with protective layers in order to avoid corrosion or the formation of thick passive films that may result in elevated ICR. Coatings should be conductive and adhere to the base metal without exposing the substrate to corrosive media.

The durability of bipolar plates is defined by the length of their lifetime in combating corrosion, while maintaining low ICR and not experiencing any drastic loss of power. Metallic plates have proven to surpass the mechanical strength of graphite bipolar plates but they are more prone to corrosion in the fuel cell environment. Considerable research has been conducted to combat the metallic bipolar plate durability issue, in order to enhance the material corrosion resistance and interfacial contact resistance.

Cost and durability are still the two pronounced challenges for the PEM fuel cell industry. The cost of large supplies of fuel cell materials and high volume manufacturing processes must be reduced for PEM to reach economic viability, to allow it to penetrate the energy market and compete with other systems. The durability of the PEM fuel cell is another important parameter that must be improved to enhance the reliability of the two main components, namely bipolar plates and MEAs. Further research and development must be conducted to rectify the four main bipolar plates corrosion mechanisms: corrosion failure by pinhole formation, electrocatalyst poisoning, membrane ion exchange with metal ion and passivation formation.

## Chapter 3

# Mitigation strategies for commercial PEM fuel cells stacks

For a commercial PEM fuel cell stack for back-up application, the most critical issues for durability to solve are:

- 1) Carbon corrosion of the catalyst support. The oxidation of the catalyst carbon support leads to the catalyst detachment from the active site producing a loss of catalyst activity. A further consequence of the carbon oxidation is a formation of hydrophilic OH groups [7] enhancing the flooding tendency of the fuel cell.
- 2) Membrane degradation. The peroxides, OOH• and OH• radicals (collateral reaction products) tend to destroy the polymeric chains and the membrane loses material. This causes membrane thickness reduction and the enlarging of small pinholes through the membrane that increase the risk of direct combustion (sudden cell death).
- 3) Pt catalyst dissolution. The Pt catalyst can detach from the site and dissolve into the ionomer even if no physical damage of the carbon support occurs. This happens mostly as a consequence of a quick cell voltage variation.

### 3.1. *Mitigation strategies against the membrane degradation*

In a PEM fuel cell, water accounts for up to a quarter of the weight of the membrane itself. The consequences of this are two-edged. Since water increases the conductivity of the polymers, it is seen as a welcome guest in the membrane. At the same time, moisture acts as a plasticizer, which sets membrane degradation in motion. Researchers have shown that at the “beginning of the end” of a PEM fuel cell, membranes frequently have specific faults that are caused by operational changes in their water content. Researchers think of the degradation process in the following way: in the typical start and stop operations of a fuel cell, like those in a car driving through city traffic, a greater or lesser amount of power is produced over time. Thus the amount of the by-product of electricity generation (water) is variable. Variations in moisture (water content) lead to alternate shrinking and swelling, and therefore to deformation of the membrane. This phenomenon is also called “creep”. In fact, after many operating cycles, the membrane can adopt, in places, a shape resembling a crawling “caterpillar”. At some points, this caterpillar becomes exposed to higher mechanical stress and is thus more susceptible to fracture. At the weak points, small pinholes can now form. These holes are too small at first to inflict much damage as they typically occupy only a few parts per million of the membrane surface area, and their impact on fuel cell functioning at this stage is still too small to measure.

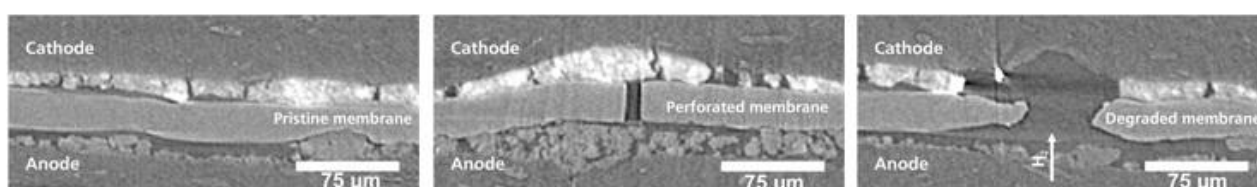


**Figure 3.1.** Pinhole formation and evolution in a polymer electrolyte membrane [42].

However, these small pinholes can start further problems, because gas molecules (hydrogen and oxygen) can pass through these open channels in the initially gas-tight membrane. Hence, hydrogen molecules can now reach the cathode, where they can react with oxygen and form free radicals. These free radicals are highly reactive, and chemically damage the membrane in the vicinity of the pinhole. As a result, the chains of carbon atoms from which polymer membranes are made get broken. And since shorter chains are less strong, the membrane fails far more easily under mechanical stress, and the holes grow larger. Then a vicious cycle sets in: more gas flows through these larger holes, and more free radicals are formed. Ultimately, the holes in the membrane are so large, that enough gas can pass through the membrane to ignite a combustion reaction between the oxygen and hydrogen. In a very short time, the heat released by the combustion can cause the membrane to melt and eventually the cell to fail. Experts refer to this as “sudden

death”. Until now, it has not been entirely clear whether combustion can occur inside a fuel cell after a gas leak caused by the combination of mechanical and chemical degradation.

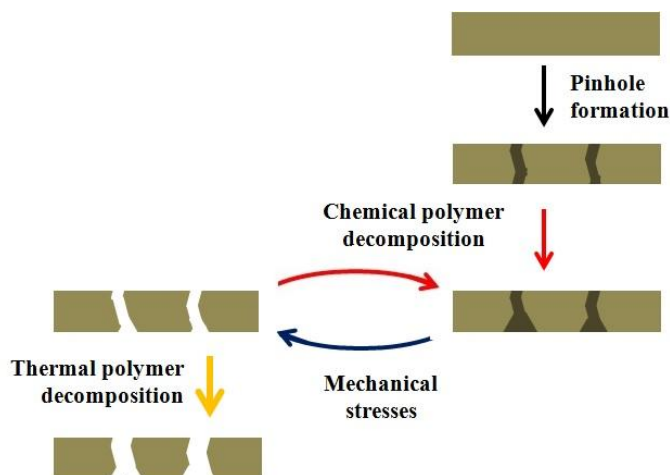


**Figure 3.2.** Scheme of the membrane degradation process [42].

In order to limit this degradation mechanism, Electro Power Systems has adopted membrane being mechanically reinforced and chemically stabilized. The materials and preparation techniques used to produce those membranes are proprietary to the MEA producer and not disclosable. Figure 3.3. shows the fuel crossover leak through the membrane as a function of operating time of at OCV condition.

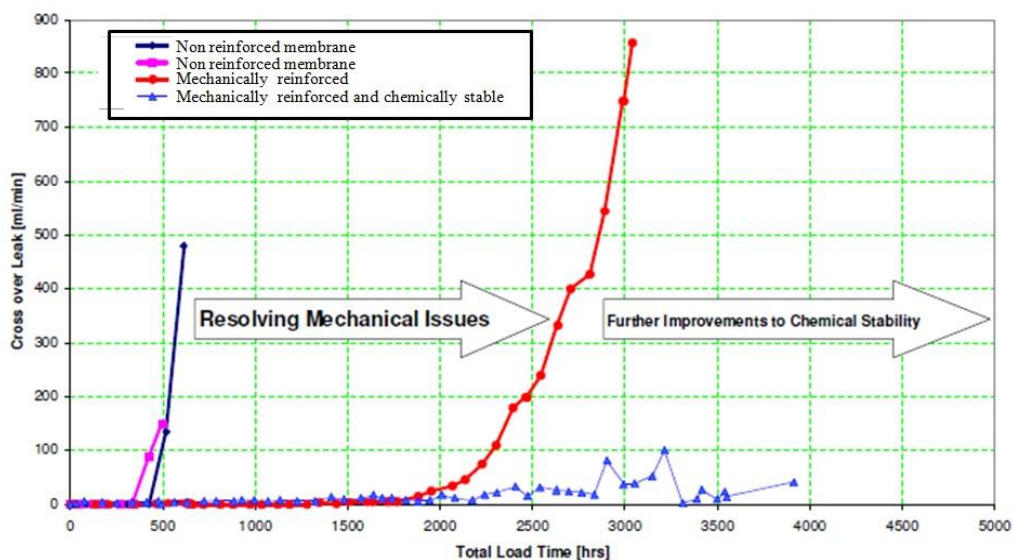


**Figure 3.3.** Comparison between non-reinforced membrane, mechanical reinforced membrane and mechanical reinforced – chemically stabilized membrane in an OCV condition stress test. The gas crossover leaks appear at longer operating times after improving the mechanical and chemical degradation issues.

Since the most critical operation for the membrane is the OCV condition (in which more gas crossover occurs leading to peroxides and radicals formation) and this can take place only during the start and stop

phases of the fuel cell, a test consisting of repetitive starts and stops has been performed in order to understand the membrane's behavior inside a commercial stack in start and stop operations.

Figure 3.4 shows the SEM image of an MEA cross-section at the EOL and after 350 startup-shutdown cycles. The membrane thickness remained stable and no physical or chemical changes occurred [43].

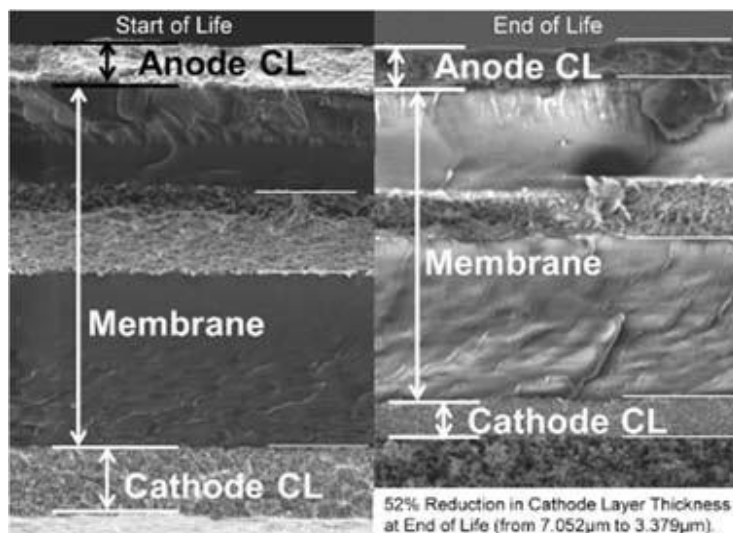


**Figure 3.4.** SEM images of a MEA at the BOL (left) and after 350 start and stop cycles (right); while the cathode catalyst layer was considerably thinned, the membrane thickness remained unchanged [43].

### 3.2. *Mitigation strategies against the Pt dissolution*

The Pt dissolution in an acid media is strongly increased if the electrode potential overcomes 1.2 V according to the oxidation reaction:



However, for dispersed nano-particulate Pt on carbon supports in PEM fuel cells, the Nernst potential for Pt dissolution is expected to decline to 1.160 V for 5 nm Pt particles, and to **1.088 V** for 1 nm Pt particles [25].

It is well known that the Pt dissolves more easily into the electrolyte during voltage cycling conditions [25],[28],[44]; and a few tentative explanations of the root cause can be found in bibliography. In the following paragraphs, the interpretation of the platinum dissolution mechanism during voltage cycling is elaborated by S. S. Kocha.

During the first complete voltage cycle (potential increase followed by potential decrease), irregular island/mesa-like structures are formed and the displaced low-coordinated Pt atoms do not revert to their

original positions during the reduction sweep when the potential is decreasing. During the following voltage cycle, the atoms at the edges of these islands are obviously more active and susceptible to attack and dissolution. When the potential sweep is extremely fast, the coverage of oxide species on the Pt surface is slightly lower (due to less time for oxide formation); this results in more bare Pt atoms being exposed and subjected to the high potential at the peak of the cycle, accelerating dissolution. In addition, the oxidation stage in a fast potential sweep very likely results in a structure that has a greater number of smaller islands (less time for diffusion to islands) and is also more irreversible. In slower potential sweeps, there is more time for Pt ions to diffuse to and stick to islands that already exist, therefore lowering the dissolution rate. In the case of cycling within the oxide regime only, larger islands form on the surface and the inner atoms of the island are protected/passivated from further attack and dissolution [25].

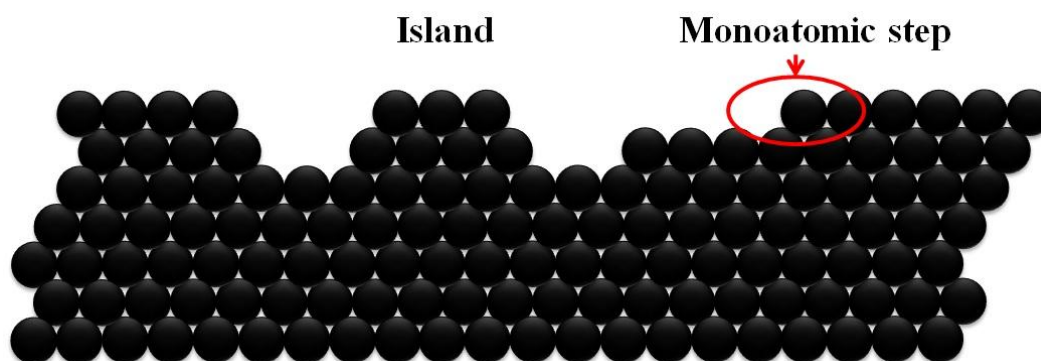


**Figure 3.5.** Schematic of the Pt atoms re-deposition after a dissolution process. Monoatomic steps exit on clean uncycled, unoxidized surfaces, while irreversible islands are formed after cycling to high potentials; surfaces with islands possess a larger number of less-coordinated atoms.

When platinum dissolution occurs, there are two possible consequent phenomena: a) the platinum dissolved in the electrode's ionomer phase can redeposit on the surface of other Pt particles leading to particle growth [45], [26]; and b) the Pt diffuses into the membrane and precipitates inside it through the reduction reaction with a hydrogen molecule [46]:



The first phenomenon is more frequent at the anode side because there is enough hydrogen to induce the Pt reduction and re-deposition on the Pt particles. On the cathode side, the high electrode potential facilitates the Pt dissolution. Then the dissolved Pt ions can easily diffuse into the membrane towards the anode side since they do not immediately meet a reducing environment. However, the  $\text{Pt}^{+2}$  is reduced and deposited in the Pt form as soon as a hydrogen molecule reacts with it.

If the Pt is deposited close to the membrane cathode side, it can easily re-dissolve to the ion form and re-diffuse because of the high potential. The only steady-state condition for the Pt non-ionic form is at a position inside the membrane where the molar flux of  $\text{O}_2$  equals one half of the molar flux of  $\text{H}_2$ , allowing for complete consumption of both gases [47]. In this condition, an isolated Pt band is formed corresponding

to the interface where the molar flux of  $O_2$  equals one-half of the molar flux of  $H_2$ . The Pt line brings to zero the concentration of hydrogen and oxygen, so towards the cathode the hydrogen partial pressure is zero (see Figure 3.6) and the Pt cannot precipitate until it reaches the Pt band.

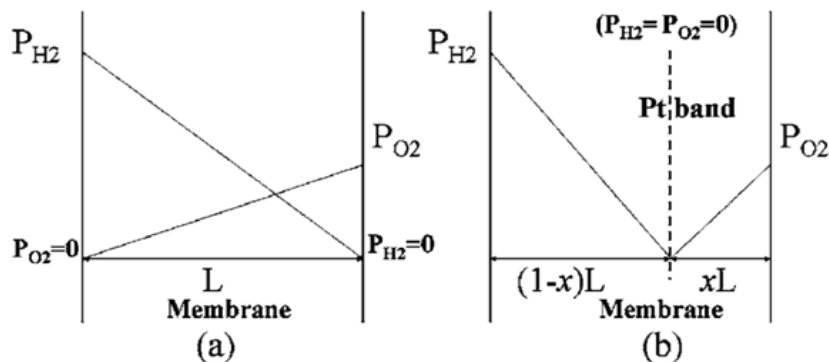


**Figure 3.6.** Simplified linear gas pressure profiles of hydrogen and oxygen in membrane (a) before Pt deposition and (b) after the Pt band formation [15].

The relative local flux of hydrogen and oxygen within the membrane determines the location of Pt deposition. Figure 3.7 [47] and Figure 3.8 [46] show how the Pt line inside the membrane can change position according to the  $H_2$  and  $O_2$  partial pressures. If the cell operates with pure  $H_2/O_2$  gases with similar pressure, the Pt line will form in the middle (Figure 3.7, left). In the case of  $H_2$ /air operation, the Pt band shifts towards the cathode (Figure 3.8-c). For two other extreme cases: 20% $H_2$  in  $N_2/O_2$  (Figure 3.7, right) and  $H_2/N_2$  (Figure 3.8-b), the Pt band was found respectively close to the anode and at the membrane-cathode interface.

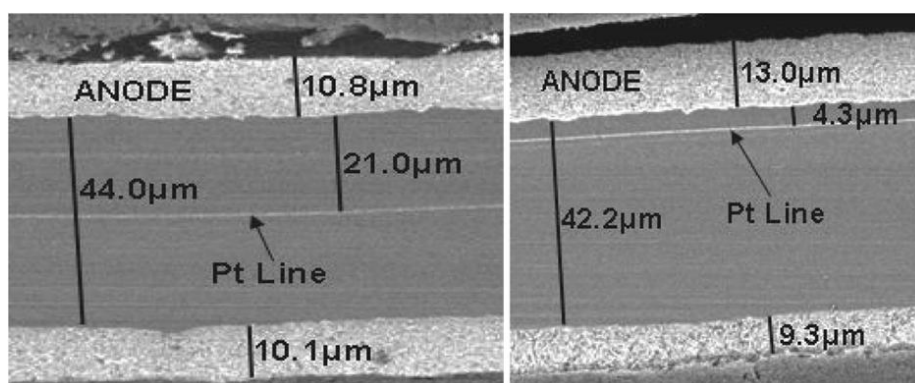


**Figure 3.7.** Cross-sectional SEM photomicrographs of the MEA after operating for 700 h at OCV with pure  $H_2/O_2$  (on the left); and after operating for 1,750 h at OCV with 20%  $H_2(N_2)/O_2$  (on the right) [47].

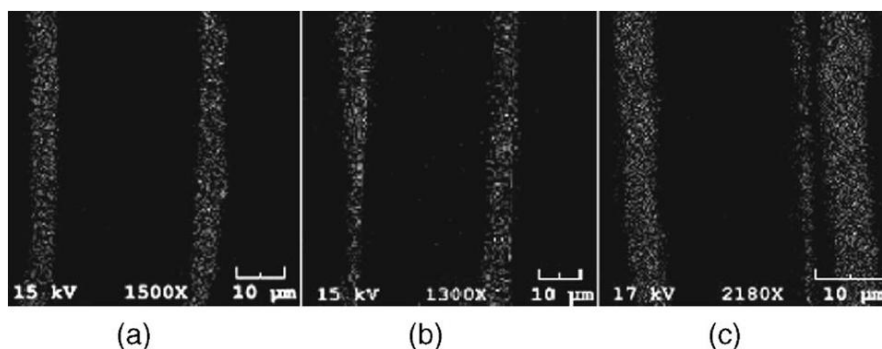


**Figure 3.8.** Pt distribution maps in the MEAs (left: Anode; right: Cathode). (a) Fresh, (b)  $H_2/N_2$  potential cycled, and (c)  $H_2/air$  potential cycled [46].

The most evident consequence of the platinum dissolution in the electrode's ionomer phase is the active area loss due both to the Pt particle growth and to the Pt leaving the catalyst layer. This leads to an irreversible activation loss enhancement, which reduces the overall cell performance.

In the case of catalyst dissolution issue, a few material-based mitigation solutions can be found in bibliography. However, it has been proved that the Pt dissolution phenomenon is enhanced during voltage cycling, in particular in case of sudden voltage change and quick voltage profile increments or decreases. For these reasons, Electro Power Systems decided to adopt a system-based strategy able to allow smooth and gradual voltage changes especially during the start and stop of the fuel cell stack when respectively a quick voltage decrease and a quick voltage increase can occur.

The mitigation strategy consists of including in the Balance of Plant an auxiliary storage (battery or super-capacitor) with a stack current control using a DC-DC converter and a control logic (see the scheme represented in figure 3.9). The system control logic must analyze the voltage of every single cell of the stack and gradually increase or decrease the output DC-DC current so that the “cell voltage change profile” remains below a certain limit (e.g. 30 mV/s).

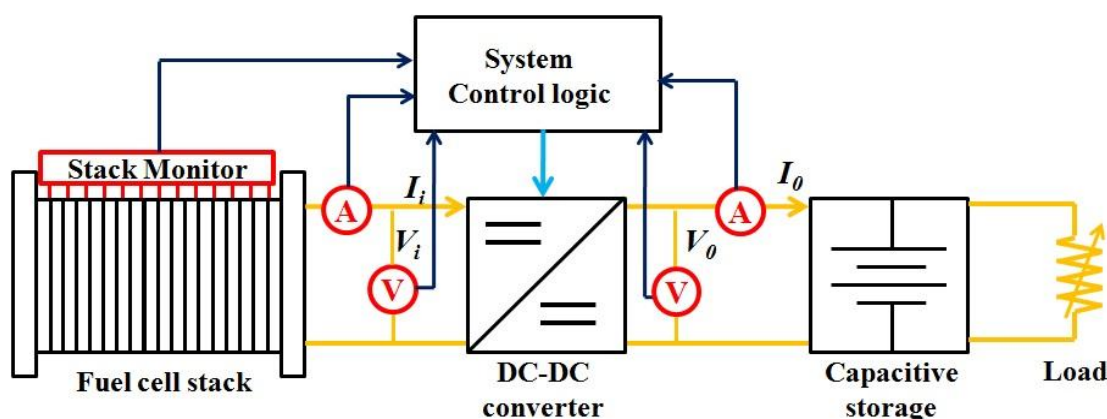


**Figure 3.9.** System improvement developed by Electro power Systems for mitigating the Pt dissolution: every cell voltage is scanned and controlled by the stack monitor while the control logic allows only smooth current variations, according to the cell voltage status, in order to have slow cell voltage changes.

### 3.3. Catalyst carbon support corrosion

In the state of the art of PEMFC, the electrodes are composed of an ionic conductor, typically a perfluorosulfonic acid ionomer, and Pt nano-particles dispersed onto the surface of carbon supports, the Carbon Blacks, which provide electronic transport and enable increased Pt catalyst activity with very low noble metal loadings [48]. The deposition of Pt on the carbon support increases the specific activity of the platinum catalyst by enhancing the surface-to-volume ratio of the platinum. Furthermore, this microstructure provides the catalyst layer with the high porosity needed to avoid mass-transport losses.

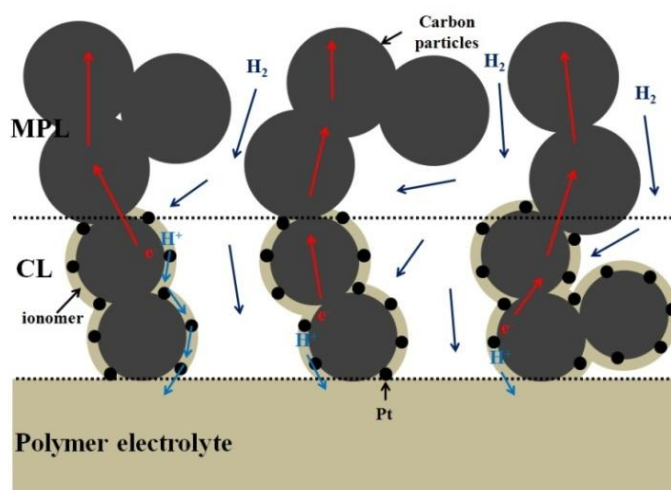


**Figure 3.10.** Carbon Black-based catalyst layer structure.

The electrochemical oxidation of Carbon Blacks is considered a major contribution to performance degradation. As shown in the following reactions, the oxidation of carbon is thermodynamically favored at the PEMFC cathode working potential range (0.6–0.9 V), compared to the Standard Hydrogen Electrode (SHE):



Nevertheless, the carbon oxidation reactions are also kinetically slow at typical PEMFC operating temperatures, and require significant overvoltage to produce a significant corrosion rate. Thus, the rate of carbon oxidation is negligible during normal operation [49]. However, Raiser et al. [34] calculated that the cathode interfacial potential difference should increase up to 1.44 V when the anode is partially exposed to hydrogen and partially exposed to air, as happens after a fuel cell shutdown or during its restart. Further

electrode potential measurements performed when the anode compartment contains an air/hydrogen mix revealed that local cathode potentials increased up to 1.4 V [35], [50]. This high potential can significantly increase the carbon corrosion rate [49], [51]; in-situ CO<sub>2</sub> and CO measurements performed by Kim et al. [35] together with cathode catalyst layer thinning and a loss of kinetic catalyst activity [35], [52] seem to confirm it.

Most of a fuel cell performance deterioration caused by Carbon Black corrosion is usually attributed to the loss of catalyst activity. The electrochemical carbon corrosion breaks down the support structure for Pt, allowing Pt particles to agglomerate or migrate into the ionomer and consequently re-deposit in the membrane or on another Pt particle. The overall result is a decrease of the Pt surface area, which implies a loss of catalyst activity [53], [54].

As suggested by Hao Tang et al. [55], the presence of Pt could accelerate the corrosion rate and the corrosion may be more severe at places where Pt particles reside. So, the resulting support impairment can facilitate the platinum detachment. Then the platinum particles can both sinter together leading to particle growth [53] or dissolve into the ionomer area of the catalytic layer [45], [53].

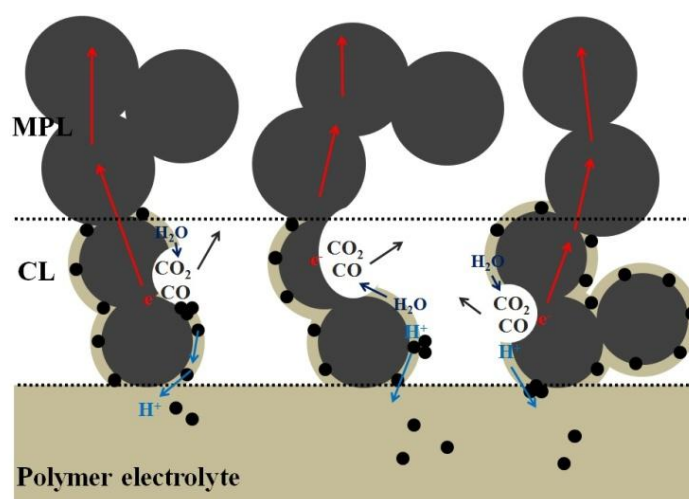


**Figure 3.11.** Catalyst support corrosion effects [56].

A further consequence of the carbon corrosion is the change in the surface chemistry of the carbon [29] resulting in an increase in the hydrophilicity of the Catalyst Layer (CL), the Micro Porous Layer (MPL) and the Gas Diffusion Layer (GDL), which negatively affects the transport behavior of gas and water [30]. This modification of the carbon surface properties is due to the formation of hydroxyl and carboxyl groups (hydrophilic in nature) in the aromatic hexagonal ring composing the graphene planes of the carbon support [31]. A clear correlation of the increased mass transport loss to the carbon oxidation activity also was reported by Hartnig and Schmidt [52], who observed an increase of the mass transport losses when testing all types of carbon supports.

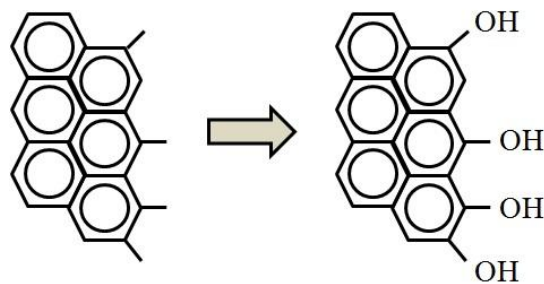


**Figure 3.12.** Hydrophilic OH groups forming on the surface of Carbon Blacks during the carbon oxidation process.

During the carbon oxidation process of the Carbon Black surface, hydrophilic surface groups are initially formed resulting in an increased flooding tendency of the electrode. Then, if the carbon oxidation of the catalyst supports is prolonged, the connectivity between carbon blacks can be compromised and the catalyst electron conduction capability deteriorates. So, the carbon corrosion initially increases the wettability of the carbon surfaces but, at longer times, a section of carbon can be completely removed.

Even if carbon corrosion should occur more easily near the Pt sites, the Micro Porous Layer structure is similar to the catalyst layer (carbon black); and, in principle, it can be subjected to carbon corrosion as well. The major consequence is an increased flooding tendency due to both the hydrophilic OH surface groups forming onto the carbon supports surface and the PTFE content loss. Typically, a membrane electrode assembly (MEA) affected by carbon corrosion can easily show high mass transport loss due to the reduced hydrophobic properties that once prevented water flooding.

### **3.3.1. Carbon corrosion during startups and shutdowns**

During a typical shutdown, air can enter into the anode compartment from the cathode by diffusion through the membrane or from the outside [34], [55]. Typical air sources in the anode compartment can be small defects in component sealing or the anode purge exhaust port. In any case, a hydrogen/air boundary is forming during and after the fuel cell shutdown. Reiser et al. [34] identified and modeled this phenomenon for the first time, explaining the mechanism involved during the fuel/air boundary formation. The boundary creates four different regions, two in the anode electrode and two in the cathode electrode, with each region characterized by different reactions and different electrode potentials [34], [55]. In Figure 3.13, a schematic model shows the four different regions involved. Opposite to the air-rich region B at the anode, a high electrode potential is forming in region C at the cathode, allowing both the carbon corrosion reaction and water electrolysis to take place. The same situation occurs during the startup of the cell when the hydrogen feeds the anode compartment full of air.

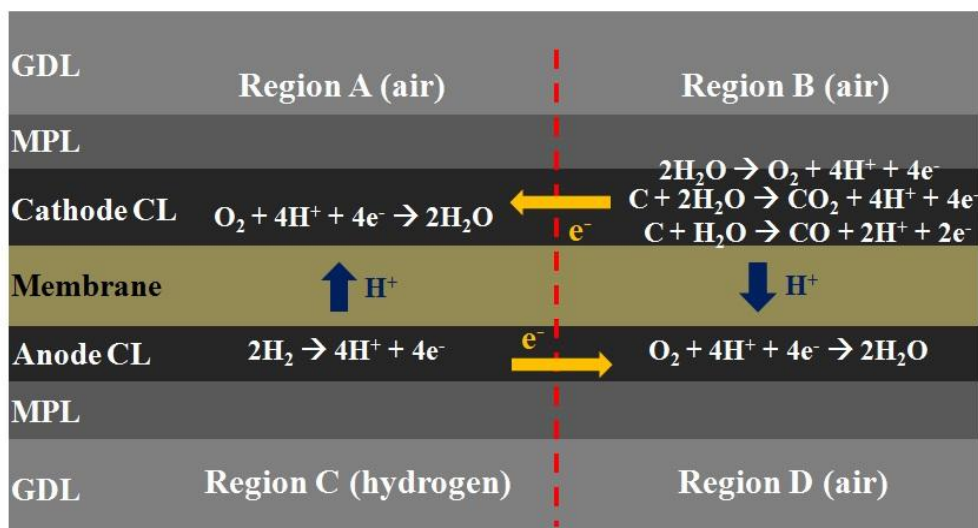


**Figure 3.13.** Catalyst carbon support oxidation mechanism when oxygen and hydrogen are present in the anode while no load is applied to the cell.

A further proof that the cathode carbon corrosion takes place due to the high electrode potential appearance was given by Kim et al. [35] who measured simultaneously the CO and CO<sub>2</sub> concentration an experiment reproducing the cell conditions during startup or shutdown. The results show that the CO concentration increased only when the cathode potential rose above 1.1 V; while the CO<sub>2</sub> was detected during the entire temporal window in which the H<sub>2</sub>/air boundary was present, even if the production fell exponentially when the potential decreased (see Figure 3.14).

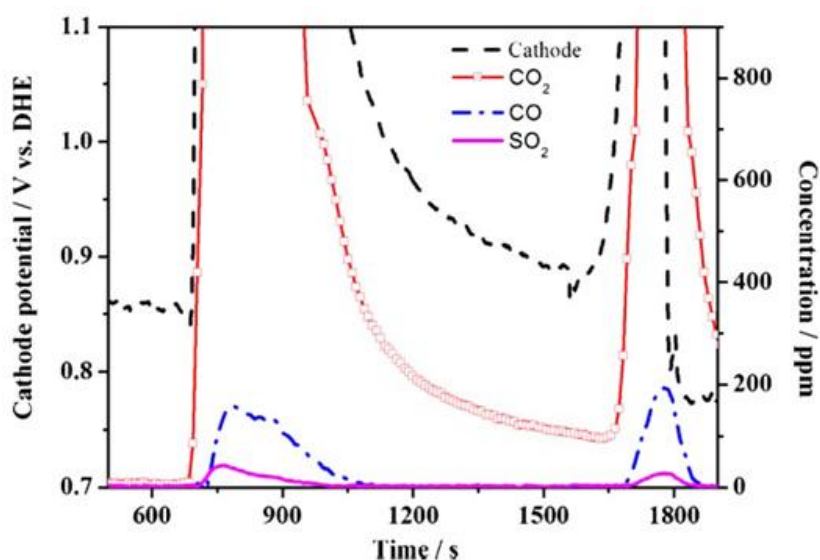


**Figure 3.14.** Quantitative analysis of the cathode outlet gases with change in cathode potential during starts and stops [35].

### 3.3.2. Carbon corrosion during fuel starvation

The fuel starvation occurs when the hydrogen does not reach the anode catalyst layer during normal operation mode (with current  $> 0$ ). This condition can occur mainly by the blockage of GDL or a flow field channel due to water flooding, excessive compression of the gas diffusion layer, presence of inert gas ( $N_2$ ) not purged during the startup or ice formation before the startup.

When the hydrogen can no longer sustain the current, another oxidation reaction must supply the hydrogen ions and electrons needed for the oxygen reduction reaction at the cathode. The possible candidates are water oxidation:



Together with carbon oxidation giving  $CO_2$  as byproduct (eq. 3.3), and carbon oxidation giving  $CO$  as byproduct (eq. 3.4).

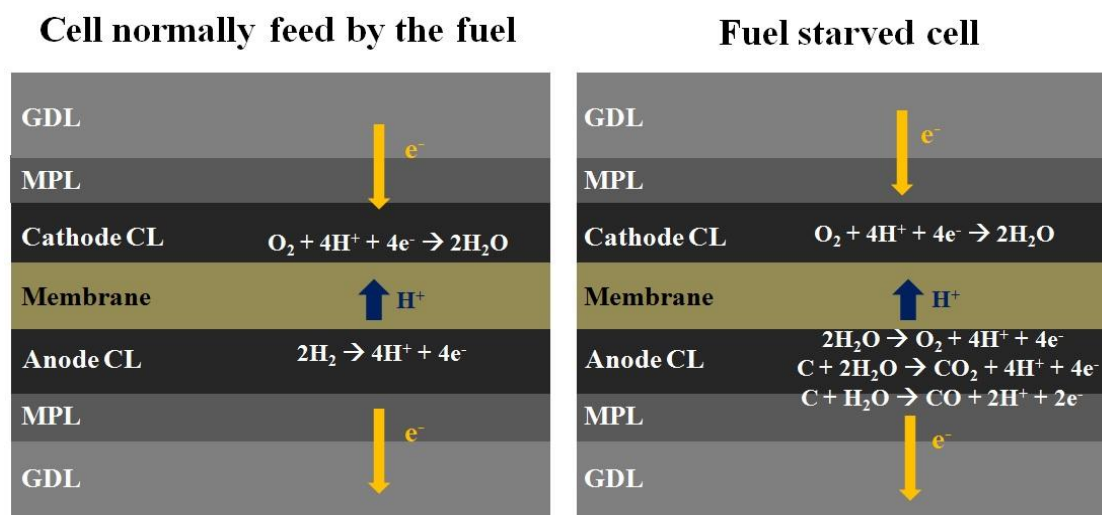


**Figure 3.15.** On the left: fuel cell reaction in normal condition; on the right: reactions occurring in case of fuel starvation

In a study carried out by T. R. Ralph et al. [57], fuel starvation was simulated by replacing  $H_2$  with  $N_2$ . One of their results is presented in Figure 3.16. Some MEAs tested were subjected to a fixed current density of  $0.04 \text{ A cm}^{-2}$  with  $N_2$  gas flowing at the anode. The cell potential was recorded during the entire test duration.

They reported that when the cell operates with  $H_2$  at the anode side and air at the cathode side, the cell voltage was positive. When the  $N_2$  gas was introduced into the anode maintaining the current constant, the hydrogen was no longer present and another oxidation reaction would have supplied electrons to the outlet circuit and  $H^+$  to the membrane to maintain the current density.

The two candidate reactions are water oxidation and carbon oxidation. As confirmed by the experiment, as long as the water content is enough to sustain the current, water oxidation will occur. Carbon oxidation has lower kinetics with respect to water oxidation, so the amount of O<sub>2</sub> produced is greater than CO<sub>2</sub> at the anode. However, once water content is depleted, the only reaction that can sustain the current flow is carbon oxidation, and the CO<sub>2</sub> becomes the most common byproduct at the anode. While the CO production was not detected, it is probable that when the cell potential became even more negative, the CO content at the anode outlet increases.

Since both water and carbon oxidation reactions require water as a reactant, further investigations are necessary in order to find the root cause linking the high carbon corrosion rate at low water content. In any cases, additional confirmation that carbon corrosion prevails only at low water content comes from a side experiment [57] in which some PTFE was added to the anode catalyst layer in order to retain more water, improving the electrode tolerance to carbon oxidation.

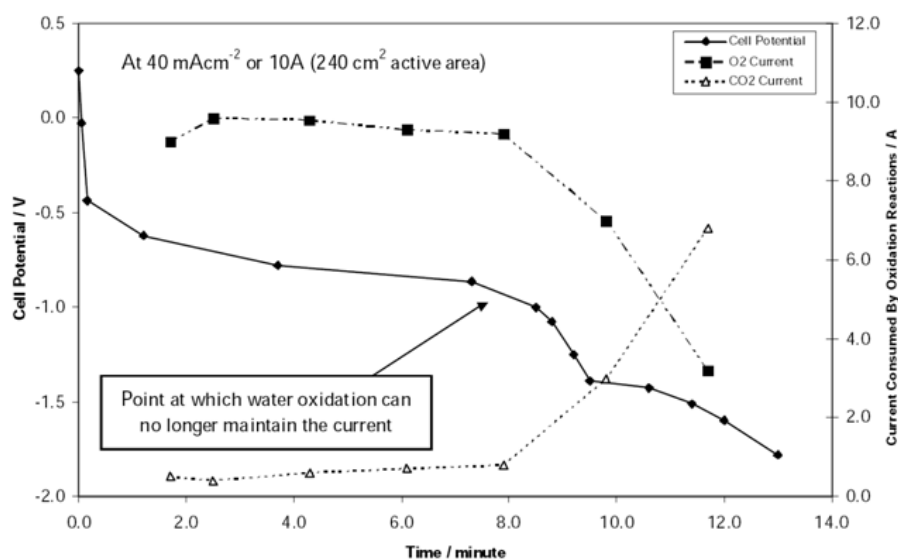


**Figure 3.16.** O<sub>2</sub> and CO<sub>2</sub> production at the anode and cell potential over time during the fuel starvation [57].

Even if the carbon corrosion reactions and the water oxidation reaction can occur at the same time, typically only one of them prevails depending on the voltage and availability of the reactants:

- If the water content is enough high, only  $2\text{H}_2\text{O} \rightarrow \text{O}_2 + 4\text{e}^- + 4\text{H}^+$  prevails: the O<sub>2</sub> is the most common byproduct.
- If the water content is low and the anode electrode potential is relatively low, only  $\text{C} + 2\text{H}_2\text{O} \rightarrow \text{CO}_2 + 4\text{H}^+ + 4\text{e}^-$  prevails: the CO<sub>2</sub> is the most common byproduct.
- If the water content is low and the anode electrode potential is relatively high, only  $\text{C} + \text{H}_2\text{O} \rightarrow \text{CO} + 2\text{H}^+ + 2\text{e}^-$  prevails: the CO is the most common byproduct.

Figure 3.17 depicts the above reactions that occur during conditions of fuel cell starvation.

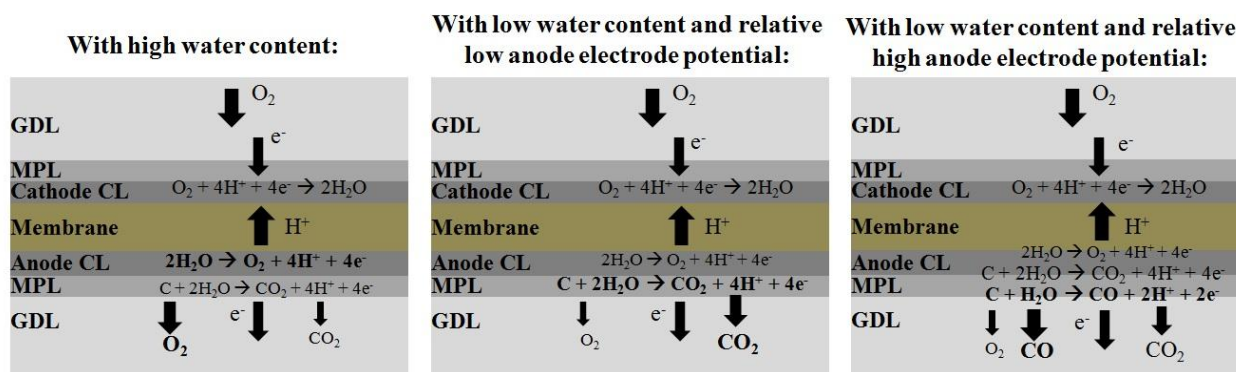


**Figure 3.17.** All possible reactions configurations during the fuel starvation conditions in PEM fuel cells.

If a cell is in a condition of fuel starvation, it can no longer produce power and shows negative voltage values. So, it starts to absorb power from the other cells (if it is in a stack) and/or from an external power source (if possible). Thus, when a PEM fuel cell has the active area in a fuel-starved condition, carbon corrosion can occur at the anode side if the other cells of the stack or an external power source are able to supply enough energy to reach a certain required cell potential.

### 3.3.3. Carbon corrosion detection methods

The detection of carbon corrosion events has a twofold purpose: a) investigate and study the phenomenon; and b) reveal *in situ* the carbon oxidation reaction activity during the fuel cell operation in order to have the opportunity to mitigate the issue.

Four detection methods can indicate carbon corrosion *in situ*:

- I. CO<sub>2</sub> detection
- II. Activation loss measurement
- III. Cell voltage monitoring
- IV. Voltammetry analysis

The *in-situ* carbon corrosion detection can be very useful if associated with an automatic control system able to detect the problem in time and make a control intervention, for example shutting down the system to avoid an ultimate failure.

However, in order to study the carbon corrosion phenomenon and its effects, some *ex-situ* methods can be very useful. For this purpose, the voltammetry analysis is again effective if used to analyze the MEAs at the end of life. Then, a SEM analysis of the MEA cross section can reveal the carbon corrosion effects, as well as measure changes in the catalyst layer thickness.

**I. CO<sub>2</sub> Detection.**

Using a CO<sub>2</sub> sensor to detect the carbon dioxide presence in the reactant gas outlets is an effective method for detecting the occurrence of a carbon corrosion reaction. For this purpose, S. Maass et al. [58] used a Non-Dispersive Infrared (NDIR) spectrometer, while T. R. Ralph et al. [57] preferred a CO<sub>2</sub> gas chromatography analysis.

Concerning the NDIR sensors, the CO<sub>2</sub> is revealed using an IR light source without a dispersive element and an IR light detector able to reveal the IR spectrum absorption peaks. See Figure 3.18.

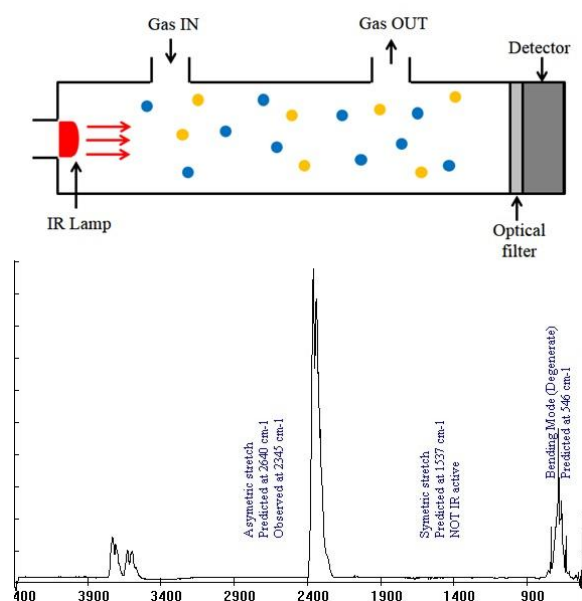


**Figure 3.18.** NDIR sensor schematic diagram and CO<sub>2</sub> absorption spectrum.

The CO<sub>2</sub> has a strong absorbance peak at a wave number of 2350 cm<sup>-1</sup>. The gas concentration is obtained by analyzing the intensity of the peak.

The gas chromatography technique consists of a chemical sensor in which the gaseous compounds being analyzed interact with the wall of a column coated with different stationary phases. The stationary phases are microscopic layers made by a liquid or a polymer on an inert solid support. They represent the sensitive part able to interact with specific chemical species.

A simple adaptation in a commercial PEM fuel cell system would be monitoring the carbon dioxide concentration in the reactant gases, and in particular, measuring the CO<sub>2</sub> concentration difference between the incoming and outgoing gas flows. The sensor used can be a Non-Dispersive Infrared (NDIR) CO<sub>2</sub> Sensor or a chemical CO<sub>2</sub> sensor. At the cathode, the CO<sub>2</sub> concentration should remain constant if the current does not change and if the inlet air is not polluted, with any variations indicative of carbon corrosion. The CO<sub>2</sub> concentration at the anode should remain close to zero, and any increase should be alarmed along with a

check of the electrode condition. One disadvantage of this method is that it can become less precise if the concentration of CO<sub>2</sub> at the air inlet is too high, for example, due to a polluted environment.

### **II. Activation Loss Measurement.**

When carbon corrosion occurs, the catalyst carbon support begins to degrade, and even more catalyst is removed together with the carbon material. So even more catalyst active area is removed from the catalyst layer and the activation loss starts to increase. Indeed, carbon corrosion is always connected to an increase of the activation loss. Measuring the activation loss can be a simple way to monitor the fuel cell status and determine if the catalyst layer maintains its functionality. A sudden increase in activation loss can be a symptom of possible carbon corrosion taking place.

There are three possible methods to measure activation loss: a) obtain the activation loss value from the polarization curve; b) using the electrical impedance spectroscopy; or c) adopt the current interrupt technique.

With the electrical impedance spectroscopy, a variable frequency alternating current is driven through the cell, the voltage is measured, and the impedance calculated [59], [60]. At higher frequencies, the capacitors in the circuits will have less impedance. By plotting graphs of impedance against frequency, it is possible to find the values of the equivalent circuit of the fuel cell. It is sometimes even possible to distinguish between the losses at the cathode and the anode, and certainly between mass transport and activation-type losses. Because the capacitances are large and the impedances are small, special signal generators and measurement systems are needed. Frequencies as low as 10 MHz may be used, so the experiments are often rather slow [60].

The current interrupt technique (Figure 3.19) is an alternative that can be used to give accurate quantitative results [59], [60]. It can be performed using standard low-cost electronic equipment.

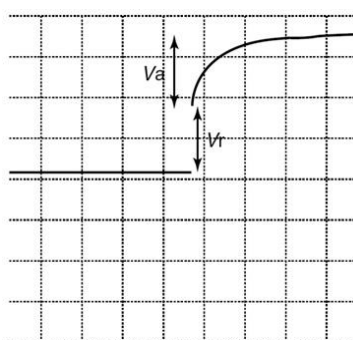


**Figure 3.19.** Current interrupt test for a low-temperature, ambient pressure, hydrogen fuel cell. The ohmic and activation voltage drops are similar (Time scale 0.2 s/div<sup>-1</sup>,  $i = 100\text{mAcm}^{-2}$ ) [60].

Suppose a cell is providing a current at which the concentration (or mass transport) overvoltage is negligible. The ohmic losses and the activation overvoltage will in this case cause the voltage drop. Suppose

now that the current is suddenly cut off. The charge double layer will take some time to disperse, and so will the associated overvoltage. However, the ohmic losses will immediately reduce to zero [60].

### III. Cell Voltage Monitoring.

The Cell Voltage Monitoring is another more practical method able to detect the potential risk of carbon corrosion formation directly in an operating fuel cell or stack. This method is useful especially for detecting the fuel starvation.

The voltage is a good estimation of the health of the cell. A decrease in cell voltage can be the result of fuel starvation; and if the cell voltage becomes negative, this can be an indication that the cell is completely starved.

If cell voltage monitoring is adopted, then system control software can be used to verify if the cell voltage shows the expected value and make a control intervention (for example shutting down the system or lowering the current) if the voltage drops below a certain reference value or a certain reference I-V curve. A solution of this kind (Figure 3.20) has been developed by Meltser et al. [61] whose apparatus was able of monitor both the fuel cells voltage status and the  $H_2$  concentration at the cathode in order to send output alert signals if the cell performance is declining or the  $H_2$  concentration exceeds the typical diffusion rate of hydrogen gas through the membrane.

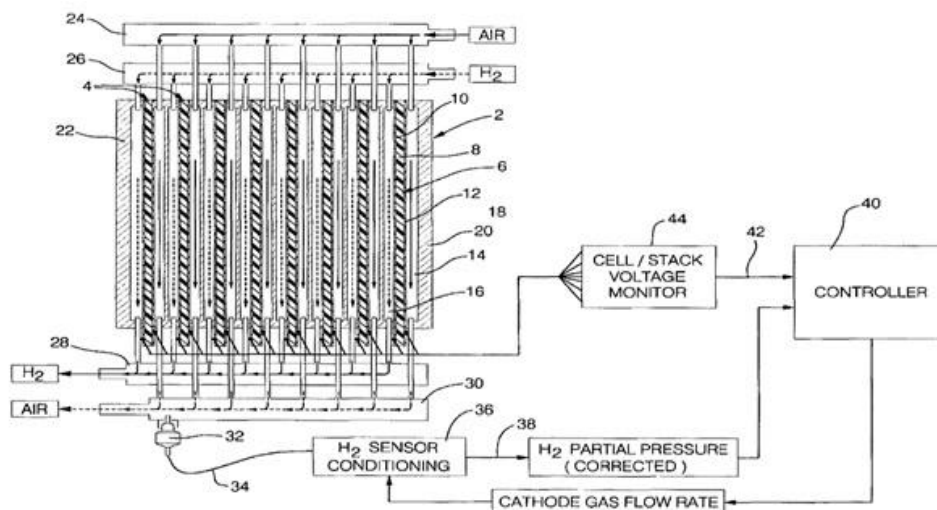


**Figure 3.20.** Patented scheme of a control system able to both monitor the cells voltage and the  $H_2$  presence in the cathode exhaust gas [61].

The cell voltage monitoring when used as a unique carbon corrosion detection method could become compromised, since the cell voltage is affected by many phenomena, and a voltage value decrease can be generated by many issues.

In any case, a constant cell voltage monitoring is recommended, since most often the majority of issues linked to cell voltage drop are directly connected to carbon corrosion. For example, cell flooding decreases the cell voltage and is responsible for fuel starvation.

### IV. Voltammetry Analysis.

The voltammetry analysis is an electro-analytical method used to determine the total active surface area of the catalyst. In particular, “cyclic” voltammetry and “CO stripping” voltammetry are commonly used.

In the first case, a triangular wave potential is imposed on the electrode and the current wave produced by electrochemical reactions is studied. The electrode potential changes between two potential ends, and for each voltage value a different number of electrons are transferred between the electrode and the electrolyte, varying the current output [62]. Each current peak corresponds to a particular reaction. To calculate the catalyst active area, for example, the hydrogen adsorption/desorption charge can be used. A description of this method is presented by Akira Taniguchi et al. [63] and it is mentioned by W. R. Baumgartner et al. [64], Hao Tang et al. [55], and Rohit Makharia et al. [51]. In Figure 3.21, an example of cycling voltammetry analysis is reported.

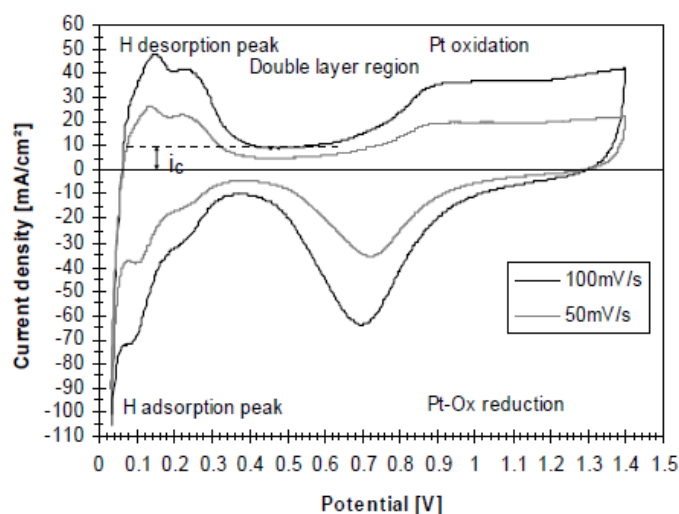


**Figure 3.21.** Typical cyclic voltammogram of the PEM fuel cell cathode; the different potential dependent reactions can be detected and correlated with the gas analysis [64].

The cycling voltammetry can be used both for qualitative and numerical evaluation. For example, Makharia et al. [51] performed a cycling voltammetry analysis with the aim to measure the Pt surface area loss (Figure 3.22).

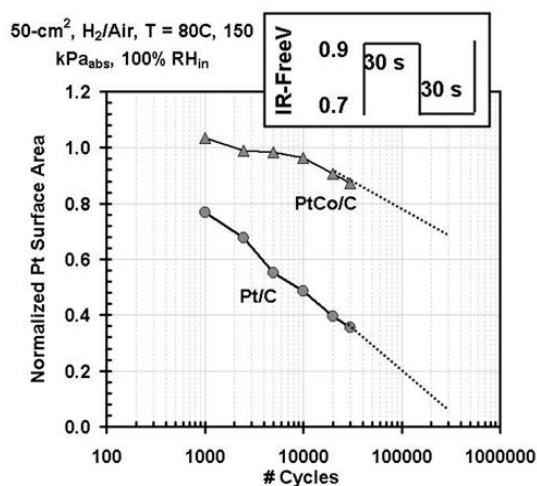


**Figure 3.22.** Normalized Pt surface area loss as a function of voltage-cycles [51].

The other voltammetry method often used to evaluate the electro-catalyst area is the CO stripping voltammetry. In this case, it is possible to distinguish 3 phases. During the first phase, the CO is pre-concentrated on the catalyst sites and a potential is applied at the electrode, then a rest period is followed maintaining the potential stable. During the last phase (stripping phase), an inverse potential scan is applied and the CO is desorbed. As a result, at a certain voltage a current peak is obtained with intensity proportional to the CO desorbed from the catalyst sites. The more catalyst active area is available, the higher the current peak [51], [55]. See Figure 3.23.

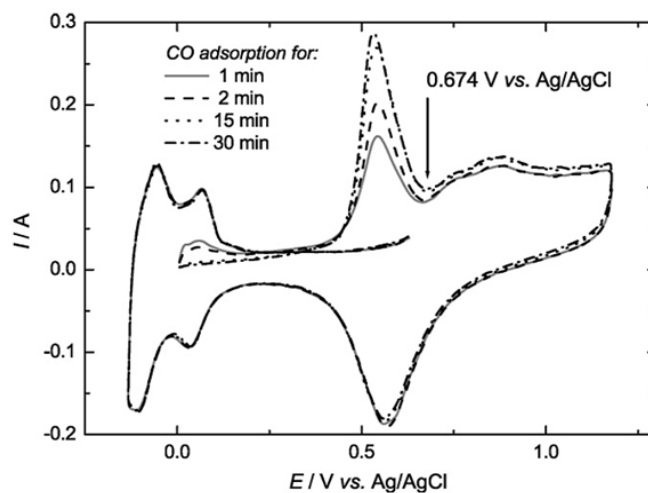


**Figure 3.23.** CO stripping voltammetry of unsupported Pt MEA after CO adsorption at 0 V compared to Ag/AgCl for different adsorption times [65].

Both cycling voltammetry and CO stripping voltammetry are the only precise methods to calculate the catalyst active area; however, these methods are not practical for a commercial fuel cells stack because every cell has to be fed with a variable potential and a Standard Hydrogen Electrode must be used. Furthermore, a variable potential is dangerous because it can increase Pt dissolution as well as carbon corrosion. Thus, these

methods are best confined to laboratory single cell testing because it is impractical to monitor the status of catalyst layers for all cells in a commercial stack.

However, the voltammetry analysis can be an interesting technique for post-mortem *ex-situ* investigations for both single cells and stacks. In this case, normally only the MEAs are considered and analyzed.

### V. SEM Analysis.

Beside the voltammetry, the Scanning Electron Microscope (or SEM analysis) is another *ex-situ* method that can be used to analyze the post-mortem MEAs and investigate the carbon corrosion effects at the EOL.

In the case of PEM fuel cells, the most common application is a cross-section image scan of the MEA, which can provide the thickness data of the different layers comprising the MEA (membrane, GDLs, MPLs, catalyst layers).

An MEA cross-section SEM analysis can be particularly useful in order to understand if the MEA was affected by carbon corrosion. The method consists in comparing the catalyst layer thickness with the nominal values. An eventual thinning would be indicative of the catalyst layer degradation.

In Figure 3.24, an example of SEM image of an MEA cross-section is shown. The catalyst layer thinning is often matched with a Pt band deposition inside the membrane and a SEM image can easily reveal it, as in this case.

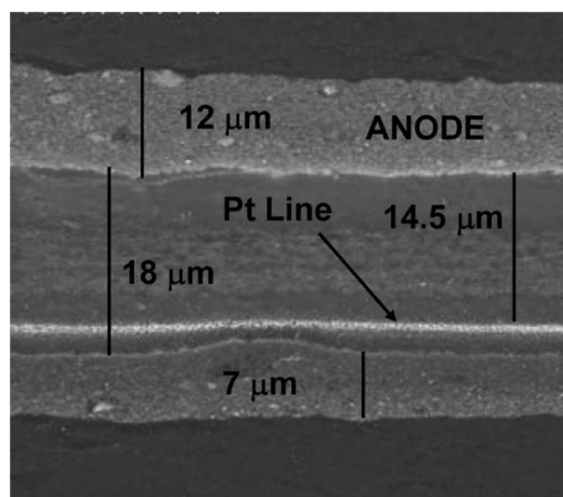


**Figure 3.24.** MEA cross-sectional SEM photomicrograph after operation for 2,000 h at OCV conditions with H<sub>2</sub>/air [47].

A disadvantage of this method is that the measurement is site-specific and not integrative for the whole MEA, since each measurement shows only a small portion of the MEA. So, analysis of additional cross-sections would be required to better define the extent of the affected area.

### **3.3.4. *Material-based carbon corrosion mitigation strategies***

Once the corrosion mechanism of the catalyst carbon support is completely understood, it is more likely that a suitable mitigation strategy will be developed.

Up to now, due mainly to the limited knowledge about this issue, many fuel cell system companies or fuel cell stack manufacturers have not adopted any kind of solution to mitigate carbon corrosion. Also, the materials for catalyst layers are standardized: almost all fuel cells produced by manufacturers contain catalyst layers composed of carbon support particles such as carbon blacks.

Several articles in the literature and patents by fuel cell companies propose solutions that are very different from each other. However, in general, only a few clear and demonstrated solutions have been presented up to now.

While some authors are aware, for example, that “unprotected” [55] startups and shutdowns have an impact on degradation, they do not specify any “protection” protocols. Other articles like the work of Akira Taniguchi et al. [63] confirm that the failure modes for PEM fuel cells, such as catalyst area loss due to carbon corrosion, are not well documented and the cause of degradation mechanisms are not fully understood. S. Maass et al. [58] instead declare that only limited information has been reported in the literature about carbon corrosion in a real PEM fuel cell environment under potentiodynamic operating conditions.

The fact that no definitive solutions have emerged until now indicates that the carbon corrosion issue is not well understood.

Here, the approach was to identify and collect the possible solutions to mitigate the problem, dividing them into two categories: a) research of new, more carbon corrosion resistant materials; and b) system management to make the fuel cell operate at conditions that will decrease the carbon corrosion activities.

Recent R&D efforts are concentrated on identifying new materials that are able to mitigate the carbon corrosion problem. These studies concern both the catalyst layer and other components including the membrane. The purpose is twofold: first, researchers want to find a new Pt support with good electron conductivity; and second, they attempt to mitigate the corrosion reaction that leads to the degradation of the carbon support.

The most effective solution for avoiding the carbon oxidation would be simply the adoption of non-carbon materials as catalyst supports. However, the challenging requirements of both high chemical inertness and good conductivity have disqualified the use of many oxides (low conductivity) and metals (low inertness) up to now. Lately some research had shown interesting results concerning the use of nanotube oxides structures, such as TiO<sub>2</sub> nanotubes, as catalyst support for the electron conduction. While still at a premature stage, this research seems very promising for future development of corrosion resistant catalyst supports.

It is possible to distinguish five different areas of research in the literature:

- I. Lower  $O_2$  diffusivity membranes
- II. Oxygen evolution reaction (OER) favorable catalysts
- III. Higher PTFE loading within the catalyst layer
- IV. More chemically resistant carbon supports
- V. Non-carbon based catalyst support

### ***I. Lower $O_2$ diffusivity membranes***

Lowering the  $O_2$  diffusion rate through the membrane will decrease the amount of oxygen reaching the anode side, and limit the oxygen reduction reaction at the anode side. During the cell startup or shutdown, the presence of oxygen at the anode side is one of the main factors leading to carbon corrosion at the cathode.

Using a lower  $O_2$  diffusivity membrane can be effective especially during a shutdown, when the fuel is consumed and the anode pressure can be lower than the cathode pressure. In fact, in this condition the oxygen crossover is favored.

Jingwei Hu et al. [66] developed a 2-dimensional model to simulate carbon corrosion. Figure 3.25 shows the impact of the Carbon Corrosion Reaction (CCR) dependence on the  $O_2$  diffusivity calculated with the simulation.

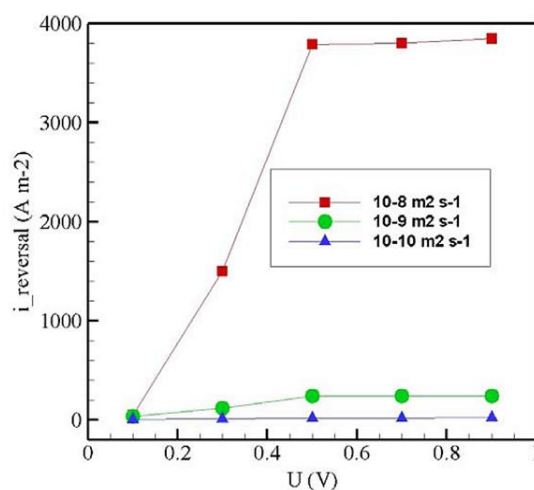


**Figure 3.25.** CCR dependence on  $O_2$  diffusivity in membrane; the simulation gives higher reversal current density values as  $O_2$  diffusivity decrease [66].

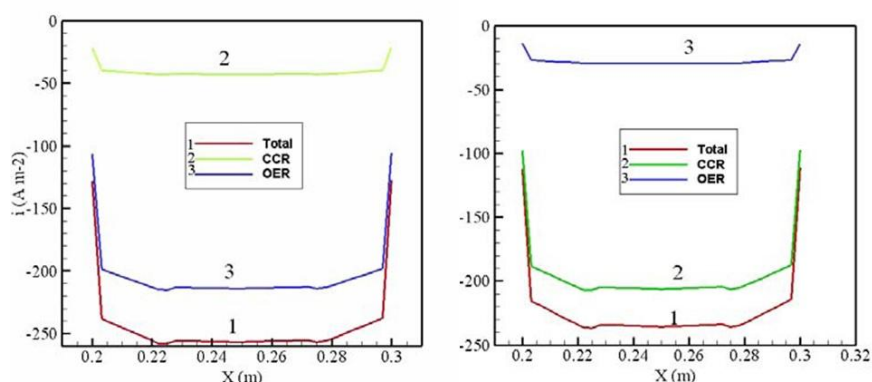
### ***II. Oxygen evolution reaction (OER) favorable catalysts***

If the catalyst layer is made of water oxidation favorable catalyst (also defined as Oxygen Evolution Reaction-favorable catalysts) such as Pt-Ir/C, the carbon corrosion reaction is less competitive with respect to the water oxidation reaction. This happens, for example, when a Pt-Ir/C catalyst is used and the required

activation energy for water oxidation is lower compared to the energy to activate the carbon oxidation. So, water oxidation is promoted over carbon corrosion, and the catalyst tolerance to carbon oxidation is increased.

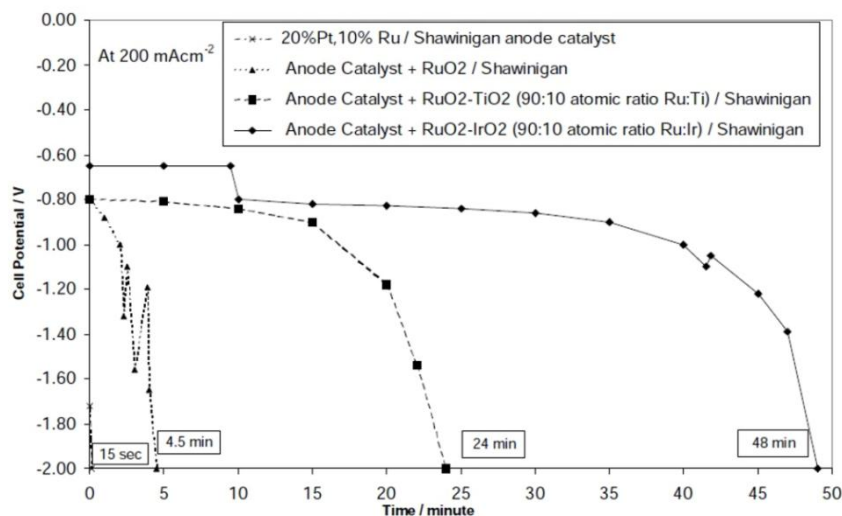
Jingwei Hu et al. [66] demonstrated with their 2-dimensional model that the use of anode OER-favorable catalysts is the best mitigation strategy when combined with the use of lower  $O_2$  diffusivity membrane.

Figure 3.26 from Jingwei Hu’s article shows the difference between OER catalysts and normal catalysts. The simulation gives lower reversal current density values as the catalyst is changed from normal Pt/C to Pt-Ir/C.



**Figure 3.26.** Left: OER favorable catalyst, right: normal catalyst [66].

The use of OER-favorable catalyst at the anode is also mentioned by T. R. Ralph et al. [57]. Their experiments confirm that the carbon corrosion tolerance is improved when using OER-favorable catalysts. The best electrocatalyst examined was unsupported  $RuO_2-IrO_2$  (see Figure 3.27).



**Figure 3.27.** Impact of adding  $RuO_2$ ,  $RuO_2-TiO_2$  and  $RuO_2-IrO_2$  as water oxidation electrocatalyst to the “20 wt% Pt, 10 wt% Ru” electrocatalyst [57].

### III. Higher PTFE loading within the anode catalyst layer

Normally PTFE is added to the GDL and most of all in the MPL to increase the hydrophobicity and avoid electrode flooding. The role of PTFE is to increase the water droplet contact angle, so that water is less attracted to the carbon fibers or Carbon Blacks, and can easily be removed with a gas flow. When PTFE is not present, the adhesion force of water droplets is higher and it is more difficult to remove them from the surface of carbon fibers and Carbon Blacks. The retained water droplets tend to agglomerate, and this situation leads to water flooding. Conversely, excessive PTFE loading (in the GDL for example) can result in water flooding because PTFE can form a completely hydrophobic layer that blocks water coming from the cathode oxygen reduction reaction.

Based on the Ralph et al. experience, the PTFE added within the anode catalyst layer tends instead to retain more water (generated by the cathode reaction) within the membrane so that the Oxygen Evolution Reaction is favored with respect to the carbon corrosion [57]. This seems to increase the anode catalyst layer carbon corrosion tolerance in fuel starvation condition. They explain that the hydrophobic character of the anode was increased by adding PTFE. Additional research may confirm if the root cause is the hydrophobicity effect, or is it partially or totally dependent on other factors, such as formation of a physical barrier. However, T. R. Ralph et al. demonstrated that a cell operating with air as oxidant and humidified  $N_2$  as fuel (to simulate starvation) can tolerate a higher current before having a failure if liquid water is supplied to the anode and if PTFE is added to the anode catalyst layer, as shown in Figure 3.28.

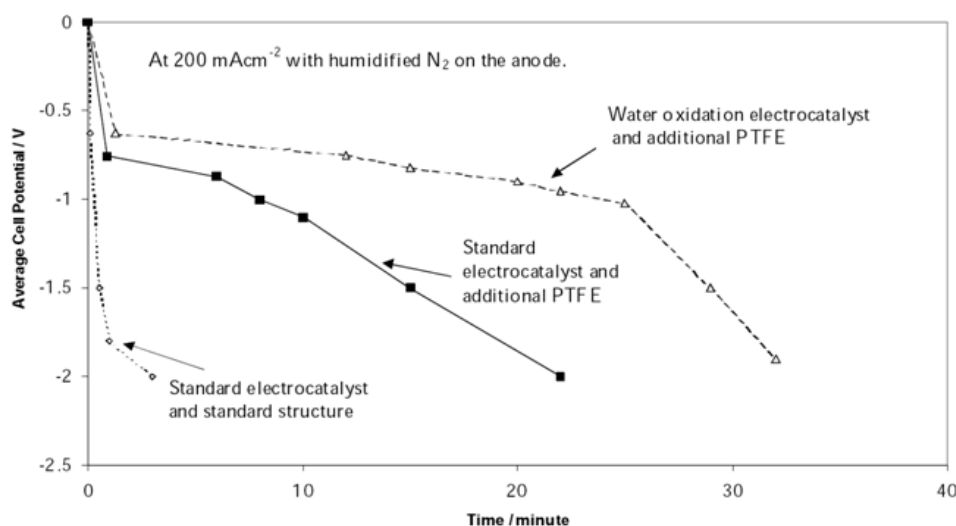
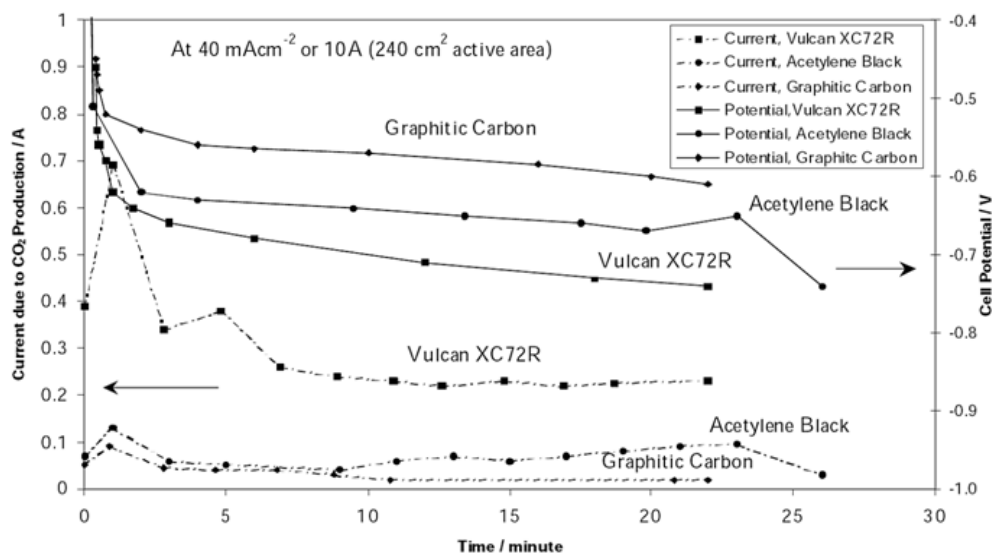


Figure 3.28. Cell reversal tolerance by using PTFE and OER-favorable catalyst [57].

### IV. More chemically resistant carbon supports

T. R. Ralph et al. performed an interesting test with the aim to analyze the carbon corrosion resistance of three different catalyst carbon supports: Vulcan XC72R, Denka acetylene black and graphitized Vulcan

XC72R. The corrosion resistance was measured in 1 mol dm<sup>-3</sup> H<sub>2</sub>SO<sub>4</sub> at 80°C and 1.2 V vs. RHE. They found the cell reversal tolerance of the anode decreases in the order: graphitized Vulcan XC72R > Denka acetylene black > Vulcan XC72R, as shown by the less negative cell potential and the much lower current attributable to the production of CO<sub>2</sub>. Figure 3.29 compares the performance results for these three catalyst options.



**Figure 3.29.** Cell voltage reversal and CO<sub>2</sub> production using Vulcan XC72R, Denka acetylene black, and graphitized Vulcan XC72R. The graphitized Vulcan XC72R shows the best corrosion resistance (lower cell reversal values and lower CO<sub>2</sub> production) [57].

The graphitized carbon support shows a considerable higher carbon corrosion resistance with respect to traditional non-graphitized supports: carbon weight loss after 24 hours is less than 0.5 wt% instead of 30%. Thus, the carbon corrosion rate is also better when compared to a lower surface area carbon support, like Denka acetylene black.

However, acetylene blacks offer a more economical alternative to the graphitized supports. In fact, the additional graphitization process increases the catalyst layer cost (consider that carbon blacks have to be processed in a furnace exceeding 2,400 °C for at least 24 hours and then the furnace must be cooled slowly over several days [57]). Furthermore, this process lowers performance because it results in a lower surface area and the catalyst active area is reduced (same problem with Denka acetylene black). The reasons for the reduction in the active area are principally two: a) most of graphitized carbons do not have sufficient surface area for making highly dispersed catalysts; and b) they present low surface energy (few active sites such as dislocation, vacancies, etc...) which is mostly responsible for forming larger precious metal particles [31].

Another solution to make the catalyst carbon support more resistant could be carbon nanotubes. Carbon nanotubes are one of the most studied allotropes of carbon in recent years because have many interesting mechanical and electrical properties. Furthermore, they are also very chemically stable. Xin Wang et al. [67] compared the carbon oxidation resistance of traditional carbon blacks and Multi-Walled Carbon Nanotubes (MWNT) following potentiostatic treatment up to 168 h at a constant potential of 0.9 V. The MWNT showed

a considerable electro-catalyst area loss reduction compared with carbon blacks (Figure 3.30). Furthermore, the catalytic effect of Pt on MWNT is less significant and the Pt particles agglomeration in time is reduced.

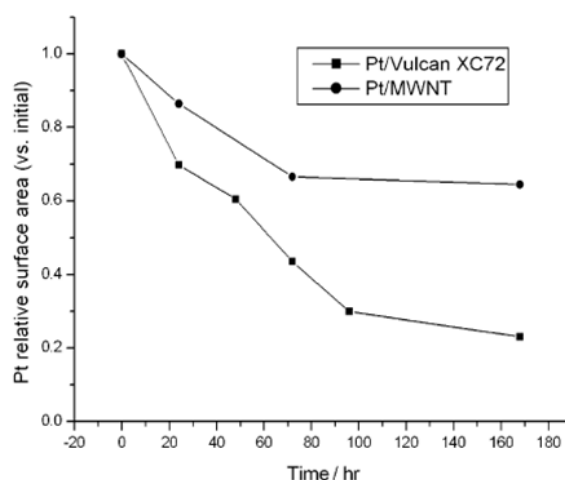


**Figure 3.30.** Comparison of Pt active surface area loss for the case of Vulcan XC-72 and MWNT at different time intervals during the oxidation treatment [67].

However, while the carbon corrosion tolerance advantage of carbon nanotubes seems to be effective, this material has been evaluated only in laboratory settings. So additional studies are necessary to understand if carbon nanotubes can be used as catalyst support in large-scale applications and at low cost.

### V. *Non-carbon based catalyst supports*

Several studies have recently converged to develop new non-carbon based supports for fuel cell catalysts. Above all,  $\text{TiO}_2$  seems to be the most promising material because of its low cost, commercial availability, stability in water, and the ease to control size and structure [68]. Like other oxide supports, it is commonly used for heterogeneous catalysis, but in recent years, it became considerably attractive especially for the many potential applications in solar cells, biotechnology, photocatalysis, and gas sensors.

However, the relatively low electrical conductivity is still the issue to overcome before  $\text{TiO}_2$  catalyst supports can successfully replace traditional carbon-based catalyst supports. As reported by Kyung-Won Park and Kwang-Su Seol [68], the current methods used to improve the electrical conductivity include reducing pure titanium oxide by producing oxygen vacancies, introducing an appropriate dopant, and adding conducting materials in oxide (and annealing under  $\text{N}_2$  or  $\text{NH}_3$ ).

S. Vinod Selvaganesh et al. [69] and Satheesh Sambandam et al. [70] adopted the last strategy, and tested Pt- $\text{TiO}_2/\text{C}$  nano-composite electrocatalysts. Results reported in Sambandam's work show performance degradation of 10% after 5,000 test cycles compared to a 28% decline for Pt/C.

As regards new methods for improving electrical conductivity, encouraging results have been obtained by Robert Hahn Dipl et al. [71], who imparted semi-metal conductivity to  $\text{TiO}_2$  nanotubes through

carbonization in acetylene gas atmosphere at 850 °C, and Chinmayee Subban et al. [72] who measured an electrical conductivity of approximately 100 S cm<sup>-1</sup> in pressed powders of W-doped TiO<sub>2</sub>.

However, all the characterizations have been done with the catalyst alone, while further tests using complete MEAs are needed in order to obtain comparable data with respect to the present carbon-based catalyst supports that remain the “state-of-the-art”.

Table 1.1 summarizes the primary carbon corrosion mitigation strategies under review, including comparison of advantages and disadvantages for each method.

**Table 1.1.** Summary of the mitigation strategies based on material improvements and their characteristics.

| <b>Method</b>                                     | <b>Advantages</b>   | <b>Disadvantages</b>  |
|---|---|---|
| Oxygen evolution reaction favorable catalyst      | Very effective method based on T. R. Ralph et al. [57] and Jingwei Hu et al. studies [66]   | Additional research needed to understand the performance difference with respect to Pt catalyst   |
| Lower O <sub>2</sub> diffusivity membrane         | Very effective method based on Jingwei Hu et al. study [66]   | Additional research needed to determine if there are any changes in the membrane ionic conductivity and water transport properties  |
| More PTFE loading within the anode catalyst layer | The water retention at the anode side favors the oxygen evolution with respect to oxygen reduction  | Additional research needed to understand the performance difference with respect to Pt catalyst   |
| More resistant carbon supports                    | Some carbon supports such as graphitized supports, smaller surface area carbon blacks, and carbon nanotubes, show high resistance to carbon corrosion | <ul style="list-style-type: none"> <li>• Low performance (graphitized carbon blacks, smaller surface area supports)</li> <li>• High cost (graphitized carbon blacks, carbon nanotubes)</li> </ul> |

### **3.3.5. System-based carbon corrosion mitigation strategies**

An alternative approach to mitigate the problem is to concentrate on fuel cell operating conditions and avoid or limit all situations leading to carbon corrosion.

One solution is based on the fact that, if the amount of reactants is smaller than the products, the reaction is limited. In the case of carbon oxidation  $C + 2H_2O \rightarrow CO_2 + 4H^+ + 4e^-$ , the possible actions to limit the carbon oxidation are decreasing the water content in the place where carbon oxidation can occur, or having more hydrogen ions and electrons available than equilibrium.

Another possibility is to decrease the electrode potential to zero so that the carbon corrosion reaction does not have the proper potential energy to occur.

The system management strategies can be divided into two categories, depending if the issue is fuel starvation or carbon corrosion during startup/shutdown.

As previously mentioned, fuel starvation can occur when the load (and current requirements) exceed the required fuel (hydrogen) supply to the anode electrode. The origin of fuel starvation is a blockage in the bipolar plate channels, GDL or MPL; the most common conditions able to generate it include anode water flooding, excessive GDL compression, nitrogen gas not purged during the startup in the anode passages and ice formation before the startup.

Normally, an optimal design of fuel cell components will avoid or minimize most causes of fuel starvation. Channel lands of the bipolar plate flow field, for example, represent one of the most critical features because they are the contact area where the GDL is compressed. Also determining the correct cell hardware bolting torque is important to avoid over-compressing the GDL.

It is also important to prevent the cell from operating with a low fuel stoichiometric ratio (close to 1), because the active area in the anode outlet zone can suffer from fuel starvation.

Residual nitrogen gas in the anode passages resulting from an inadequate startup purging procedure is another possible cause. A more common situation is that air is present in the anode before hydrogen is supplied, but soon oxygen is consumed and the remaining inert gas is composed almost entirely of nitrogen. If this inert gas is not purged during the startup, the active area exposed to hydrogen decreases and local fuel starvation occurs.

Indeed, the most common cause of fuel starvation during fuel cell operation is probably fuel blockage due to water flooding in the bipolar plate channels, GDL and MPL. The system control, if present, must check that the fuel cell is operating in a non-mass transport regime. Often, if the mass transport loss is increasing, the cause is just due to water flooding. Also, if the mass transport loss does not decrease after raising the cathode side airflow, then the problem is most likely due to water flooding on the anode side. In this case, the possible options are:

- Decrease current density since the water production is proportional to the current
- Increase  $H_2$  flow (if  $H_2$  is recirculated) or initiate a periodic anode side purge → this will facilitate the water removal from the anode side

During a startup or shutdown, oxygen is always mixed with the incoming  $H_2$  (startup) or outgoing  $H_2$  (shutdown). As previously explained, the co-presence of  $O_2$  and  $H_2$  leads to carbon corrosion on the cathode side.

UTC Fuel Cells [36-41] thoroughly investigated this phenomenon and proposed several mitigation methods.

System strategies to avoid this situation and mitigate carbon corrosion during a startup or shutdown include the following:

- I. Purging both anode and cathode with inert gas
- II. Drying the cathode
- III. Purging with H<sub>2</sub> at both anode and cathode
- IV. Cell shunting

### ***I. Purging both anode and cathode with inert gas***

If before a startup or after a shutdown of the fuel cell, an inert gas, like nitrogen, is introduced at both the anode and cathode, no possible reduction and oxidation reactions can occur and, above all, the oxygen-hydrogen boundary presence at the anode is completely avoided. So, if the N<sub>2</sub> purging procedure is well done, carbon corrosion at the cathode side can be totally avoided. For this reason, this solution represents the best mitigation strategy of all even if, in practice, this can become complicated and costly to achieve.

In fact, you have to: a) add another gas circuit and a N<sub>2</sub> cylinder in the fuel cell system; b) introduce another gas pressure reducer besides the H<sub>2</sub> one; and c) introduce at least as many valves to close and open independently the H<sub>2</sub>, N<sub>2</sub> and air circuit.

### ***II. Drying the cathode***

Shyam Kocha [73] proposed a method consisting of driving dry gas through the cathode flow field for an amount of time sufficient to reduce the water content to a level that suppresses both carbon corrosion and catalyst dissolution. In this case, the aim is to eliminate one of the two main reactants in the carbon oxidation reaction, which is just the water. A practical and economical way to drying the fuel cell is, for example, to use non-humidified heated air from the existing system blower. Degradation rate comparisons for combinations of temperature and RH values tested by Kocha are shown in Figure 3.31.

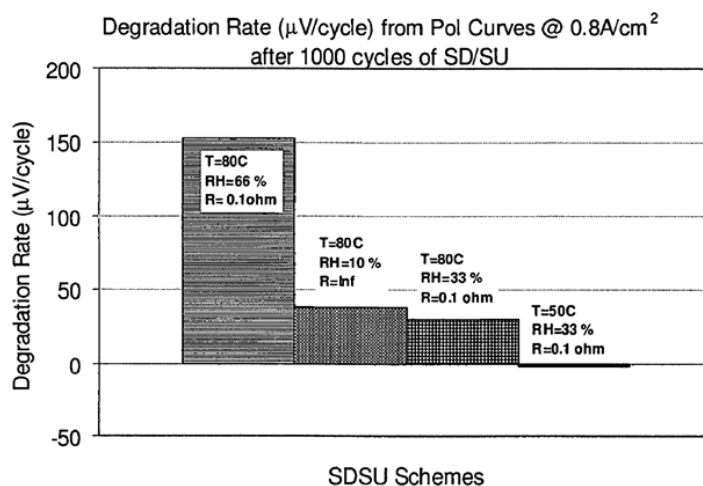


**Figure 3.31.** Comparative degradation rates under cycling condition at specific temperature and RH values [73].

### III. Purging both anode and cathode with hydrogen

Yu et al. [74] presented a method to mitigate carbon corrosion by introducing hydrogen gas into the cathode passages to consume and purge oxygen in both the anode and cathode passages. When hydrogen is introduced into the cathode channels, the open circuit voltage declines very rapidly. Without a potential, reactions cannot take place because they need an activation energy to occur. Furthermore, introduction of hydrogen at the cathode consumes and purges oxygen, avoiding O<sub>2</sub> crossover through the membrane. Then, in a second phase, air is introduced to remove water droplets from the cell, which further reduces the risk of carbon corrosion, as water is the second reactant.

However, additional studies of this method are needed to verify that any peroxides, OOH• and OH• radicals formed during H<sub>2</sub> introduction into the “air filled” cathode do not negate the benefits of rapid O<sub>2</sub> consumption and open circuit voltage decrease.

### IV. Cell shunting

An important characteristic to mitigate carbon corrosion with the above mentioned methods was the rapid reduction in open circuit voltage that avoids having a high voltage on the cell, and, in particular on the cathode side. Without a cathode potential, carbon corrosion cannot occur because it uses this potential to activate the reaction. Bekkedahl et al. [36] exploited this principle to provide a very simple method to decrease cell voltage: “cell shunting”. In a fuel cell stack, each cell is provided with a shunt between the anode and the cathode. The shunt can be a discrete resistor, a diode or a strip of carbon cloth; or a small amount of conductive carbon black mixed with an ionomer polymer mixture, similar to the ionomer used for the proton exchange membrane.

However, inserting a shunt in every cell of a stack could be impractical and costly in stack manufacturing (consider for example that an automotive stack can have 300-400 cells). Even Ralph et al. remarked on the high cost of using diodes connected to each cell in the stack [57].

Furthermore, the nearby cells can quickly degrade if a cell shunt is damaged and does not function. In fact, all the cells will discharge except the one with the damaged shunt. When all the other cells reach the null potential, the hydrogen is no longer present at the anode catalyst layer in those cells and they are fuel starved. However, a potential still exist in the cell with the damaged shunt, and a current will be drawn by all the shunted cells even if they remain fuel starved. As previously explained, this situation can lead to reverse voltage and, above all, to the carbon corrosion of the catalyst layer.

Also, a permanent shut will certainly decrease the cell performance because the cell has to supply two currents in parallel, one for the shunt, and one for the load. So, the cell works at a higher current and the efficiency decreases for higher current values.

**Table 3.2.** Summary of the system management mitigation strategies able to mitigate cathode carbon corrosion during startups or shutdowns.

| Method  | Advantages  | Disadvantages  |
|---|---|--|
| Purging anode and cathode with N <sub>2</sub>           | Probably the most effective method                          | Complicated and costly to realize  |
| Drying the cathode after the operation mode             | Simple and low-cost   | The cell is operated at OCV condition during the drying period   |
| Introducing H <sub>2</sub> both at anode and at cathode | The open circuit voltage drops rapidly and oxygen is purged | The system design becomes more complicated; more studies needed about the formation of peroxides, OOH• and OH• radicals during the H <sub>2</sub> purging phase  |
| Cell shunting   | Simple and low-cost   | <ul style="list-style-type: none"> <li>• Impractical to realize a shunt in every cell during the stack assembly</li> <li>• If a shunt has a failure, the cell degrades more rapidly with respect to nearby cells</li> <li>• A permanent shunt lowers the cell performance</li> </ul> |

### ***3.4. Mitigation strategies testing and validation***

In order to validate some mitigation strategies studied and developed in Electro Power Systems, two durability tests (with two different protocols) has been performed. In particular, the aim was to understand the effectiveness of three techniques:

- 1) Stack shunting for mitigating the catalyst carbon corrosion during starts and stops.
- 2) Cell voltage monitoring and stack current modulation for preventing fuel starvation events leading to irreversible performance losses.
- 3) Stack current modulation for preventing quick stack voltage changes that would produce high Pt dissolution rates.

The experiment used a 24-cell PEM fuel cell stack designed and assembled by Electro Power Systems SpA. The design of the reactants and coolant manifolds featured a U-profile that positioned all the inlets and outlets at the same end of the stack. The bipolar plates were made of pure graphite and machined with a proprietary flow field design for both the reactant and cooling sides. The reactant flow fields were multi-serpentine design for both the anode and cathode. A cooling flow field was present between every cell.

The MEA specification included: chemically stabilized and mechanically reinforced perfluorosulfonic ionomer membrane, carbon paper Gas Diffusion Layers (GDLs), catalyst active area of 200 cm<sup>2</sup>, and Pt/C-based catalyst layers with anode Pt loading of 0.2 mg/cm<sup>2</sup> and cathode Pt loading of 0.6 mg/cm<sup>2</sup>.

Figure 3.32 shows a schematic representation of the test bench used for the stack. The air was supplied by a blower to a humidifier and then into the stack. The wet outlet air was used to exchange water with the dry inlet air through a polymer electrolyte membrane present in the humidifier. The calculated inlet air RH was 78% for the operating conditions specifically chosen for the durability test (see Table 3.3). The hydrogen came from a cylinder at a pressure of 6 bar absolute (5 barg), followed by a pressure reducer that stabilized the pressure at 1.3 bar absolute (300 mbarg). A pump recirculated the hydrogen, and the supply line was purged periodically in order to remove water and avoid anode flooding. The stack was cooled using circulating demineralized water in the primary circuit. The primary circuit then exchanged heat with a secondary circuit that included a fan-cooled radiator. The entire coolant circuit was design for cooling a thermal load generated by a 2 kW stack.

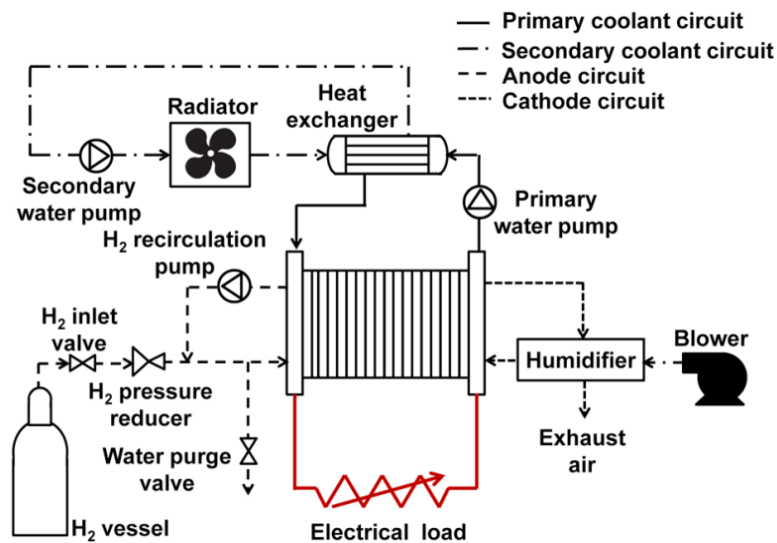


**Figure 3.32.** Schematic of the test bench used for the experiment with unprotected startups and shutdowns [28].

The entire system management used proprietary software to control all phases of the stack operation. The software controlled the electrical load such that the stack gradually reached the selected regime current operating point (180 A), thus regulating the voltage ramp rate from the cell Open Circuit Value (about 0.96 V in this case) up to a cell voltage value at 180 A (about 0.67 V). It intervened by limiting sudden current changes when the load request varies quickly in time. The missing part of power required by the load was supplied by an auxiliary battery. This protocol, including the **current modulation**, avoids rapid potential changes that are well known to accelerate the Pt dissolution rate [25], [44].

Data generated by three temperature sensors (two in the primary coolant circuit and one in the secondary coolant circuit) and a pressure sensor in the H<sub>2</sub> circuit were essential for the software to automatically monitor and control the main physical stack parameters during the entire duration of the tests.

The **cell voltage monitoring** techniques was included in the experimentation and each single cell voltage was measured. The system software always scans in real time each single cell voltage and evaluates it with an average cell voltage. If a cell shows a deviation with respect to the average value, the control starts to decrease the stack current. In the same time, the oxidant flow is increased and, since the recirculation pumps are kept in operation, overall this helps to increase the stoichiometric ratio. In this way if the cell is flooded at the anode or at the cathode, it is likely that the water can be quickly drained out from the cell. When the performance is then restored the flows and the current return at the starting value. The missing power required by the load is again supplied by the auxiliary battery. So even in this case, a current modulation technique is combined with cell voltage monitoring. The aim here is not to prevent sudden voltage changes, but to prevent failure events mostly due to cell flooding. The cell flooding is particularly dangerous at the anode because the hydrogen blockage causes fuel starvation, which is another root cause of carbon corrosion.

For the cell voltage detection and acquisition, the digital voltmeter described in chapter 2 was used. The software control logic managed the blower air flow, the hydrogen supply and water purge procedures, and was able to maintain a constant stack temperature with limited excursions ( $\pm 2$  °C). The main operating parameters selected for the test are summarized in Table 3.3.

**Table 3.3.** Principal operating parameters of the experiment [28].

| Item   | Value                        |
|--|------------------------------|
| Average stack temperature                              | 62 °C                        |
| Operating current point                                | 180 A                        |
| Fuel   | Hydrogen (purity 99.995 %)   |
| Fuel stoichiometric ratio (at operating current point) | 1.6 (with recirculation on)  |
| Fuel inlet pressure                                    | 1.3 bar absolute (300 mbarg) |
| Estimated inlet fuel RH (at operating current point)   | 78 %                         |
| Oxidant  | Laboratory quality air       |
| Oxidant stoichiometric ratio                           | 3                            |
| Estimated inlet air RH (at operating current point)    | 90 %                         |

The durability tests consisted of repetitive cycles, alternating a phase of operation for 15 minutes with a phase of stand-by for 6 minutes. The 15 minutes of operation were chosen because this was the average operation period of the EPS power systems installed in customers' sites. However, the "6 minutes" stand-by period was selected to allow time for the stack to cool down to a temperature below 35 °C.

Two different tests were performed:

- one including the current modulation and the cell voltage monitoring techniques but with "unprotected" startups and shutdowns. The aim was to evaluate the effectiveness of the cell voltage monitoring and the current modulation techniques.
- the other one using the stack shunt method for mitigating catalyst support carbon corrosion.

Both tests used the same operating conditions reported in Table 3.3.

A stack polarization curve was recorded before starting the first durability test with unprotected startups and shutdowns in order to document the initial stack performance. The same characterization was repeated at the end of the test and compared to the initial results.

The voltage of each cell, the stack voltage and the stack current were continuously monitored and recorded in real time during the entire duration of the experiment.

After the end of the first test, the three worst performing MEAs were analyzed using the FE-SEM technique. The goal was to measure the thickness changes of the anode and cathode catalyst layers and the membrane by comparing the measurements with a fresh MEA.

After the first test was completed with unprotected startups and shutdowns, the stack was refreshed with a set of new MEAs. Then a second test was run using the stack shunt protocol and modified test bench as

shown in Figure 3.33. The stack hardware remained unchanged for the purpose of verifying if the same cell positions in the first test also experienced the highest degradation rate in this test.

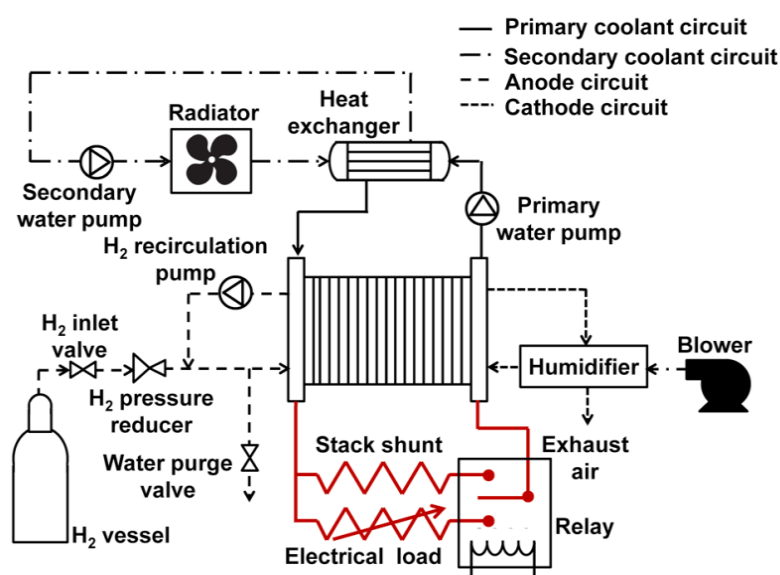


**Figure 3.33.** Schematic of the test bench used for the experiment adopting the stack shunt protocol [28].

The hardware modification for implementing the stack shunt protocol consisted of an additional relay switch and a 5-ohm shunt resistor inserted in parallel to the electrical load. In addition, the software was modified to allow automatic control of the shunt relay switch during shutdown and startup.

During the stack normal operation, the shunt switch status is set to OFF, corresponding to connecting the stack to the electrical load. When the stack operation stops, the load returns to an open circuit condition, and the control software sends a command to switch ON the relay and connect the stack to the shunt resistor. The resistor remains connected until the next stack startup, when the software sends the command “switch OFF” to the relay because the electrical load changed from the open circuit condition.

The selected shunt was able to completely discharge the 24-cell stack in about 30-40 s. The current measured with the shunt connected was 4.2 - 4.4 A; while the stack voltage was 21.5 V corresponding to an average cell voltage of 0.89 V.

In order to be effective, the stack shunt protocol requires three important features to be applied during the shutdown:

- **Anode gas recirculation:** this prevents a localized fuel starvation condition during hydrogen consumption while the shunt is connected to the stack during the shutdown phase, avoiding anode carbon corrosion of the catalyst support [32], [33]. Furthermore, it equalizes the fuel distribution within the stack, limiting voltage differences between cells.
- **Oxidant Flow:** together with the anode gas recirculation, promotes equal reactant gas distribution within the entire stack, limiting the voltage differences between cells. This prevents a localized oxidant starvation condition during oxygen consumption while the shunt is connected to the stack

during the shutdown phase, avoiding cathode activity degradation due to Pt particle agglomeration [75].

- **Venting procedure:** this prevents excessive pressure drop in the anode compartment, which can quickly fall below 0.05 MPa absolute (- 500 mbarg) in a few seconds. A high-pressure difference between anode and cathode (which is open to ambient air) can damage the polymer electrolyte membrane, which typically is no more than 25-30  $\mu\text{m}$  thick.

If these three features are included with the shunt, then high cathode potential excursions due to the co-presence of hydrogen and air in the anode compartment can be avoided, or at least mitigated, and high voltage differences between cells can be limited.

The gas recirculation avoids fuel starvation and oxidant starvation in the outlet area of each cells, which is unavoidable in a dead-end mode [32], [33]. In the meantime, the fuel is consumed continuously by the hydrogen oxidation reaction; and when the hydrogen is totally consumed, the cell voltage will drop off.

During the shutdown phase, the stack shunt remains connected until the next startup in order to avoid any possible voltage generation due to residual un-reacted hydrogen. However, the anode gas recirculation system is stopped once the voltage drops to zero volts.

Cell voltage data were recorded and analyzed to establish the plot of the “average cell voltage” performance for each startup/shutdown operation cycle during the lifetime of the stack. The “average cell voltage” for each cell was calculated from data only when the stack was operating at 180 A. Therefore, the calculation did not use voltage data recorded during the initial and final transient periods, when the stack respectively reached the maximum current and when the current was lowered to 0 A.

The cell data was recorded using the following numeration: the first cell, “Cell #0”, was the cell closest to the stack end where all the reactants and coolant inlets and outlets were located. Therefore, the last cell was #23 at the opposite end of the stack.

The End of Life (EOL) voltage was defined as 560 mV for this study. Therefore, when an individual cell voltage dropped below this selected value, the test was considered finished. Based on past stack experience, when a cell voltage dropped below this value, the cell experienced rapid performance degradation. In addition, voltage decline can be influenced by the operating conditions and stack hardware design; however, further investigation of these factors was outside the scope of this work. Other criteria for defining EOL voltage can be considered, such as a certain percentage of voltage degradation (e.g. 5% or 10%). Probably the criterion that is most relevant to fuel cell applications is to establish a “minimum average cell voltage” that insures that the stack will supply the required load.

Figure 3.34 shows the plot of each cell voltage versus the number of cycles. At the Beginning of Life (BOL) the cells had an average performance of 668 mV and the difference between the maximum and minimum performance was about 25-30 mV. Typically, the cell voltage tends to decrease faster during the first cycles, followed by a slower steady trend, and finally a dramatic drop off. The EOL limit was reached after 354 startup/shutdown cycles when cell #4 voltage fell below 560 mV. After about 310 startup/shutdown cycles, the cells started to show high mass transport losses, and the cell performance decreased considerably

with each new cycle. A proposed explanation is that the MEAs started to lose their hydrophobic properties and the cells began to flood. Since any residual water was not removed prior to the next startup, the cells performed even worse at each following cycle. The worst performing cell was #4, which showed more mass transport losses, with respect to the others.

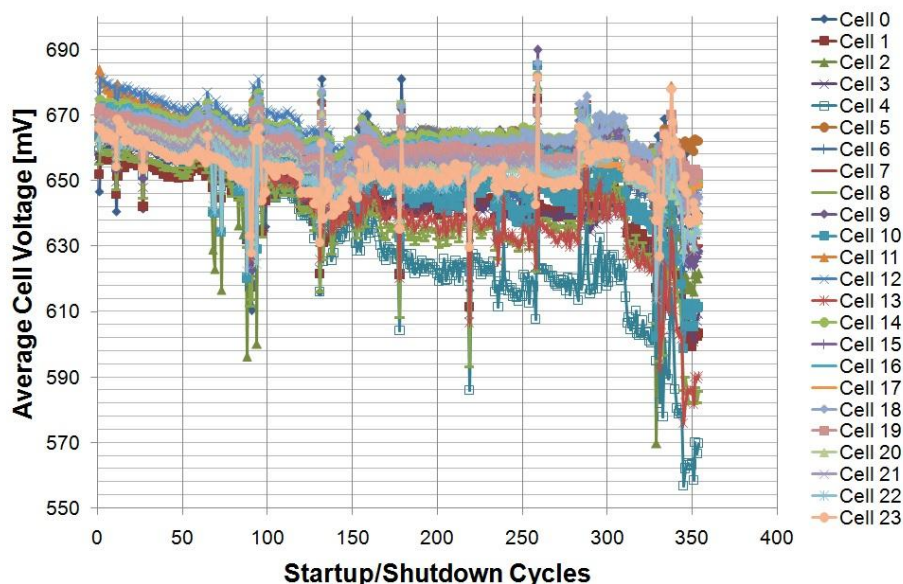


Figure 3.34. Voltage graph of the cells with unprotected startups and shutdowns [28].

The voltage degradation values for the “average cell voltage” and cell #4 are based on the collected stack data. The results have been reported in Figure 3.35, along with two degradation trend lines, where each slope approximates the average and the maximum (cell #4) degradation rates, which were respectively 72 and 205  $\mu\text{V}/\text{cycle}$ .

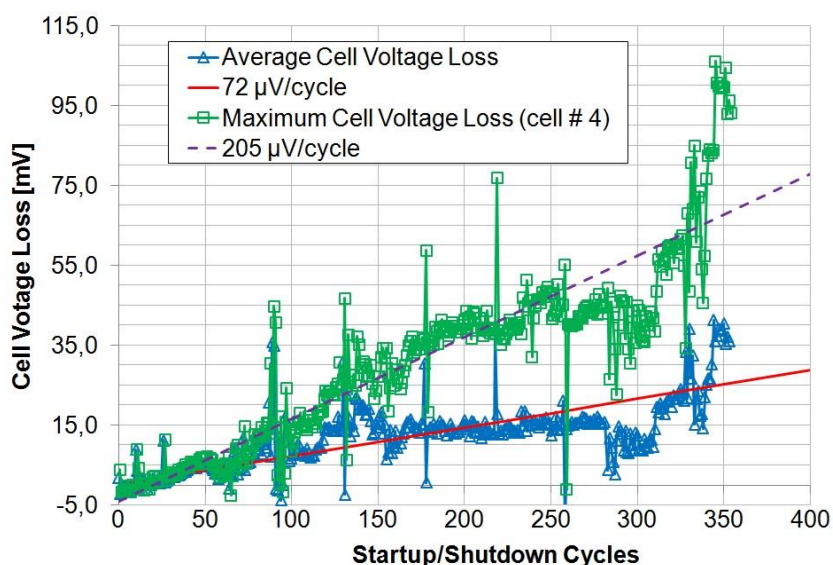
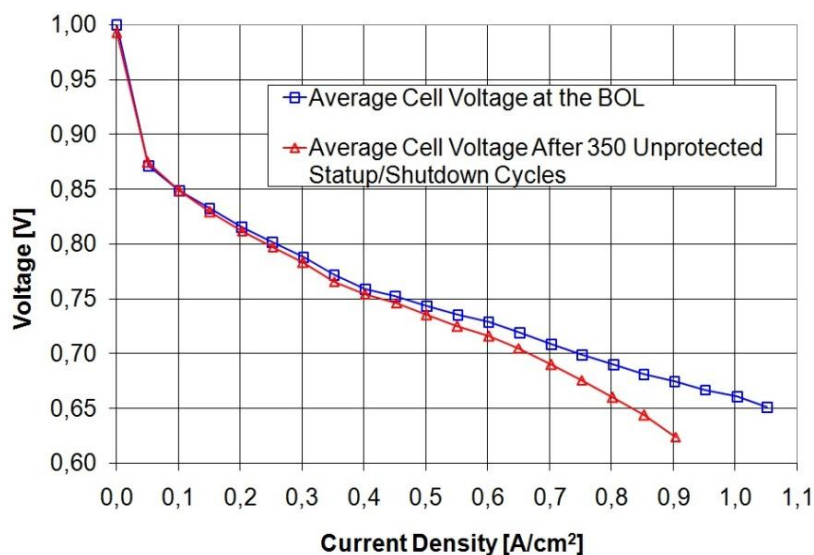


Figure 3.35. Average and maximum cell voltage degradation rate with unprotected startups and shutdowns [28].

Figure 3.36 reports the polarization curves for the stack tested with unprotected startups and shutdowns. The EOL curve shows a significant deviation from the BOL curve especially at high current density, indicative of decreased mass transport properties. Atanassova et al. [31] report that one type of performance loss related to catalyst support carbon corrosion is the mass transport losses due to some hydrophilic surface groups forming and leading to electrode flooding.



**Figure 3.36.** Stack polarization curve at the BOL and at the EOL [28].

The proposed model of catalyst degradation caused by carbon corrosion is the following [28]. At the beginning, the carbon oxidation reaction acts on the surface chemistry of the carbon support surface increasing its hydrophilicity, which will decrease the rate at which the MEA can expel excess water at high current density operation, and lead to an earlier appearance of reduced mass transport and performance loss [30]. The tendency for enhanced wettability can further promote carbon oxidation due to the increased water retention. At this point, carbon support damage can become so pronounced that it leads to Pt particle detachment from the carbon surface. Also, the Pt detachment is favored by its high catalytic activity for the carbon oxidation, which focuses the carbon corrosion events near the Pt-site [25], [49], [53]. Once the Pt is detached, it can sinter into another Pt particle, or dissolve into the ionomer and re-deposit again into a Pt site or inside the membrane [44], [53], [76].

In this stack experiment, the carbon corrosion occurring during the startup and shutdown periods could be still at an initial phase, since only a loss in mass transport has occurred without any substantial effect on catalyst activity.

The worst performing cells at the end of the test with unprotected startups and shutdowns were #4, #8 and #13, having cell voltage values respectively of 558 mV, 581 mV and 582 mV. The three MEAs coming from these cell positions, together with a fresh MEA for comparison, were examined using the Field Emission Scanning Electron Microscopy (FE-SEM) technique.

The principal difficulty encountered during the FE-SEM analysis was the Micro Porous Layer (MPL) detachment from the catalyst layer, especially at the anode side. This occurred during the sample exposure to liquid Nitrogen (freeze fracture technique), which was unavoidable in order to create a good cross section of the MEA. All the MEAs coming from the durability test showed the detachment of the anode catalyst layer when immersed into liquid Nitrogen. Thus, it was not possible to be totally confident with the thickness measurements of the anode catalyst layer, since it could have been partially attached to the MPL and separated with it. However, the cathode catalyst layer remained well bonded to the MPL in all the samples; and the membrane remained anchored to both the Catalyst Layers (CLs).

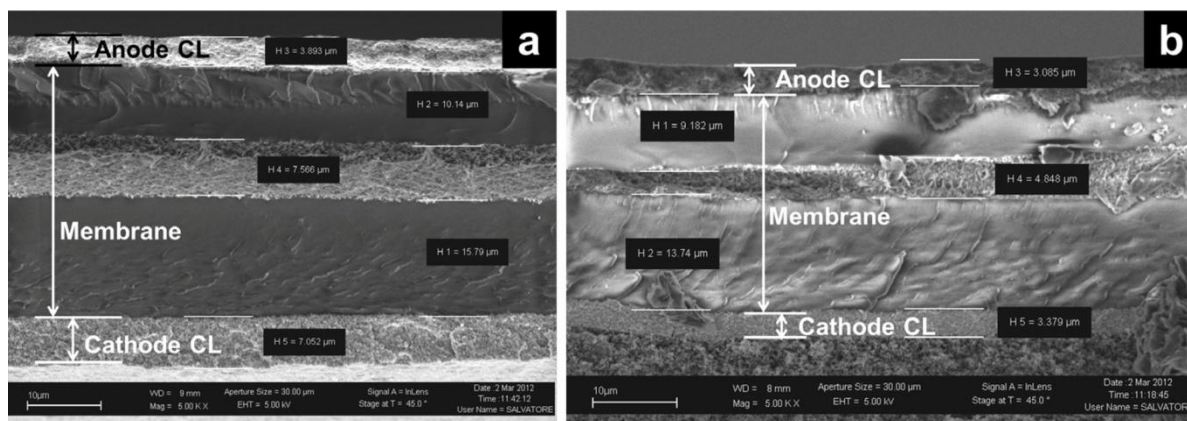
Results reported in Table 2 show that while the membrane thickness is still within the manufacturing tolerances range (reference value = 30  $\mu\text{m} \pm 10\%$ ), the cathode catalyst layer is starting to diverge from the thickness reference value (7  $\mu\text{m} \pm 15\%$ ), especially at the cell outlet.

Therefore, from the FE-SEM analyses two important points can be confirmed: (a) the membrane was not significantly thinned during the test; and (b) the cathode catalyst layer started to degrade, especially at the cell air outlet.

**Table 2.** Thickness values of membrane and cathode CL for a fresh MEA, and the MEAs coming from the three worst performing cells of the unprotected stack [28].

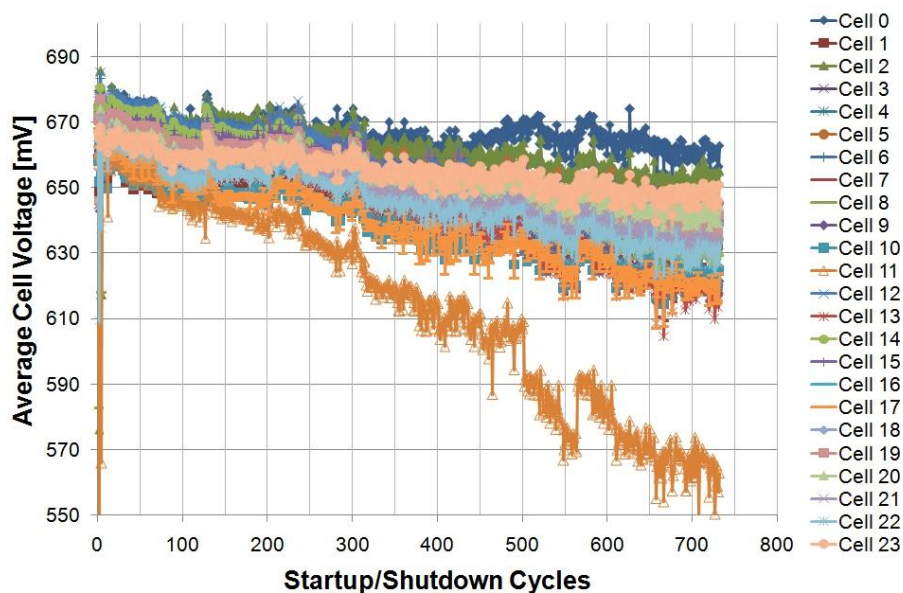
| Sample           | Membrane Thickness | % Deviation vs. Membrane Thickness Value | Cathode Layer Thickness | % Deviation vs. Cathode Layer Thickness Value |
|------------------|--------------------|--|-------------------------|---|
| Fresh MEA inlet  | 30.6 $\mu\text{m}$ | + 2 %                                    | 7.0 $\mu\text{m}$       | + 0 %   |
| Fresh MEA outlet | 28.7 $\mu\text{m}$ | - 4 %                                    | 6.8 $\mu\text{m}$       | - 3 %   |
| Cell #4 inlet    | 28.8 $\mu\text{m}$ | - 4 %                                    | 5.6 $\mu\text{m}$       | - 19 %  |
| Cell #4 outlet   | 28.1 $\mu\text{m}$ | - 6 %                                    | 4.6 $\mu\text{m}$       | - 34 %  |
| Cell #8 inlet    | 31.7 $\mu\text{m}$ | + 6 %                                    | 6.5 $\mu\text{m}$       | - 6 %   |
| Cell #8 outlet   | 28.0 $\mu\text{m}$ | - 7 %                                    | 4.0 $\mu\text{m}$       | - 43 %  |
| Cell #13 inlet   | 29.4 $\mu\text{m}$ | - 2 %                                    | 6.5 $\mu\text{m}$       | - 7 %   |
| Cell #13 outlet  | 28.8 $\mu\text{m}$ | - 4 %                                    | 4.7 $\mu\text{m}$       | - 32 %  |

The cross section of each sample was examined at three different locations. So, a total number of 24 cross sections were screened with FE-SEM. The thickness values reported in Table 2 are in fact the result of the average of these three positions in order to minimize the impact of thickness tolerances on the measurements. Figure 3.37 shows two of the 24 FE-SEM images evaluated. The membrane total thickness (about 30  $\mu\text{m}$ ) can be obtained by summing the thicknesses of the two-ionomer layers plus the center reinforcing layer.



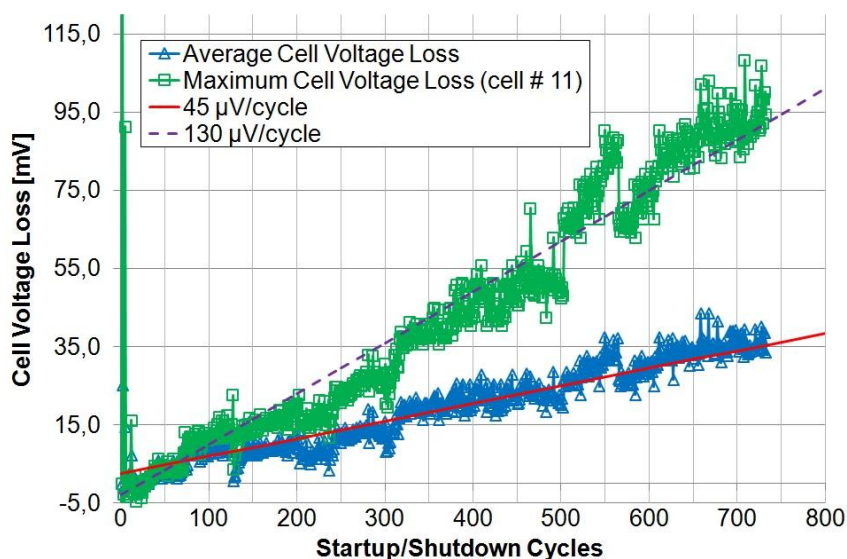
**Figure 3.37.** (a) On the left: FE-SEM scan of an MEA at the BOL. (b) On the right: FE-SEM scan of MEA coming from cell #4 after the cycling test [28].

After having substituted all the MEAs with new ones and modifying the test bench for implementing the stack protocol, the durability test was repeated using the same operating conditions, test bench and stack hardware. The average cell voltage at the BOL was 770 mV while the difference between the maximum and the minimum performance was slightly lower with respect to the first test (20-25 mV). As shown in Figure 3.38, the EOL limit was reached after 732 startup/shutdown cycles when the voltage for cell #11 dropped below 560 mV. The cells, even towards the end of the test, showed a linear degradation trend. Furthermore, mass transport issues at high current density did not influence the behavior of all the cells, except #11. On the other hand, Cell #11 already started to show marked mass transport losses after 200 cycles.



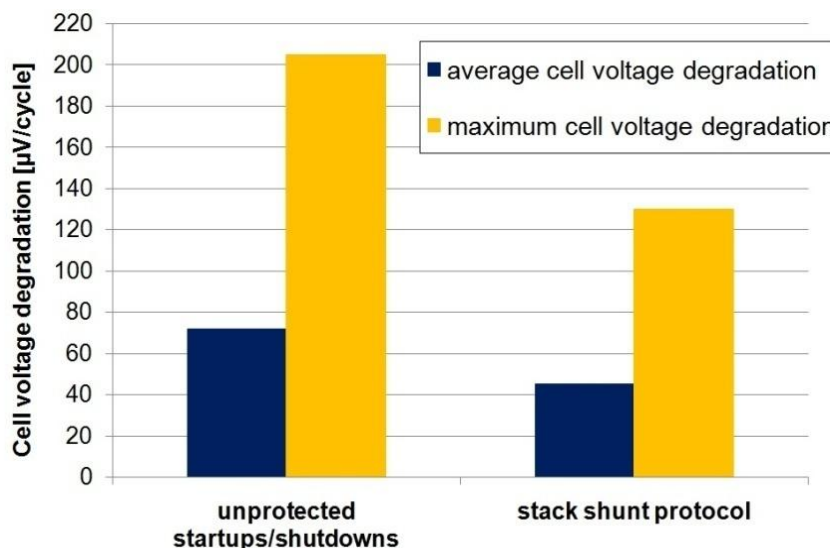
**Figure 3.38.** Voltage graph of the cells using the stack shunt protocol [28].

Figure 3.39 summarizes the cell voltage degradation as a function of the number of startup/shutdown cycles for the stack average cell voltage and for cell #11. The corresponding degradation trend was respectively 45 and 130 μV/cycle.



**Figure 3.39.** Average cell voltage and degradation rate using the stack shunt protocol [28].

The test results show a significant decrease in the degradation rate for startup/shutdown cycling with the protected stack using the shunt protocol, compared to the stack with unprotected startups and shutdowns. Figure 3.40 shows the comparison of the degradation rate values for each stack average cell voltage and for the worst performing cell in each stack test. The stack shunt decreased both the average and the maximum degradation rate by about 37% with respect to the case of unprotected startups and shutdowns.



**Figure 3.40.** Comparison of the degradation rate/cycle with unprotected startups and shutdowns and using the stack shunt protocol [28].

In both cases, the performances of one or more cells deviated considerably from the average value. The principal degradation result was an increased mass transport loss probably due to an enhanced flooding tendency of the electrodes because of the carbon oxidation effects. The worst performing cells were different

in the two tests (cell #4 in the first one and cell#11 in the second one). The higher degradation rate cannot be attributable to the stack hardware, since it was the same in both tests. A plausible explanation might be that partial flooding of these particular cells persisted during the shutdown. This could have blocked and isolated certain regions of the MEA and promoted the formation of air-rich and hydrogen-rich areas on the anode side of the cell, and thus accelerating the cathode catalyst carbon support corrosion.

The main effect of carbon corrosion observed during unprotected startups and shutdowns was a decrease of the fuel cell performance, which is attributed to high mass transport losses. FE-SEM analyses prove that the carbon oxidation reaction caused a thinning of the cathode catalyst layer.

Results obtained with the stack shunt protocol report a decrease in the voltage degradation rate by 37% per startup-shutdown cycle, as compared to unprotected startups and shutdowns. This improvement allowed double the number of cycles before the stack reached a pre-defined “End of Life” operating voltage.

At the end of the first test (with unprotected startups and shutdowns) the main considerations are:

- No failure events due to fuel starvation had been registered. So the cell flooding prevention, exercised by the contemporary actions of the current modulation and the cell voltage monitoring, had been effective.
- Figure 3.35 shows that the polarization curve at the Beginning of Life is practically coincident to the curve at the End of Life, indicative of similar activation losses. So, since the performance losses are not due to a catalyst activity decrease, also the current modulation technique avoiding sudden voltage changes had been effective.
- The cathode catalyst layer thinning proved that the carbon corrosion at the start and stop is the dominant degradation mechanism in back-up application.

However, the second test proved that the stack shunt protocol effectively helps to decrease the degradation rate at the start and stop allowing the doubling the lifetime of the stack in terms of start-stop cycles.

In conclusion, this experimentation has proved that:

- 1) The stack shunt method is capable of mitigating the impact of carbon corrosion at the cathode during the startup and shutdown phases.
- 2) The cell voltage monitoring together with the current modulation have been effective since no failure events occurred during all the time of the experimentation.
- 3) Limited catalyst activity losses were found after the experimentation tests, indicative of the good effectiveness of the current modulation in preventing the platinum dissolution.

The use of a stack shunt, cell voltage monitoring and current modulation indicated a definite improvement in the MEA durability by a) mitigating carbon corrosion during startup and shutdown, b) limiting Pt dissolution and c) avoiding dangerous situations such as the fuel starvation condition.

These methods do not require a complex or expensive modification in system hardware, thus are suitable for commercial fuel cell systems. The methods featured would be particularly useful for automotive

## Chapter 3 – Mitigation strategies for commercial PEM fuel cells stacks

---

applications, where, as in back-up, the number of startup/shutdown cycles and load cycles are considerably high.

Up to now, both the cell voltage monitoring and the current modulation methods have been used in all power systems manufactured by Electro Power Systems. Now, thanks to the positive results obtained at the end of the tests, the stack shunt feature has been added to new EPS products immediately after this study.

## Chapter 4.

# Performance, compactness and cost improvement of the fuel cells system

Nowadays a PEM fuel cell based system with a power output range of 1.5 – 10 kW must compete with batteries (lead-acid and Li-ions in particular) and diesel generators. Since the technologies of these traditional systems are consolidated and the sales numbers are high, the number of products ordered by the customer are high enough to spread the investment cost to a greater number of pieces decreasing the cost for each component.

Instead the fuel cell based system companies usually have to manage high overhead cost in particular for research and development and the typical production are small orders. The small sales numbers are attributable to the fact that the customer typically does not know the technology well, still needs to be convinced about reliability and, most of all, and is reluctant to buy something new and more expensive.

So this situation is a vicious cycle where sales volumes are small and the price cannot decrease due to the few orders. The only way to remedy is to find new technology solutions able to lower the system cost with similar performance.

The technology solution explored by Electro Power Systems is the **components integration**. This should allow:

- to decrease the number of components (less pipelines, electrical connections, sensors)
- to eliminate some components taking advantage of the interchange between devices

- to increase the performance optimizing the components operations

### ***4.1. DC-DC converter integration with a fuel cells stack***

The DC-DC converter is a device able to accept a continuous input voltage and generate a different amplitude output continuous voltage. DC-DC converters are commonly used in applications such as computers, medical devices and communication devices where the principal requirement is a regulated continuous power supply.

The methods used to transfer the electrical power from a DC source to a load in a controlled way are two: the linear conversion and the switching mode.

In the first case, the voltage conversion is produced by a variable resistance with a consequent considerable heat dissipation that leads to low efficiency.

With the switching mode, a commutator remains alternatively closed and open for certain periods of time. In this way, it is possible to regulate effectively the power flow according to the load by only controlling the time periods in which the commutator is closed and opened with efficiencies up to 90-95%. The need of having a continuous output voltage implies the use of reactant devices (inductors and capacitors) able to eliminate the frequency components different from zero, generated by the commutation process.

The fuel cell power system studied in this work is a UPS system for telecom applications where the requirements are typically a (theoretical) 48 V DC supply, even if in practice the voltage is always set at 52 V DC.

The power system includes conveniently a boost-type converter able to transform the input power supplied by the stack, which can generate a voltage both lower and higher than 52 V depending on the number of stacked cells and the current point, into a 52 V DC output. For this reason, the maximum allowable number of cells is 56 and a proper stack shunt resistor must be included in the Balance of Plant (BOP) in order to lower the stack voltage to 52 V during the idle periods, when the stack is disconnected to the load.

The MOSFETs and diodes, as well as the inductor present inside a DC-DC converter produce heat during the power conversion due to residual magnetic field and hysteresis phenomena in the inductor cores during the switching cycles and to the commutation losses of the MOSFETs. So MOSFETs, diodes and inductor are usually placed on a heat exchanger where a cooling liquid or air passes and removes the heat generated.

The first configuration studied by Electro Power Systems involved two separate coolant circuits: a primary connected to the stack and compatible with demineralized water only, and a secondary where common water or an ethylene glycol – water mix (for outdoor heat exchangers) can be used. In this configuration, the DC-DC converter was cooled by the secondary coolant circuit and was electrically connected to the stack with two separate electrical cables (see figure 4.1).

This cooling system requires a considerable amount of piping, auxiliaries, electric connection material and insulating material that leads to high cost, increased ohmic losses, longer thermal dynamic response and higher failure issues due to the intrinsic complexity.

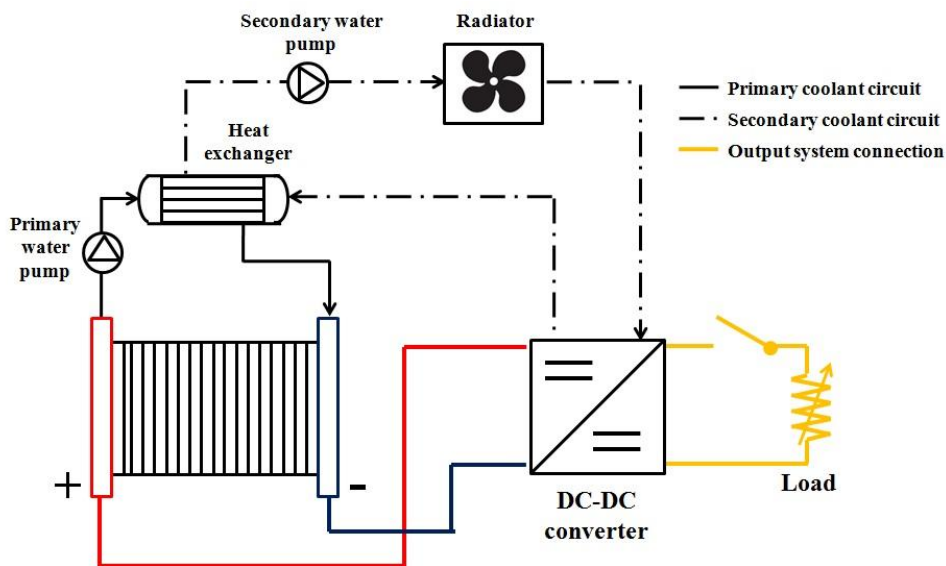


**Figure 4.1.** Scheme of the first system configuration proposed by Electro Power Systems.

With the invention “Stack of improved fuel cells and electric power generator comprising said stack” [77], the DC-DC converter is conveniently integrated with the fuel cell stack increasing considerably the compactness of the entire system. The integration comprises:

- a) integration with the stack cooling circuit
- b) electrical integration with the cathode electrode of the stack

Figure 4.2 shows the entire stack with the cathode electrode 211 thermally and electrically connected to the DC-DC converter 216 [77].

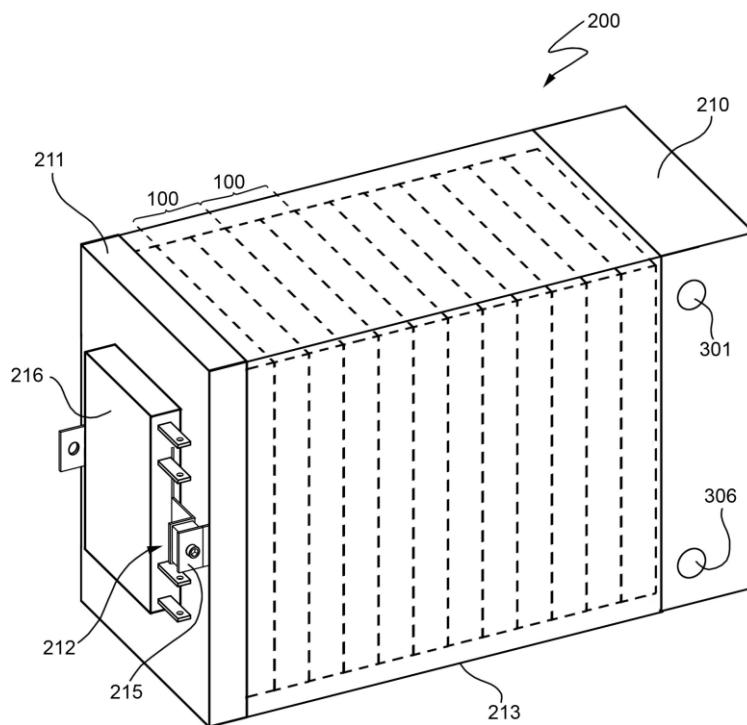


**Figure 4.2** Schematic drawing of a stack with a DC-DC converter thermally and electrically integrated with one of the stack head [77].

Since the efficiency is never 100%, the electric conversion usually produces a significant amount of dissipative heat especially for power system that needs to manage 5 or more kW. So an adequate cooling system must manage efficiently this heat in order to maintain the DC-DC converter in an optimal temperature range for the operation.

A dedicated cooling system for the DC-DC converter is usually costly and bulky. So using the stack cooling circuit can increase considerably the system compactness and at the same time reduce the global cost. Another important collateral advantage produced by this invention is the minimization of the thermal drift and thermal gradients between parts of the power generator due to the reduction of the number of independent components and the physical distance between the components themselves [77].

The thermal integration with the DC-DC converter is achieved using a thermal coupling between the stack cathode electrode 211 and one of the fuel cell cooling circuit 130'. Every cell, in fact, comprises a flow field for the coolant (see Figure 4.3) which is usually used to cool the fuel cell during the operation. By adding an additional coolant flow field after the last cell at the cathode end of the stack, the thermal coupling with the cathode electrode takes advantage of the stack cooling circuit and uses it to cool the DC-DC converter.

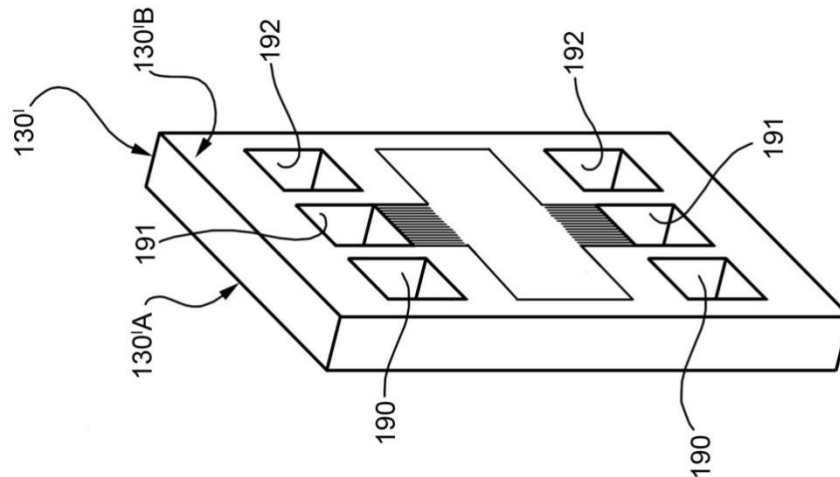


**Figure 4.3** Schematic drawing of the stack fuel cells cooling side [77].

Concerning the electrical integration, two main changes are present with respect to traditional fuel cells systems:

- a) the cathode end plate has the double function of tightening stack head and cathode current collector
- b) the inductor of the DC-DC converter is reasonably fixed and electrically connected to the cathode head of the stack 211.

The solution presented avoids an expensive copper current collector at the cathode and other electrical connections. Furthermore, there is no longer the necessity of insulating the cathode current collector from the tightening head of the stack, so the need of insulating material is greatly reduced.

The outlet current from the stack is usually addressed to the DC-DC converter inductor whose purpose is to dampen current harmonics generated by the DC-DC converter 216, in order to reduce the total harmonic component of the current drawn from the stack. With this invention, compared to other known solutions, the length of the electrical connections between the stack and the inductor is significantly limited. In this way it is possible to reduce the harmonic emission by radiation related to the connection (possibility to use less sophisticated and less expensive harmonic filter) and ohmic losses are significantly limited (increased conversion efficiency). Furthermore, the elimination of contacts and connections increases the overall reliability of the converter.

Figure 4.4 shows the first stack prototype integrated with a DC-DC converter. While the anode of the stack is electrically connected to the converter with a short cable, the cathode is electrically coupled with it. The stack cathode head is made by C40 steel, material with relatively high thermal conductivity but with also high flexural strength (indispensable for having a good mechanical pressure distribution on the entire fuel cell area). Thanks to this material and a thermal paste spread between the stack head and the converter, the DC-DC converter can be cooled by the stack's internal cooling circuit but without the necessity of additional pipes and connections with an external dedicated circuit.



**Figure 4.4.** Picture of the first prototype implementing the DC-DC thermal and electrical integration with the stack.

A further system improvement has been the unification of primary and secondary coolant circuits into a single one. This was possible thanks to the use of a commercial coolant prepared with a mixture of demineralized water, ethylene glycol and other additives that protect the metal surfaces, avoiding their ionic release.

The ethylene glycol helps also in reducing the freezing point temperature up to  $-20\text{ }^{\circ}\text{C}$ : this is a requirement linked with the fact that the system can be also installed outdoor in many climatic conditions. When the fuel cell stack is not working, the freezing of the water content inside membranes can be prevented by drying the membranes after every shutdown.

The system, including the unified coolant circuit and the stack integrated with the DC-DC converter, represents a considerable step forward since it is capable of solving the cost, performance and reliability issues listed at the beginning of this section 4.

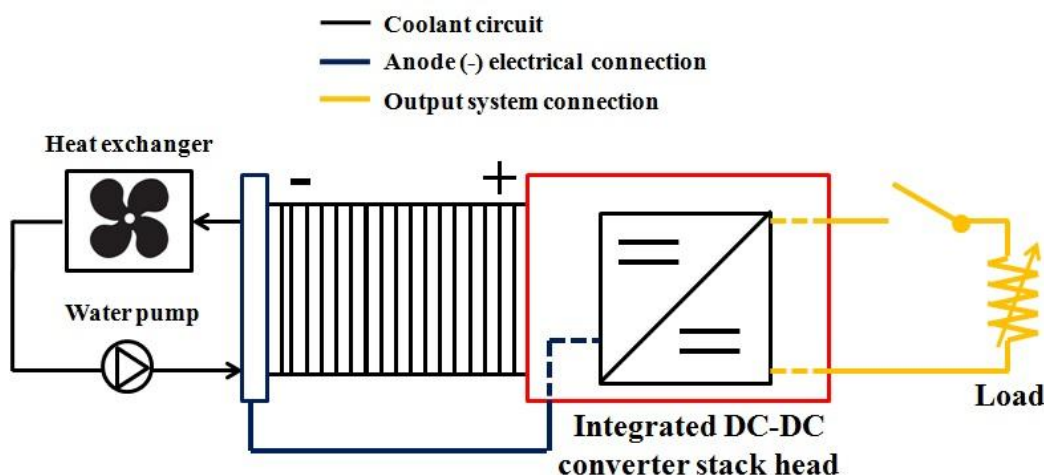


**Figure 4.5.** Scheme of the improved system design including the DC-DC integration with the stack and the unification of primary and secondary circuit into a unique coolant circuit.

## 4.2. Functionalized stack head with integrated heat exchanger for reactant gases processing

The fuel cell stack comprises, in addition to a plurality of cells connected in series, a first and a second head. Usually the heads have the primary function of structural support for the cells, and they can be bonded through a system of tie-rods. So the cells connected in series are positioned between the first head and the second head. In the previously presented invention [77], the second head has the above described additional functions of direct electrical connection and thermal coupling with the DC-DC converter.

Instead, the other head shown here has a more complex structure formed by:

- fluidic connections for the feeding of the reactants and for the discharge of reaction products or excess reactants
- fluidic connections for the feeding and the discharge of the coolant
- a heat exchanger able to transfer heat to a fluid, such as a reactant gas (hydrogen or oxygen)

While functions a) and b) are common in every PEM fuel cell stack, the function c) is specific of the invention “Stack of improved fuel cells and electric power generator comprising said stack”.

Figure 4.6 shows the first head that, apart from fluidic connections for the reactants and the coolant, defines advantageously, internally, a volume through which a fluid may pass thermally coupled with the stack coolant. In this way, this fluid can be heated up to the operation temperature of the stack (typically 55-60 °C).

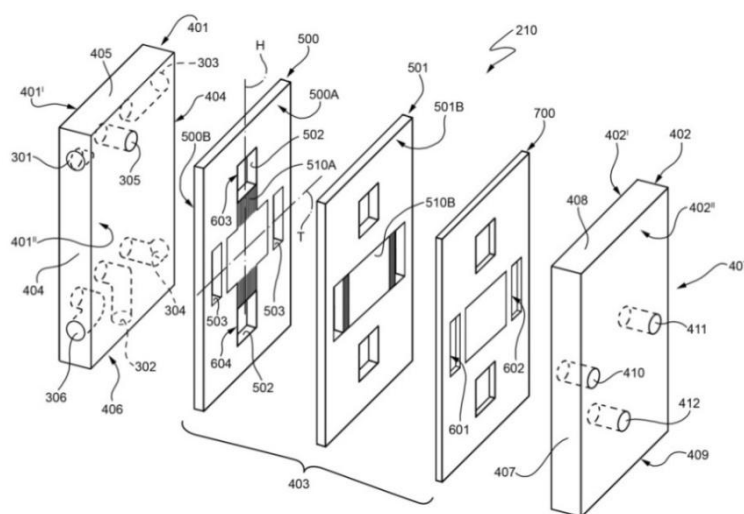


**Figure 4.6.** Schematic drawing of a stack head including a heat exchanger able to heat a fluid using the thermal power produced by the stack itself [77].

This is a great advantage if the fluid used is one of the reactants (hydrogen or pure oxygen) because in this way it is possible to a) reduce considerably the startup time of the stack and b) reduce the flooding tendency inside the reactants flow field channels if a reactant gas recirculation is used.

So, since the reactant is pre-heated up to the stack temperature, the high flooding tendency acting during the startup is considerably limited. This flooding phenomenon is due to the water condensing when the cold gas flows in the cell encounters the by-product water gas coming from the MEA. During the startup, the issues linked to even small flooding are particularly severe due to the presence of inert gas that enhances the mass transport losses. If the gas entering into the cells is instead pre-heated, it is possible to raise the stack current output faster (and so the stack power output) without significant flooding risk. Furthermore, even when the stack reaches the operating temperature, the flooding risk is still present if recirculation of the reactant gas is used. The recirculation is very useful for increasing the stoichiometric ratio and to avoid a low reactant concentration at the cell outlet. However, in this way, the gas with high RH values is carried to the stack inlet and this contributes to make water management more difficult within the cells.

Usually the highest flooding risk in this case is due to the conjunction between the cold reactant gas coming from the external feeding pipeline and the humidity-rich recirculation gas. The conjunction produces some water condensing that can promote cell flooding. If instead the recirculation gas is pre-heated up to the stack temperature, as described above, the gas mixing does not produce water condensing and the water flooding risk is reduced.

In the following, a detailed description of the head containing the “internal” gas heat exchanger is presented. The head comprises a first and a second end plate 401 and 402 (see Figure 4.6) having a development substantially parallel-piped and dimensions comparable with those of bipolar plates 130 and 130', and at least one heat exchange module 403. The heat module 403 is positioned between the first and the second end plates 401 and 402.

The feeding inlets and the outlets of hydrogen, comburent and coolant are defined internally by the first end plate 401. The first plate has a first face 401' and a second face 401'' opposite to each other; the first face is facing, in use, the rest of the stack 200, the heat exchange module 403, two sidewalls 404, an upper wall 405 and a lower wall 406. Similarly, the second end plate 402 has a first face 402' and a second face 402'' opposite to each other; the first face 402' is facing, in use, the heat exchanger module 403, two sidewalls 407, an upper wall 408 and a lower wall 409. The feeding inlets and the outlets for hydrogen and the comburent are obtained in the sidewall 404 of the first end plate 401. Instead, the feeding inlet and the outlet for the coolant are obtained in the second face 401'' and in the lower wall 406 of the first plate 401, respectively. Moreover, in the second plate 402 are formed an inlet 410 and an outlet 411 of the working heat-transfer fluid flow and an outlet of the coolant.

The heat exchange module 403 comprises a first and a second plate 500 and 501, which are identical but arranged one rotated by 180° with respect to the other with reference to a longitudinal axis H. The first plate 500 has two first openings 502 symmetrically arranged with respect to the transverse axis T of the first plate 500 and crossed by the longitudinal axis H. In addition, the first plate has two additional openings 503

arranged symmetrically with respect to the longitudinal axis H. In addition it defines, on a respective surface 500 facing the second plate 501, a first flow field 510A facing the second plate 501, a first flow field 510A comprising a plurality of ducts through which the working heat-transfer fluid flow pass and in fluidic communication with the second openings 503. The first plate 500 also defines, on a respective surface 500B opposite to the surface 500A and facing the first end plate 401, a second flow field 510B.

The first and the second plate 501 and 502 are made of a material having appropriate thermal conduction properties in order to facilitate the heat exchange between the two flows of coolant and working heat-transfer fluid.

In this way, the coolant is fed in at the level of the first head 210 through the inlet 302, passing through the fuel cells 100, removing the excess heat locally developed from the electrochemical reaction to then return to the first head 210. Here, said flow crosses the flow field 510A between the first plate 500 and the second plate 501 and then leaves the first head. Note that, once leaving the first head 210, the coolant can be recirculated by a pump at the inlet 302.

Moreover, in this way, the working heat-transfer fluid flow is fed at the level of the first head 210 through the inlet 410, flowing along the duct 601, crossing the flow field 510B between the second plate 501 and the second end plate 402, to then go along the outlet duct 602 and leave the head 211 through the outlet 411.

In this way, the thermal coupling between the coolant and the working heat-transfer fluid flows is achieved. The coolant and the working heat-transfer fluid flows lapping from opposite faces the second plate 501, through which heat is exchanged, whereby at least part of the excess heat developed by the reaction and removed from the coolant is transferred to the working heat-transfer fluid.

So, a stack head modified as described above, can be useful, for example, to pre-heat and dry the hydrogen. In this case, especially when the hydrogen is recirculated with a high water content (high RH values), using this invention contributes to lowering the flooding risk and helps to stabilize the cells voltage especially at high current. See Figure 4.7.

Another possibility is to use the heat exchanger contained in this stack head in order to dry the recirculated oxidant when the oxygen is used as oxidant at the cathode instead of the ambient air. This probably can produce even more evident benefits on the cell performance at high current with respect to the case of recirculated hydrogen because almost all the by-product water produced inside the fuel cells is sent in the oxidant circuit.

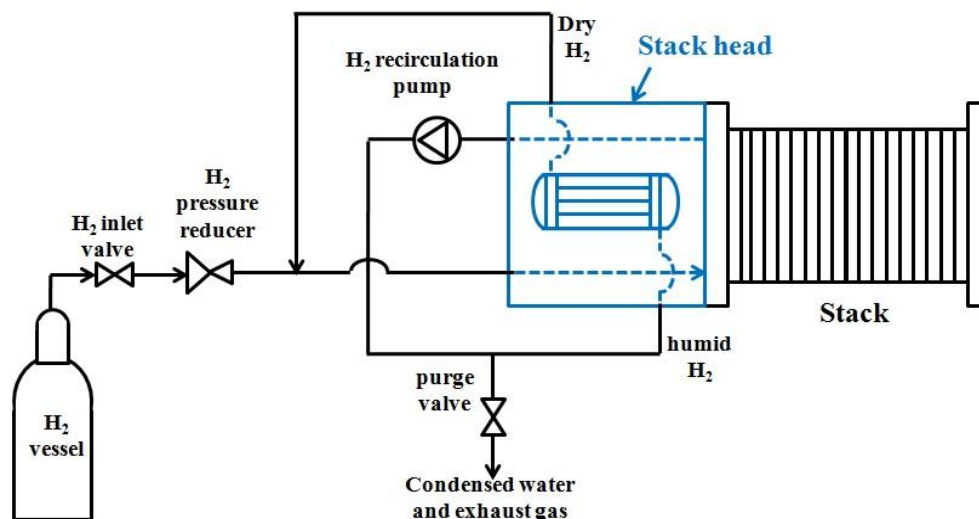


**Figure 4.7.** Scheme of the system including a stack head able to pre-heat and dry the hydrogen before entering into the stack, allowing a better performance at high current.

### ***4.3. Sensors integration for the process parameters measurement directly inside the stack***

The invention “Stack of improved fuel cells and electric power generator comprising said stack” also comprises, advantageously, a plurality of sensor means of corresponding relevant parameters for the process of producing electric power, such as, in particular, temperature and conductivity for the coolant fluid, pressure and humidity for the gas streams of reactants.

Preferably, such sensor means are housed directly within the stack, so as to obtain a high measurement accuracy. More particularly, said sensor means can be suitably housed in proximity to the housing of the gaskets, or at the flow fields. Said sensor means are operatively connected to a control unit, which is programmed to adjust, based on the physical quantity values detected by the sensor means and of the set point parameters, which can be predetermined, or selected from time by the user, the flow rate of the coolant and of the heat exchanged gas flows within the stack. For this purpose, the control unit is operatively connected to the sensor means housed in the stack, as well as to suitable flow regulation means arranged on respective ducts.

In use, by appropriate adjustment of the coolant and the heat-exchanged gas fluid flows within the stack, the temperature of the system is thus advantageously maintained within a predetermined range that is optimal for the stack operation.

In order to test the effectiveness of the sensor integration inside fuel cells, an experimentation was conducted with the aim of measuring the temperature distribution map inside operating PEM fuel cells.

The sensors used for this purpose were commercial platinum thin-film chip sensors acting as a Pt1000 thermistor. The chosen sensors were already encapsulated in order to protect the sensor from the humid environment present inside a PEM fuel cell and avoid the modification of the resistance response to temperature.



**Figure 4.8.** Schematic drawing of the thin film sensor used.

Concerning the most proper location where to insert temperature sensors, the graphite bipolar plate was considered the best option since the graphite is a good material to be machined with the aim of obtaining channels for sensors and connecting cables. The plate side chosen was the coolant side because it offered large areas to obtain those channels. Since the graphite is a good thermal conductor (80-240 W/mK) and the plate thickness is only 2 mm, the temperature difference calculated between the reactant side and the cooling side was negligible.

Overall, 9 sensors were placed: 6 inside the active area, 2 on the sides and 1 close to the inlet cooling manifold. Figure 4.9 shows schematically the sensors distribution inside the cell.

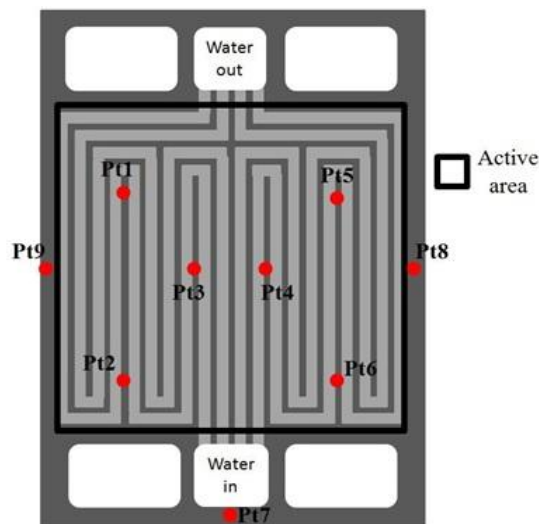


**Figure 4.9.** Sensors positions inside the cell.

The sensor integration inside the bipolar plate required four different steps:

- I. LASER machining of the channels for placing the sensors and for connecting enameled copper wires
- II. Welding of the enameled copper wire ends with the sensors

- III. Sensor inserting and covering with an insulation resin
- IV. Test for excluding possible shorting events

The bipolar plate is made of electrical conductive material and it is essential that the sensors are perfectly insulated from the plates. However, having a high thermal conduction nearby the sensors is fundamental as well. These requirements contributed to increase the difficulty of implementation.

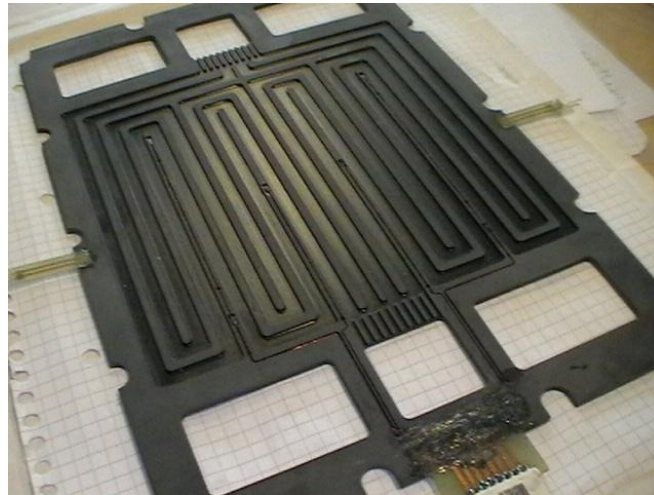


**Figure 4.10.** Plate with the MEMS sensors integrated on the coolant side.

The temperature variation inside a PEM fuel cell can lead to serious issues. In particular, the most dangerous problem is the water management.

If a sudden temperature fall occurs, the water vapor condenses generating and accumulating liquid water inside the bipolar plate channels or inside the GDL. As a consequence, the water flooding results in a gas reactants blockage, restricting feed to the catalyst layer where the reaction occurs.

On the contrary, if the temperature rises excessively, the polymer electrolyte membrane starts drying and the ionic conduction falls, leading soon to huge ohmic losses.

Usually if the temperature remains in the range 5 – 70 °C, a variation of 3-5 °C inside the fuel cell is still tolerable and does not generate local issues. If the temperature difference between the coolant inlet and the outlet exceeds 5 °C, some local drying or water flooding effects can occur.

The plate with the integrated sensors has been tested first inside a climatic chamber at the INRIM Institute in Turin. In the temperature range between 0 and 80 °C, the error with respect to the reference value remained below 0.5 °C for temperatures under 40 °C, while it reached 1.1 – 1.3 °C when over 60 °C. The difference between the reference value rose over 2 °C when the temperature approached 80 °C. However the control logic developed by Electro Power Systems in any case avoids temperatures over 70 °C. If the temperature reaches 70 °C and does not decrease immediately, the control logic stops the power system and an error message of over-temperature appears.

Another relevant result obtained from the characterization at the INRIM Institute was the stability test on a humid environment: even at RH 100 % the sensors do not suffer from any drift effects thanks to the encapsulation.

| difference from the reference temperature |            |            |            |            |            |            | Expanded uncertainty of calibration |              |              |              |              |              |              |
|---|------------|------------|------------|------------|------------|------------|-------------------------------------|--------------|--------------|--------------|--------------|--------------|--------------|
| REF °C                                    | Pt7-REF °C | Pt6-REF °C | Pt4-REF °C | Pt3-REF °C | Pt2-REF °C | Pt1-REF °C | REF °C                              | u_tar Pt7 °C | u_tar Pt6 °C | u_tar Pt4 °C | u_tar Pt3 °C | u_tar Pt2 °C | u_tar Pt1 °C |
| 0,27                                      | 0,4        |            |            | 0,4        | 0,2        | 0,5        | 0,27                                | 0,2          |              |              | 0,2          | 0,2          | 0,2          |
| 0,28                                      | 0,4        | 0,4        | 0,5        |            |            |            | 0,28                                | 0,2          | 0,2          | 0,2          |              |              |              |
| 20,65                                     | 0,1        | 0,0        | 0,2        |            |            |            | 20,65                               | 0,2          | 0,2          | 0,2          |              |              |              |
| 20,64                                     | 0,1        |            |            | 0,1        | -0,1       | 0,1        | 20,64                               | 0,2          |              |              | 0,2          | 0,2          | 0,2          |
| 40,71                                     | -0,4       |            |            | -0,4       | -0,7       | -0,4       | 40,71                               | 0,2          |              |              | 0,2          | 0,2          | 0,2          |
| 40,86                                     | -0,4       | -0,5       | -0,3       |            |            |            | 40,86                               | 0,2          | 0,2          | 0,2          |              |              |              |
| 61,05                                     | -1,1       | -1,1       | -1,0       |            |            |            | 61,05                               | 0,3          | 0,3          | 0,3          |              |              |              |
| 60,92                                     | -1,1       |            |            | -1,1       | -1,3       | -1,0       | 60,92                               | 0,3          |              |              | 0,3          | 0,3          | 0,3          |
| 80,88                                     | -1,8       |            |            | -1,9       | -2,1       | -1,8       | 80,88                               | 0,2          |              |              | 0,2          | 0,2          | 0,2          |
| 80,89                                     | -1,8       | -1,9       | -1,7       |            |            |            | 80,89                               | 0,2          | 0,2          | 0,2          |              |              |              |

Figure 4.11. Gap respect to the reference value and calibration uncertainty.

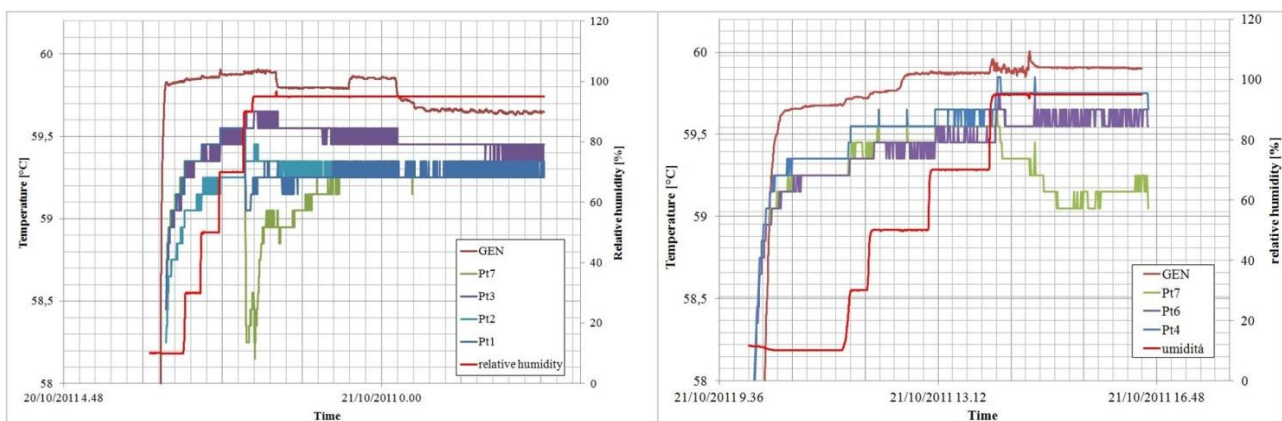


Figure 4.12. Stability test for different RH values.

The plates then was used to assembly a 40-cell stack with the following features:

- Operating voltage: 25-40 V
- Maximum power: 5.7 kW
- Weight: 28 kg
- Fuel / Oxidant: pure H<sub>2</sub> (purity 99.995%) / ambient air
- Coolant: demineralized water
- Working temperature: 62 °C



Figure 4.13. Pictures of the stack including the bipolar plates with the MEMS temperature sensors integrated.

The test bench used to perform the characterization was equipped with:

- A power system modified to work without the DC-DC power converter and the relative electronic boards controlling the electrical stack parameters. Since the electrical parameters are measured inside the DC-DC converter, in this way it was possible to connect directly the stack to a load without generating software alarms coming from the absent signals of the electrical parameters.
- 6 polypropylene pipes transporting air, hydrogen and demineralized cooling water to and from the stack.
- An electronic load reaching 12 kW.
- An acquisition system with 4 independent channels able to read and record the MEMS sensors temperature data.

The test was performed in two phases:

- 1) Stack heating at low load (2 kW) for 15 minutes in order to reach the working temperature (62 °C).
- 2) Temperature data acquisition at maximum load (5.7 kW) in stable working conditions.

All 9 sensors were cabled and connected, but since the acquisition system was able to read only 4 channels at a time, the sensors cables were manually and periodically changed during the test in order to investigate all the positions inside the fuel cell.



**Figure 4.14.** Pictures of the test bench used for the experimentation.

From the test data, two important features can be observed:

- The temperature close to the cell coolant inlet and in the side of the cell is considerably more stable with respect to the one recorded inside the active area. Since the current, the reactants flows and the humidity were constant, the fluctuations could be produced by the coolant system only: for the test done, a simple temperature controller switching on and switching off a fan when the temperature respectively increased above or decreased below 62 °C was used. This kind of control is not precise and was used expressly for this test in order to study frequent and high temperature variation. For

the standard power system assembled by Electro Power Systems, the type of temperature controller used is instead the PID type.

- It is possible to distinguish two different areas inside the fuel cell (see Figure 4.17):
  - A central strip with a large thermal gradient
  - Two side strips with more uniform and stable temperature conditions

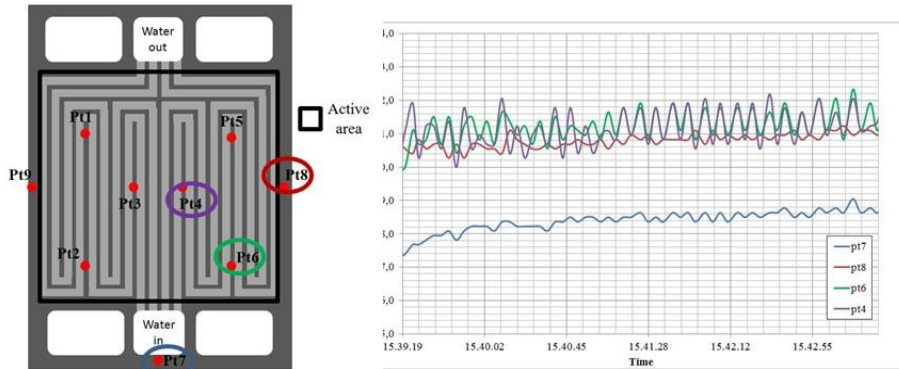


**Figure 4.15.** Temperature data coming from sensors #7 (coolant inlet), #4 and #6 (active area), and #8 (border region).

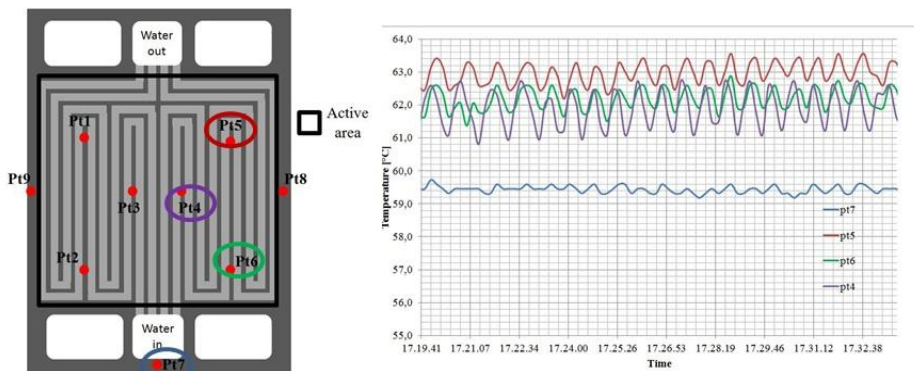


**Figure 4.16.** Temperature data coming from sensors #7 (coolant inlet), #4, #5 and #6 (active area).

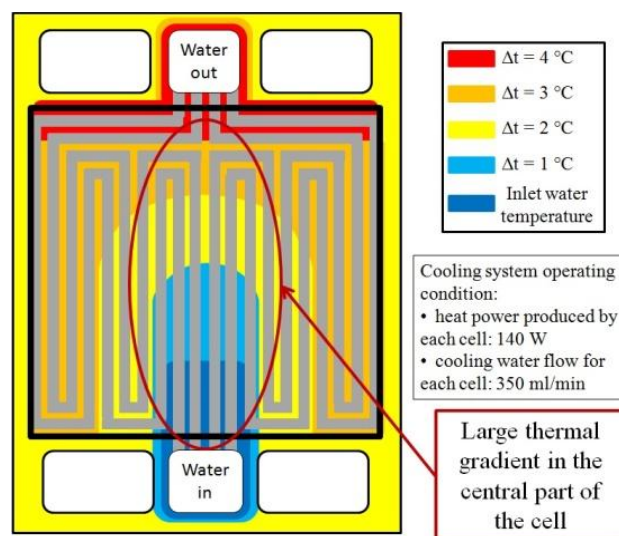


**Figure 4.17.** Schematic temperature distribution map obtained from the temperature data collected during the test.

Thanks to this temperature investigation inside a fuel cell, it was possible to obtain a first complete temperature distribution map of a PEM fuel cell.

The sensors integrated inside the fuel cell did not suffer from instability issues produced by the humidity influence or oxidation problems, and their behavior was stable for every RH value.

The temperature map realization allowed discovering three different areas: two side regions more stable and uniform, and a large central region featured by a high thermal gradient.

From a deep analysis on the behavior of the three thermal areas, it was clear that the large central thermal gradient increases the risk of water flooding, particularly in the zone close to the coolant inlet. So in this area, the water vapor contained in the reactant compartment condenses and produces liquid water leading to gas blockage.

Even if the thermal gradient detected during the test was only 4 °C, it is not uncommon to find out a thermal gap between the stack inlet and the outlet exceeding 6-10 °C especially during some particular events as load peaks. So, it is presumable that in these situations the cell suffers from water flooding at least in some zones (as those close to the coolant inlet of the fuel cell).

When a water flooding occurs, the reactant is unable to reach the catalyst and generate the reaction. So, in this situation:

- All the current absorbed by the load is generated by the remaining non-flooded free part of the active area. This leads to a loss of efficiency because the ohmic losses due to the electron flow and the ions flow increase.
- The flooded area is in a fuel-starved status, so the catalyst support is subjected to carbon corrosion. As we have seen in the previous chapters, the carbon corrosion involves: a) a further carbon surface wettability increase and b) carbon structure damaging with relative Pt detachment and loss of catalyst activity

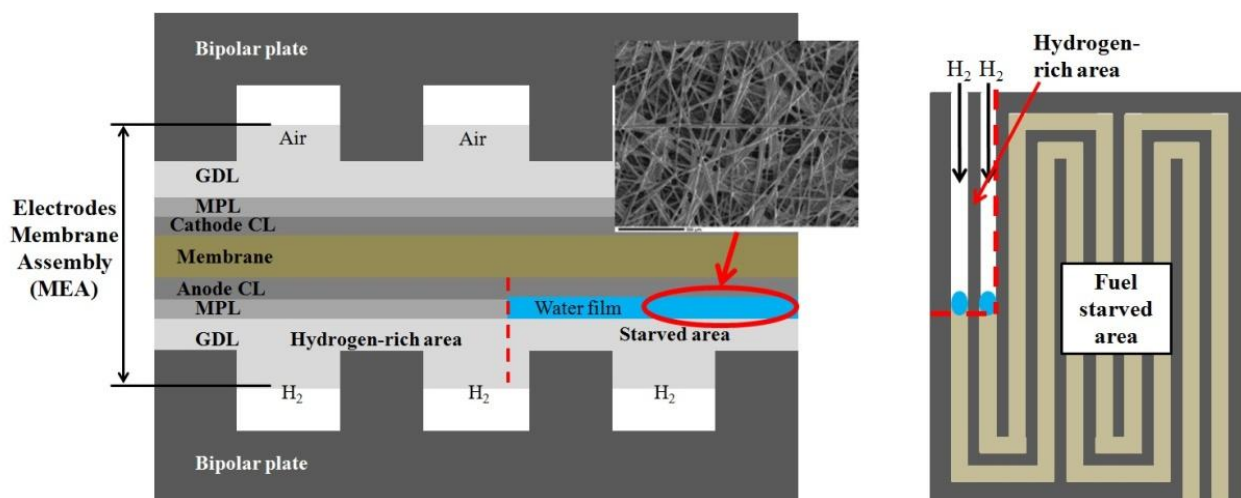


**Figure 4.18.** Most frequent locations inside a PEM fuel cell where it can exhibit water flooding.

Local over-temperature induces the membrane drying. Since the membrane needs a certain water content in order to show a good ionic conductivity, the dry zones become less conductive and most of the current flows in the remaining areas (see Figure 4.19).

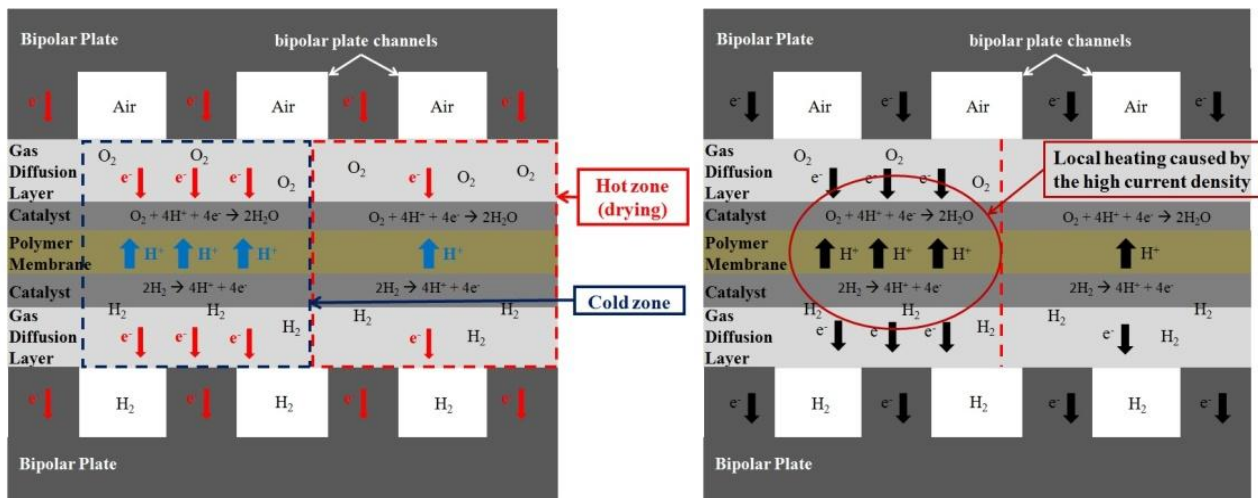


**Figure 4.19.** On the left: different ionic current distribution producing after the membrane drying of a hot area; on the right: consequent overheating produced by the current concentration.

The current concentration in a smaller area induces local overheated zones. Often the dry zone is so wide that the current is concentrated in a very local point. In this case, a “hot spot” is formed due to the heat produced by high current density.

Typically, the mechanism leading to local overheating started by a drying membrane zone is a vicious cycle in which the current is gradually concentrated in a smaller area where the temperature starts to rise. As a consequence, the higher temperature favors the membrane drying also in this area. Again, the current becomes even more concentrated in the remaining well-hydrated areas until it is so concentrated that the thermal power generated in a small area produces physical damage.

In particular, the overheating produced in some confined areas can cause:

- Gas Diffusion Layer collapsing → mass transport loss increasing (performance loss)
- Membrane degradation → leads to hydrogen crossover and consequent direct burning

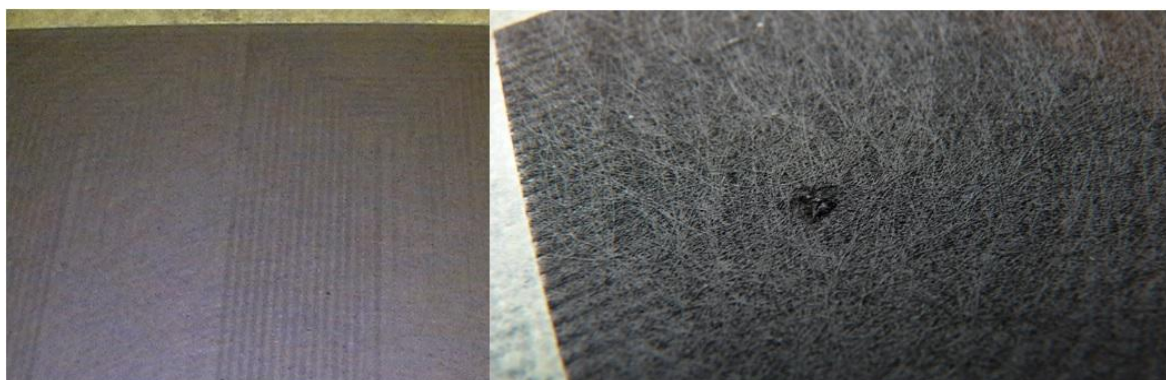


**Figure 4.20.** On the left: GDL collapsing due to local overheating; on the right: hot spot generated after a current concentration in a local point.

Concerning the temperature effects on the fuel cells, two methods can be used to increase the fuel cell performance:

- Leveling the temperature in the entire active area of the fuel cell.
- Avoiding that the reactant crosses a cold area for too long a time, especially when the reactant exhibits high RH values.

Concerning the first case, the simplest way is to increase the coolant flow rate until the temperature gap between the inlet and the outlet is under 4-5 °C. This temperature gradient distributed in an active area of 200-300 cm<sup>2</sup> is acceptable and typically does not induce particular issues.

Instead, it is important to design the reactant flow field taking into account the design of the coolant flow field. In particular, it is fundamental to avoid positioning the reactant's channel outlets in the same area corresponding to the coolant's channels inlets.

A possible future development can be the realization of MEMS temperature sensors deposited as thin film directly on the plate's surface. An example could be a Ni small strip (acting as a thermistor) deposited on an insulated oxide layer (acting as an insulator film). If properly realized, the Ni strip can act as a temperature sensor changing the internal resistance linearly with the temperature.

### ***4.4. Global advantages obtained and future developments***

The invention “Stack of improved fuel cells and electric power generator comprising said stack” provides considerable advantages to the power systems in terms of:

- i. Cost
- ii. Reliability
- iii. Size and weight

The cost reduction has been achieved mostly thanks to the integration between the stack and the DC-DC converter, and the possibility to dry the recirculated non-reacted hydrogen before it reenters the stack.

Thanks to the integration between the stack and the DC-DC converter, it was possible to eliminate or use less expensive components for: a) several electrical connections between the stack and the DC-DC converter, b) several piping runs in the coolant circuit and c) harmonic filter cutting the radio-frequency emission.

The functionalized stack head instead, if used to heat (drying) the recirculated H<sub>2</sub> before re-sending it into the stack, allows the stack to work at higher current operation with less flooding risk for the cells. This means higher performance, but if the increase in performance lets the stack supply the same power output

with less cells, this also translates to a cost reduction of the system. Furthermore, the recirculated H<sub>2</sub> drying insures also faster startup and less risk of having flooding in a cell. This means higher reliability for the power system.

The integration between stack and DC-DC converter has led to a great reduction of weight and size. The weight has been reduced mostly thanks to the elimination of the DC-DC converter’s coolant circuit and the electrical connections, while the size has been considerably reduced by coupling the stack with the DC-DC converter. In parallel, the unification of primary and secondary circuits into a unique coolant circuit contributes to further reducing cost and size, and at the same time increases thermal response and system reliability.

Finally, the MEMS temperature sensors integration inside a fuel cell provided for the first time indispensable information concerning the temperature distribution across the cell. Thanks to this information, some new fuel cell designs with improved temperature distribution have been already planned and should offer better protection from local over-heating or water flooding.

Concerning the topic of components integration inside the fuel cell system, another effort is currently under study. The idea is to eliminate the recently adopted resistive shunt for mitigating carbon corrosion with an “electronic shunt” able to simulate the stack shunt using a DC-DC converter and a capacitive storage.

A certain power  $P = V_0 I_0 = \eta V_i I_i$  can be drawn from the stack to a battery or super-capacitor, by setting the DC-DC output target voltage  $V_{target}$  higher than the battery voltage or super-capacitor voltage  $V_0$ .

The DC-DC control logic is able to set the stack current  $I_i = (V_0 / V_i) (I_0 / \eta)$  by changing the parameters  $D$  (duty cycle) or the switching frequency. When the stack shunt is engaged, the current  $I_i$  should be set to discharge the stack in a relatively short time period avoiding anode fuel starvation and inhomogeneous voltage values between cells (usually 4 to 5 amps is a good compromise). See Figure 4.21.

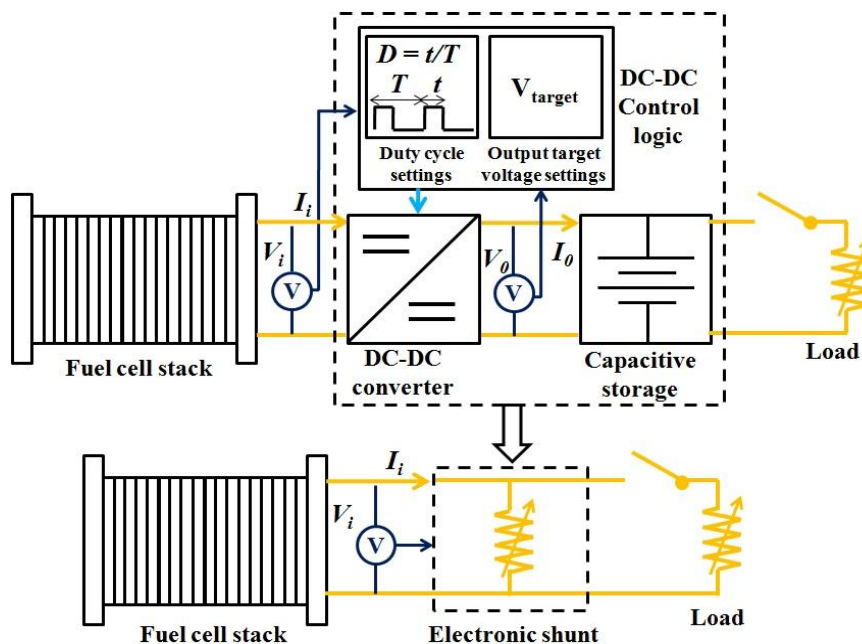


**Figure 4.21** Electronic shunt scheme: the DC-DC control logic is modified in order to make converter send power and re-charge the capacitive storage during the shutdown, simulating a resistive shunt [43].

The protocol with the electronic shunt would be the same as the resistive shunt, thus including anode recirculation, oxidant flow and venting procedure during the shutdown phase. The only difference is that with the e-shunt, the shunt cannot remain connected once the stack discharging is complete. So the only way to avoid any possible voltage generation due to residual un-reacted hydrogen is to air-purge the anode compartment.

The electronic shunt, together with appropriate hardware and protocol, has the same carbon corrosion mitigation features as a traditional resistive shunt. However, additional advantages include:

- 1) The resistor can be eliminated from the balance of plant.
- 2) The input impedance of the DC-DC converter can be set by modifying the switch duty-cycle, allowing *precise control of the current* during the entire shutdown phase.
- 3) The current sink is independent from the actual voltage of the fuel cell stack.
- 4) The current sink can be lowered in case of high voltage differences between individual cells, which can occur during cell flooding.

# Conclusion

The aim of this work was finding new and innovative solutions able to improve the fuel cell durability on one side and reduce the system cost on the other. Since to the beginning, this research followed these two requirements and its development led to the realizations of some prototypes taken as example for the effective production of commercial fuel cell power systems with increased lifetime at lower cost.

The MEMS nano-sensors integration allowed the first temperature distribution map realization inside a fuel cell. The indications obtained helped to improve the fuel cell stack and avoid local over-heating or water flooding.

The detection and mitigation methods adopted, such as the *cell voltage monitoring*, the *stack current modulation* and the *stack shunt method*, led to effective improvement in PEM fuel cell durability, doubling the lifetime of the fuel cell stack.

Other system-based and material-based mitigation strategies had then been adopted, obtaining further reliability and durability.

The system cost has been considerably reduced thanks to the DC-DC converter integration with the stack and the coolant circuit simplification.

As future developments, we are studying the possibility to develop:

- an “electronic shunt” that uses a DC-DC converter and a capacitive load to discharge and simulate the resistive shunt, allowing further system cost reduction.
- a functionalized stack head with a gas-liquid exchanger and sensors incorporated inside that can allow further increase of performance and reliability.

In conclusion, this PhD research lead to effective innovations for PEM fuel cell stacks and systems, and made significant contributions to PEM fuel cell knowledge concerning the important topic of durability. It also proved that with some focused research efforts it is possible to reduce the cost of the fuel cell systems without high sales volumes.

# References

- [1] DOE/EIA-0484(2013), International Energy Outlook 2013
- [2] <http://www.eia.gov/todayinenergy/detail.cfm?id=3130>
- [3] DOE/EIA (2008), World Energy Outlook 2008
- [4] DOE/EIA (2008), World Energy Outlook 2011
- [5] Energiläget 2050 by prof. Cristian Azar and Kristian Lindgren Chalmers, Göteborg (see also [http://en.wikipedia.org/wiki/World\\_energy\\_consumption](http://en.wikipedia.org/wiki/World_energy_consumption))
- [6] <http://www.oil-price.net/en/articles/oil-drilling-expensive-business.php>
- [7] UNCTAD 2006, p. 41. Price for new vessel \$M in 2005 (see also [http://en.wikipedia.org/wiki/Oil\\_tanker](http://en.wikipedia.org/wiki/Oil_tanker))
- [8] [http://en.wikipedia.org/wiki/Keystone\\_Pipeline](http://en.wikipedia.org/wiki/Keystone_Pipeline)
- [9] <http://www.theglobeandmail.com/report-on-business/pipeline-fees-revolt-widens/article1548807/>
- [10] [http://www.techmodular.com/oil\\_gas\\_power\\_projects.htm](http://www.techmodular.com/oil_gas_power_projects.htm)
- [11] [http://cleancaroptions.com/html/ev\\_fueling\\_time.html](http://cleancaroptions.com/html/ev_fueling_time.html)
- [12] P. G. Mura, R. Baccoli, U. Carlini, R. Innamorati, S. Mariotti, “PROPOSTE PER LA PRODUZIONE DI IDROGENO DA FONTI RINNOVABILI IN SARDEGNA PER INPIANTI INDUSTRIALI DI GRANDE POTENZA” (see <http://www.tecnosophia.org/>)
- [13] [http://www.scientific-computing.com/features/feature.php?feature\\_id=126](http://www.scientific-computing.com/features/feature.php?feature_id=126)
- [14] The Fuel Cell Today Industry Review 2013
- [15] <http://europe.autonews.com/article/20131211/ANE/131209875/toyota-targets-5000-to-10000-fuel-cell-sales-a-year#axzz2pXwLd3NK>
- [16] <http://europe.autonews.com/article/20131212/ANE/131219963/hyundai-reveals-europe-designed-intrado-fuel-cell-concept#axzz2pXwLd3NK>
- [17] <http://www.fuelcelltoday.com/news-events/news-archive/2013/may/hydrogen-infrastructure-project-launches-in-usa>

## References

---

- [18] <http://www.digitaltrends.com/cars/daimler-goes-big-on-h2-plans-to-bring-400-hydrogen-filing-stations-to-german-in-the-next-decade/>
- [19] Fuel Cell Commercialization Conference Of Japan, July 2010, Commercialization Scenario for FCVs and H2 Stations
- [20] Fuel cell 2000, Press releases 2013, “Fuel Cell Forklifts Gain Ground” (see also [http://www.fuelcells.org/base.cgim?template=press\\_releases](http://www.fuelcells.org/base.cgim?template=press_releases))
- [21] <http://www.fchea.org/index.php?id=25>
- [22] <http://www.renewableenergyfocus.com/view/23702/solvay-unveils-nedstack-1-mw-pem-fuel-cell-in-operation/>
- [23] <http://www.ballard.com/about-ballard/newsroom/news-releases/news10171201.aspx>
- [24] [http://www.nrel.gov/hydrogen/proj\\_fc\\_market\\_demo.html](http://www.nrel.gov/hydrogen/proj_fc_market_demo.html)
- [25] Mench, M. M., Kumbur, E. C., and Veziroglu, T. N., 2011, “Polymer Electrolyte Fuel Cell Degradation, 1<sup>st</sup> Edition”, Academic Press.
- [26] Jinfeng Wu, Xiao Zi Yuan, Jonathan J. Martin, Haijiang Wang, Jiujun Zhang, Jun Shen, Shaohong Wu, Walter Merida, J. Power Sources 184 (2008): 104-119.
- [27] S.D. Knights, K.M. Colbow, J. St-Pierre, D.P. Wilkinson, J. Power Sources 127 (2004) 127–134.
- [28] D. Bona, D. E. Curtin, F. Pedrazzo, E. M. Tresso, “Using a Stack Shunt to Mitigate Catalyst Support Carbon Corrosion”, Journal of Fuel Cell Science and Technology, February 01, 2014, Volume 11, Issue 1
- [29] Avasarala, B., Moore, R., and Haldar, P., 2010, “Surface oxidation of carbon supports due to potential cycling under PEM fuel cell conditions”, Electrochimica Acta, 55, pp. 4765–4771.
- [30] Fowler, M., Amphlett, J. C., Mann, R. F., Peppley, B. A., and Roberge, P. R., 2002, “Issues associated with Voltage Degradation in a PEMFC”, Journal of New Materials for Electrochemical Systems, 5, pp. 255–262.
- [31] Atanassova, P., Rice, G., Shen, J. P., and Sun, P., 2007, “Carbon Corrosion Effects in Fuel Cells”, Gordon Research Conference on Fuel Cells, Bryant University, Smithfield, RI, USA.
- [32] Chen, J., Siegel, J. B., Matsuura, T., and Stefanopoulou, A. G., 2011, “Carbon Corrosion in PEM Fuel Cell Dead-Ended Anode Operations”, Journal of The Electrochemical Society, 158, pp. B1164–B1174.
- [33] Baumgartner, W. R., Parz, P., Fraser, S. D., Wallnofer, E., and Hacker, V., 2008, “Polarization study of a PEMFC with four reference electrodes at hydrogen starvation conditions”, Journal of Power Sources, 182, pp. 413–421.
- [34] Reiser, C. A., Bregoli, L., Patterson, T. W., Yi, J. S., Yang J. D., Perry, M. L., and Jarvi, T. D., 2005, “A Reverse-Current Decay Mechanism for Fuel Cells”, Electrochemical and Solid-State Letters, 8, pp. A273–A276.
- [35] Kim, J., Lee, J., and Tak, Y., 2009, “Relationship between carbon corrosion and positive electrode potential in a proton-exchange membrane fuel cell during start/stop operation”, Journal of Power Sources, 192, pp. 674–678.

## References

---

- [36] Bekkedahl, T. A., Bregoli, L. J., Breault, R. D., Dykeman, E. A., Meyers, J. P., Patterson, T. W., Skiba, T., Vargas, C., Yang, D., and Yi, J. S., 2005, "Reducing fuel cell cathode potential during startup and shutdown", US patent 6,913,845 B2.
- [37] Van Dine, L. L., Steinbugler, M. M., Reiser, C. A., and Scheffler, G. W., 2003, "Procedure for shutting down a fuel cell system having an anode exhaust recycle loop", US Patent 6,514,635 B2.
- [38] Condit, D. A., and Breault, R. D., 2003, "Shut-down procedure for hydrogen-air fuel cell system", US Patent 6,635,370 B2.
- [39] Balliet, R. J., and Reiser, C. A., 2004, "System and method for shutting down a fuel cell power plant", US Patent 6,835,479 B2.
- [40] Reiser, C. A., Yang, D., and Sawyer, R. D., 2005, "Procedure for shutting down a fuel cell system using air purge", US Patent 6,858,336 B2.
- [41] Reiser, C. A., Yang, D., and Sawyer, R. D., 2008, "Procedure for starting up a fuel cell system using a fuel purge", US Patent 7,410,712 B2.
- [42] <http://www.psi.ch/media/from-pinholes-to-sudden-death-how-fuel-cells-age>
- [43] D. Bona, F. Pedrazzo, I. Rosso, D. E. Curtin, Dec. 11-13, 2013, "Stack Shunt Protocol: A Simple and Cost-Effective Method for Mitigating Catalyst Support Carbon Corrosion in PEMFC Stacks", Fifth European Fuel Cell Technology & Applications, Piero Lunghi Conference (Rome, Italy).
- [44] Büchi, F. N., et al.(eds), 2009, "Polymer Electrolyte Fuel Cell Durability", Springer Science + Business Media, Part III - System Perspectives, pp. 467–482.
- [45] de Bruijn, F. A., Dam, V. A. T. and Janssen, G. J. M. (2008), Review: Durability and Degradation Issues of PEM Fuel Cell Components. *Fuel Cells*, 8: 3-22.
- [46] Wu Bi, Gary E. Gray, and Thomas F. Fuller, *Electrochem. Solid-State Lett.* 10 (2007): B101–B104.
- [47] Jingxin Zhang, Brian A. Litteer, Wenbin Gu, Han Liu, and Hubert A. Gasteiger, *J. Electrochem. Soc.* 154 (2007): B1006–B1011.
- [48] Litster, S., and McLean, G., 2004, "PEM fuel cell electrodes", *Journal of Power Sources*, 130, pp. 61–76.
- [49] Chaparro, A. M., Mueller, N., Atienza, C., and Daza, L., 2006, "Study of electrochemical instabilities of PEMFC electrodes in aqueous solution by means of membrane inlet mass spectrometry", *Journal of Electroanalytical Chemistry*, 591, pp. 69–73.
- [50] Hinds, G., and Brightman, E., 2012, "In situ mapping of electrode potential in a PEM fuel cell", *Electrochemistry Communications*, 17, pp. 26–29.
- [51] Makharia, R., Kocha, S. S., Yu, P. T., Sweikart, M. A., Gu, W., T. Wagner, F. T., and Gasteiger, H. A., 2006, "Durable PEM fuel cell electrode materials: requirements and benchmarking methodologies", *ECS Transactions*, 1, pp. 3–18.
- [52] Hartnig, C., and Schmidt, T. J., 2011, "Simulated start–stop as a rapid aging tool for polymer electrolyte fuel cell electrodes", *Journal of Power Sources*, 196, pp. 5564–5572.
- [53] Wu, J., Yuan, X. Z., Martin, J. J., Wang, H., Zhang, J., Shen, J., Wu, S., and Merida, W., 2008, "A review of PEM fuel cell durability: Degradation mechanisms and mitigation strategies", *Journal of Power Sources*, 184, pp. 104–119.

## References

---

- [54] Schmittinger, W., and Vahidi, A., 2008, "A review of the main parameters influencing long-term performance and durability of PEM fuel cells", *Journal of Power Sources*, 180, pp. 1–14.
- [55] Hao Tang, Zhingang Qi, Manikandan Ramani, John F. Elder, "PEM fuel cell cathode carbon corrosion due to the formation of air/fuel boundary at the anode", *J. Power Sources* 158 (2006): 1306-1312.
- [56] D. Bona, F. Pedrazzo, I. Rosso, D. E. Curtin, E. M. Tresso, September 26-27, 2012, "Methods to Detect and Mitigate Catalyst Support Carbon Corrosion in PEM Fuel Cells", International Workshop on "Characterization and quantification of MEA degradation processes" (Grenoble, France)
- [57] T. R. Ralph, S. Hudson, and D. P. Wilkinson, *ECS Trans.* 2006 1(8): 67-84.
- [58] S. Maass, F. Finsterwalder, G. Frank, R. Hartmann, C. Merten, *J. Power Sources* 176 (2008):444-451.
- [59] G. Hinds, *Performance and Durability of PEM Fuel Cells: A Review*, NAT. PHYS. LAB, Teddington, UK, 2004.
- [60] James Larminie and Andrew Dicks, *Fuel Cell Systems Explained (Second Edition)*, John Wiley & Sons Ltd (2003).
- [61] Mark Alexander Melster, Stephens Andreas Grot, patent No.: US 5,763,113, Jun. 9, 1998.
- [62] Wenchao Sheng, Doctoral thesis: *Electrocatalytic Activities of Supported Pt Nanoparticles for Low-Temperature Fuel Cell Applications*, 2010 Massachusetts Institute of Technology.
- [63] Akira Taniguchi, Tomoki Akita, Kazuaki Yasuda, Yoshinori Miyazaki, *J. Power Sources* 130 (2004): 42-49.
- [64] Wolfgang R. R. Baumgartner, Eva Wallnöfer, Thomas Schaffer, Viktor Hacker, Volker Peinecke, and Peter Prenzinger, *ECS Trans.* 2006 3(1): 811-825.
- [65] Tanja Vidaković, Mihai Christov, Kai Sundmacher, *Electrochimica Acta* Volume 52, Issue 18, 10 May 2007, pp. 5606-5613.
- [66] Jingwei Hu, Pang-Chieh Sui, Ned Djilali and Sanjiv Kumar, *ECS Trans.* 2008 16(2): 1313-1322.
- [67] Xin Wang, Wenzhen Li, Zhongwei Chen, Mahesh Waje, Yushan Yan, *J. Power Sources* 158 (2006): 154-159.
- [68] Kyung-Won Park, Kwang-Su Seol, *Electrochemistry Communications* 9 (2007):2256-2260.
- [69] S. Vinod Selvaganesh, G. Selvarani, P. Sridhar, S. Pitchumani, and A. K. Shuklab, *J. Electrochem. Soc.* 157 (2010): B1000–B1007.
- [70] S. Sambandam, V. Valluri, W. Chanmanee, N. R. Tacconi, W. A. Wampler, W. Y. Lin, T. F. Carlson, V. Ramani, K. Rajeshwar, *J. Chem. Sci.*, Vol. 121, No. 5 (2009): 655-664.
- [71] R. Hahn, F. Schmidt-Stein, J. Salonen, S. Thiemann, Y. Song, J. Kunze, V. Lehto, P. Schmuki, *Angewandte Chemie* 121, Issue 39, pp.7372-7375, Sep. 14, 2009.
- [72] Chinmayee Subban, Qin Zhou, Brian Leonard, Chinmoy Ranjan, Heather M. Edverson, F. J. DiSalvo, Semeret Munie, and Janet Hunting, *Phil. Trans. R. Soc. A* (2010) 368:3243-3253.
- [73] Shyam Kocha, patent No.: US 7,887,963 B2, Feb. 15, 2011

## References

---

- [74] Paul Taichiang Yu, Frederick T Wagner, patent No.: US 7,799,475 B2, Sep. 21, 2010
- [75] Taniguchi, A., Akita, T., Yasuda, K., Miyazaki, Y., 2008, “Analysis of degradation in PEMFC caused by cell reversal during air starvation”, *International Journal of Hydrogen Energy*, 33, pp. 2323 – 2329.
- [76] Zhang, S., Yuan, X., Wang, H., Mérida, W., Zhu, H., Shen, J., Wu, S., and Zhang, J., 2009, “A review of accelerated stress tests of MEA durability in PEM fuel cells”, *International Journal of Hydrogen Energy*, 34, pp. 388–404.
- [77] D. Bona, P. Cherchi, G. Gianolio, L. Mercante, I. Rosso, 2012, Stack of improved fuel cells and electric power generator comprising said stack, WO 2012046192 A1